



Aeronautical Engineering Final Project

---

# Study of the optimal approach and detection phases for missions to small asteroids

---

Author: Adrià Pacheco Fuentes

Supervisor: Elena Fantino (ETSEIAT)

Collaborator: Joan Pau Sánchez Cuartielles (ETSEIB)

Thesis submitted in partial fulfillment of the requirements for the

Master Thesis in Aeronautical Engineering

in the

Department of Aerospace Engineering

January 2015



# Abstract

---

Nowadays, small asteroids are catching the space community's attention and interest. Instead of planning expensive missions to planets, missions to small asteroids (<100m) are of interest both because of their lower costs and scientific value.

Small asteroids are extremely faint objects that are serendipitously discovered while they are extremely close to the Earth. After a period of only a few days, a newly discovered small object moves far enough from the Earth so that its brightness falls below the detectability threshold of current telescopes. If the length of time that the asteroid has been visible from Earth is not long enough, the uncertainty on its ephemerides may still be high.

When a transfer is planned, the spacecraft is sent to a blind point since the asteroid cannot be seen from Earth. It becomes visible only the last days of the rendezvous trajectory. To ensure the meeting between the spacecraft and the object, only asteroids with very accurate ephemerides are targeted.

The aim of the project is to gain an insight into optimal approach trajectories in order to ensure that a small object is detected or, failing a total certainty, maximizing the probability to detect it during the close approach.

With this aim, the relative motion dynamics in the Hill coordinate frame will be studied and Matlab simulations will be performed.

# Index

<b>1. INTRODUCTION .....</b>	<b>9</b>
1.1 JUSTIFICATION .....	9
1.2 SCOPE OF THE PROJECT .....	11
<b>2. STATE OF THE ART .....</b>	<b>12</b>
2.1 NEOs DISCOVERY .....	12
2.1.1 <i>Catalina Sky Survey</i> .....	13
2.1.2 <i>Pan-STARRS</i> .....	13
2.1.3 <i>LINEAR</i> .....	14
2.1.4 <i>Spacewatch</i> .....	14
2.1.5 <i>NOEWISE</i> .....	15
2.2 ASTEROID DEVIATION.....	19
2.2.1 <i>NEOSshield</i> .....	19
2.2.2 <i>Asteroid Impact and Deflection Assessment (AIDA) Study</i> .....	20
2.3 ASTEROID SAMPLING .....	22
<b>3. MODELS .....</b>	<b>24</b>
3.1 RELATIVE ORBIT DESCRIPTION .....	24
3.1.1 <i>Hill coordinate frame</i> .....	25
3.1.2 <i>Clohessy-Wiltshire Equations</i> .....	26
3.1.3 <i>Orbit Element Difference Description</i> .....	30
3.2 OCC AND SEMI-MAJOR AXIS UNCERTAINTY .....	36
3.2.1 <i>Orbit Condition Code</i> .....	36
3.2.2 <i>Uncertainty in the semi-major axis</i> .....	37
3.3 REGRESSION MODEL FOR THE UNCERTAINTIES.....	38
3.3.1 <i>Model Validation</i> .....	41
3.4 ASTEROID DETECTION MODEL.....	42
3.4.1 <i>Additional constraints</i> .....	44
3.4.2 <i>Camera performance</i> .....	45
3.4.3 <i>Model validation</i> .....	45
3.5 VIRTUAL UNCERTAIN POPULATION.....	49
<b>4. SIMULATIONS.....</b>	<b>51</b>
4.1 STUDY 0: GENETIC ALGORITHM .....	51
4.1.1 <i>Description</i> .....	51
4.1.2 <i>Parameter evaluation</i> .....	53
Number of asteroids generated.....	53
Upper and Lower bounds.....	54
4.2 STUDY 1: PROBABILITY OF DETECTION (OCC AND CAD) .....	55
4.3 STUDY 2: PROBABILITY OF DETECTION (OCC AND ASTEROID DIAMETER) .....	57

4.4	STUDY 3: CAMERA VALUE.....	59
4.5	STUDY 4: CAD INFLUENCE ON DETECTABLE ASTEROID DIMENSIONS .....	62
4.6	STUDY 5: RESULTS ANALYSIS .....	68
4.6.1	<i>Part 1: Data loading</i> .....	68
4.6.2	<i>Part 2: Parameters selection</i> .....	69
4.6.3	<i>Part 3: Ellipsoid of uncertainty</i> .....	69
4.6.4	<i>Part 4: Optimum spacecraft and orbit analysis</i> .....	71
4.6.5	<i>Part 5: Trajectory representation and analysis</i> .....	73
	Accumulated probability .....	74
	Detection zone plot.....	77
4.7	STUDY 6: OPTIMAL APPROACHES FOR LOWER ASTEROID DIAMETERS .....	79
<b>5.</b>	<b>CONCLUSIONS</b> .....	<b>82</b>
<b>6.</b>	<b>ACKNOWLEDGEMENTS</b> .....	<b>84</b>
<b>7.</b>	<b>REFERENCES</b> .....	<b>85</b>
<b>8.</b>	<b>PROJECT BUDGET</b> .....	<b>87</b>
<b>9.</b>	<b>ENVIRONMENTAL AWARENESS</b> .....	<b>89</b>
<b>10.</b>	<b>ANNEX I: MATLAB FUNCTIONS</b> .....	<b>90</b>
<b>11.</b>	<b>ANNEX II: TIME REDUCTION</b> .....	<b>92</b>
<b>12.</b>	<b>ANNEX III: STUDY 4B</b> .....	<b>95</b>
<b>13.</b>	<b>ANNEX IV: STUDY 6 RESULTS</b> .....	<b>97</b>

# Abbreviations

---

OCC	Orbit Condition Code
NASA	National Aeronautics and Space Administration
NEO	Near Earth Object
SMA	Semi Major Axis
MPC	Minor Planet Center
LVM	Limiting Visual Magnitude
CAD	Close Approach Duration

# List of figures

---

FIGURE 1 ASTEROID SEEN IN RUSSIA (FEBRUARY 2013) .....	10
FIGURE 2 ASTEROID IMPACT IN A LAKE (RUSSIA).....	10
FIGURE 3 NEO DISCOVERIES PER FACILITY .....	12
FIGURE 4 PAN -STARRS FACILITY .....	13
FIGURE 5 PS2 TELESCOPE .....	14
FIGURE 6 SPACEWATCH FACILITY IN TUCSON, ARIZONA .....	15
FIGURE 7 NEOWISE SPACECRAFT .....	16
FIGURE 8 NEOWISE SPACECRAFT DETAILED VIEW .....	17
FIGURE 9 NEA CENSUS PREDICTION BY NEOWISE .....	18
FIGURE 10 AIDA MISSION CONCEPT .....	20
FIGURE 11 SPACECRAFT CAPTURING THE TARGET ASTEROID .....	22
FIGURE 12 ASTRONAUTS STUDYING THE CAPTURED ASTEROID.....	23
FIGURE 13 HILL REFERENCE FRAME DEFINITION .....	25
FIGURE 14 RELATIVE ORBIT DEFINITION .....	26
FIGURE 15 FILTER SELECTION .....	38
FIGURE 16 ECCENTRICITY UNCERTAINTY VS SMA UNCERTAINTY .....	40
FIGURE 17 INCLINATION UNCERTAINTY VS SEMI-MAJOR AXIS UNCERTAINTY.....	41
FIGURE 18 ASTEROID DETECTION DEFINITIONS AND CONFIGURATION .....	44
FIGURE 19 "NO DETECTION" ZONE .....	45
FIGURE 20 APPARENT MAGNITUDE (ASTEROID IN THE CENTRE) .....	46
FIGURE 21 DETECTION ZONE FOR CAMERA=15 AND ASTEROID IN THE CENTRE .....	46
FIGURE 22 APPARENT MAGNITUDE (S/C IN THE CENTRE) .....	47
FIGURE 23 DETECTION ZONE FOR CAMERA=15 AND S/C IN THE CENTRE .....	48
FIGURE 24 CLOUD OF ASTEROIDS .....	49
FIGURE 25 GENETIC ALGORITHM.....	51
FIGURE 26 TERMINATION CRITERIA EXAMPLE.....	52
FIGURE 27 DETECTION PROBABILITY FOR DIAMETER=20 M (STUDY 1).....	55
FIGURE 28 DETECTION PROBABILITY FOR DIAMETER=5 M (STUDY 1).....	56
FIGURE 29 DETECTION PROBABILITY CAD = 10 MONTHS (STUDY 2) .....	57
FIGURE 30 DETECTION PROBABILITY FOR CAD = 5 MONTHS (STUDY 2).....	58
FIGURE 31 CAMERA LMV REQUIRED FOR DIFFERENT ASTEROID DIAMETER AND OCC.....	60
FIGURE 32 EXPECTED RESULTS STUDY 4 .....	62
FIGURE 33 ELLIPSOID OF UNCERTAINTY MEASURES.....	69
FIGURE 34 ELLIPSOID PLOT (TOP VIEW) .....	70
FIGURE 35 ELLIPSOID PLOT (FRONT VIEW) .....	70
FIGURE 36 TRAJECTORY PLOT FOR OCC=4 AND CAD = 14 MONTHS (ISOMETRIC VIEW).....	73
FIGURE 37 FRONT, LATERAL AND TOP VIEW FOR OCC=4 AND CAD = 14 MONTHS.....	74
FIGURE 38 ACCUMULATED PROBABILITY FOR OCC=4 AND CAD = 14 MONTHS.....	75

FIGURE 39 FRONT, LATERAL AND TOP VIEWS WITH ACCUMULATED PROBABILITY FOR OCC=4 AND CAD = 14 MONTHS.....	76
FIGURE 40 TOP VIEW WITH ORBIT PARTS DIFFERENTIATION .....	76
FIGURE 41 LATERAL VIEW WITH DETECTION ZONE PLOTTED.....	77
FIGURE 42 FRONT VIEW WITH DETECTION ZONE PLOTTED.....	77
FIGURE 43 TOP VIEW WITH DETECTION ZONE PLOTTED .....	77
FIGURE 44 PROBABILITY OF DETECTION VS CAD FOR OCC = 5 AND DIAMETER = 4 M .....	79
FIGURE 45 TRAJECTORY PLOT FOR OCC = 5, DIAMETER = 4 M AND CAD = 30 MONTHS.....	80
FIGURE 46 SCHEMATIC ILLUSTRATION OF THE OPTIMAL TRAJECTORY .....	81
FIGURE 47 TIME DISTRIBUTION ALONG THE PROJECT (FROM JANUARY TO DECEMBER 2014) .....	87
FIGURE 48 FITNESS FUNCTION TIME PROFILE.....	92
FIGURE 49 ASTDETMODELSC TIME PROFILE .....	93
FIGURE 50 ASTDETMODELSC TIME PROFILE AFTER MODIFICATION OF "CROSS" AND "DOT" FUNCTIONS.....	93
FIGURE 51 FITNESS FUNCTION TIME PROFILE AFTER "ASTDETMODELSC" MODIFICATION .....	94
FIGURE 52 FITNESS FUNCTION TIME PROFILE AFTER CONVERSION TO MEX-FILE.....	94
FIGURE 53 ASTEROID DIAMETER VS CAD FOR OCC = 4 (1 TO 15 MONTHS) .....	95
FIGURE 54 ASTEROID DIAMETER VS CAD FOR OCC = 5 (1 TO 15 MONTHS) .....	95
FIGURE 55 ASTEROID DIAMETER VS CAD FOR OCC = 4 (1 TO 42 DAYS).....	96
FIGURE 56 ASTEROID DIAMETER VS CAD FOR OCC = 5 (1 TO 42 DAYS).....	96
FIGURE 57 DETECTION PROBABILITY FOR OCC=5, D=4 M AND CAD FROM 12 TO 36 MONTHS.....	97
FIGURE 58 DETECTION PROBABILITY FOR OCC=5, D=8 M AND CAD FROM 12 TO 36 MONTHS.....	97
FIGURE 59 DETECTION PROBABILITY FOR OCC=5, D=12 M AND CAD FROM 12 TO 36 MONTHS.....	97
FIGURE 60 TRAJECTORY FOR OCC=5, D=4 M AND CAD=12 MONTHS .....	98
FIGURE 61 TRAJECTORY FOR OCC=5, D=8 M AND CAD=12 MONTHS .....	99
FIGURE 62 TRAJECTORY FOR OCC=5, D=12 M AND CAD=12 MONTHS .....	100
FIGURE 63 TRAJECTORY FOR OCC=5, D=4 M AND CAD=18 MONTHS .....	101
FIGURE 64 TRAJECTORY FOR OCC=5, D=8 M AND CAD=18 MONTHS .....	102
FIGURE 65 TRAJECTORY FOR OCC=5, D=12 M AND CAD=18 MONTHS .....	103
FIGURE 66 TRAJECTORY FOR OCC=5, D=4 M AND CAD=24 MONTHS .....	104
FIGURE 67 TRAJECTORY FOR OCC=5, D=8 M AND CAD=24 MONTHS .....	105
FIGURE 68 TRAJECTORY FOR OCC=5, D=12 M AND CAD=24 MONTHS .....	106
FIGURE 69 TRAJECTORY FOR OCC=5, D=4 M AND CAD=30 MONTHS .....	107
FIGURE 70 TRAJECTORY FOR OCC=5, D=8 M AND CAD=30 MONTHS .....	108
FIGURE 71 TRAJECTORY FOR OCC=5, D=12 M AND CAD=30 MONTHS .....	109
FIGURE 72 TRAJECTORY FOR OCC=5, D=4 M AND CAD=36 MONTHS .....	110
FIGURE 73 TRAJECTORY FOR OCC=5, D=8 M AND CAD=36 MONTHS .....	111
FIGURE 74 TRAJECTORY FOR OCC=5, D=12 M AND CAD=36 MONTHS .....	112

# List of tables

---

TABLE 1 DIDYMOS CHARACTERISTICS .....	21
TABLE 2 AIM PROPULSION DATA .....	21
TABLE 3 OCC AND RUNOFF VALUES .....	37
TABLE 4 PARAMETERS FOR ASTEROIDS WITH OCC=1 .....	38
TABLE 5 REGRESSION PARAMETERS SUMMARY .....	40
TABLE 6 SIMULATION 1 PARAMETERS (STUDY 1) .....	55
TABLE 7 SIMULATION 2 PARAMETERS (STUDY 1) .....	56
TABLE 8 SIMULATION 1 PARAMETERS (STUDY 2) .....	57
TABLE 9 SIMULATION 2 PARAMETERS (STUDY 2) .....	58
TABLE 10 SIMULATIONS PARAMETERS STUDY 3 .....	60
TABLE 11 SIMULATION PARAMETERS STUDY 4A .....	63
TABLE 12 ASTEROID DIAMETER FOR P=99.5% (FROM 1 TO 8 MONTHS) .....	66
TABLE 13 ASTEROID DIAMETER FOR P=99.5% (FROM 9 TO 15 MONTHS) .....	66
TABLE 14 NUMBER OF DIFFERENT MEMBERS INTO THE FINAL POPULATION THAT HAVE REACHED THE MAXIMUM SCORE .....	71
TABLE 15 NUMBER OF DIFFERENT MEMBERS INTO THE FINAL POPULATION THAT HAVE REACHED THE MAXIMUM SCORE AND REPRESENTS MORE THAN 10% OF THE TOTAL POPULATION.....	72
TABLE 16 SIMULATION PARAMETERS STUDY 6.....	79
TABLE 17 BUDGET SUMMARY .....	88

# 1. Introduction

---

## 1.1 *Justification*

Near-Earth Objects (NEOs) are comets and asteroids that have been nudged by the gravitational attraction of nearby planets into orbits that allow them to enter the Earth's neighbourhood. Composed mostly of water ice with embedded dust particles, comets originally formed in the cold outer planetary system while most of the rocky asteroids formed in the warmer inner solar system between the orbits of Mars and Jupiter. The scientific interest in comets and asteroids is due largely to their status as the relatively unchanged remnant debris from the Solar System formation process some 4.6 billion years ago. The giant outer planets (Jupiter, Saturn, Uranus, and Neptune) formed from an agglomeration of billions of comets and the left over bits and pieces from this formation process are the comets we see today. (Hanslmeier, 2007) Likewise, today's asteroids are the bits and pieces left over from the initial agglomeration of the inner planets, i.e., Mercury, Venus, Earth, and Mars (Sanchez, 2009).

It also exist the theory of the "Oort cloud". This theory states that there is a cloud of one to one hundred billion objects composed by ice, methane and ammonia that were originated close to the Sun during the Solar System formation. This objects are placed almost 1 light year to the Sun due to the gravitational effect of the giant planets and, according this theory, are considered the source of all comets with large period. (Morbidelli, 2005)

As the primitive, leftover building blocks of the Solar System formation process, comets and asteroids offer clues to the chemical mixture from which the planets formed some 4.6 billion years ago. If we wish to know the composition of the primordial mixture from which the planets formed, then we must determine the chemical constituents of the leftover debris from this formation process - the comets and asteroids. (Hanslmeier, 2007)

Apart from the scientific reason, it is important to keep in mind that an asteroid impact is a real hazard. It is easy to remember the February 2013 asteroid impact in Chelyabinsk, Russia.



Figure 1 Asteroid seen in Russia (February 2013)

Some scientists and companies around the world are studying the feasibility of the different strategies to change the trajectory of potential hazardous asteroids. However these expensive technologies should be tested first, and the small asteroids that orbit near the Earth can be used as guinea pigs in this field (Sanchez, 2009).



Figure 2 Asteroid impact in a lake (Russia).

The comets and asteroids that are potentially the most hazardous because they can closely approach the Earth are also the objects that could be most easily exploited for their raw materials. It is not presently cost effective to mine these minerals and then bring them back to Earth. However, these raw materials could be used in developing the space structures and in generating the rocket fuel that will be required to explore and colonize the Solar System in the twenty-first century (SpaceGuardCentre, 2014).

Whereas asteroids are rich in the mineral raw materials required to build structures in space, comets are rich-sources of the water and carbon-based molecules necessary to sustain life. In addition, an abundant supply of cometary water ice could provide copious quantities of liquid hydrogen and oxygen, the two primary ingredients in rocket fuel. It seems likely that in the next century when we begin to colonize the inner Solar System, the metals and minerals found on asteroids will provide the raw materials for space structures, and comets will become the watering holes and gas stations for interplanetary spacecraft (Lewis, 1996).

## 1.2 *Scope of the project*

The scope of the project is structured in the following sections:

- Study and present the relative orbit equations.
- Create models that allow to:
  - Obtain the semi-major axis uncertainty from the OCC.
  - Calculate the uncertainties on the inclination and eccentricity of the orbit given the uncertainty in the semi-major axis.
  - Asses the detection probability depending on the relative position of the spacecraft and the asteroid.
- Asses the importance of:
  - Asteroid diameter.
  - Close approach duration.
  - Asteroid OCC.
- Present the optimal trajectories in order to maximize the probability of detect the asteroid.

Out of scope studies:

- Define the transfer trajectory from the Earth to the Asteroid.
- Define the asteroid rendezvous phase.

## 2. State of the art

This section shows the current state of the art of missions to small asteroids and their scientific value.

### 2.1 NEOs discovery

The first section of this chapter covers the importance of discovering the asteroids and comets orbiting near the Earth. In 1998, NASA established a goal to discover 90% of the NEOs larger than one kilometre in diameter, and in 2005, the Congress extended that goal to include 90% of the NEOs larger than 140 meters. There are thought to be about 1000 NEAs larger than one kilometre and roughly 15,000 larger than 140 meters (Johnson, 2010).

In this chapter, we illustrate the main facilities used by NASA. The major part of the information collected in these facilities is sent to the Minor Planet Center (MPC, Cambridge, MA), which directly collaborates with ESA. Fig. 3 shows the importance of each facility.

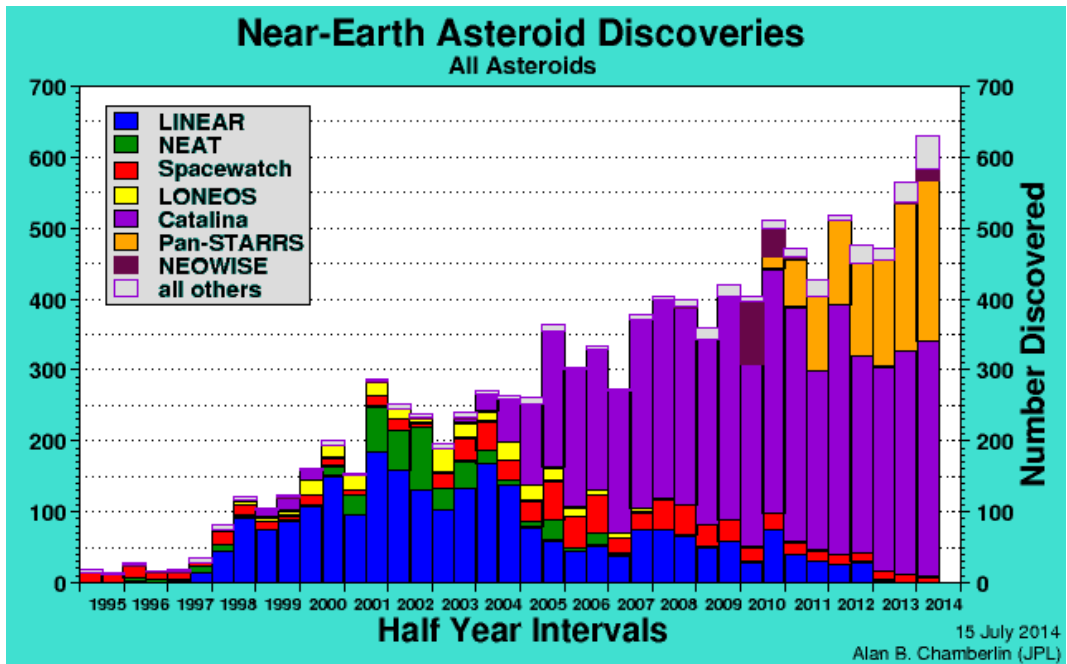


Figure 3 NEO Discoveries per facility

### 2.1.1 Catalina Sky Survey

The Catalina Sky Survey (CSS), Mt. Lemmon Survey and Siding Spring Survey (SSS) working together under the name of the FIRST Survey, are carrying out sustained, highly productive searches for NEOs, contributing to the congressional mandates of obtaining an inventory of more than 90% of the previously mentioned NASA goal. Furthermore, these surveys are operated in such a manner that same night follow-up on newly discovered objects can usually be done, making possible the rapid determination of orbits and the specific hazard posed by the newly found objects.

### 2.1.2 Pan-STARRS

Pan-STARRS stands for Panoramic Survey Telescope and Rapid Response System, located in Honolulu, Hawaii.

Like the CCS project, the major goal of Pan-STARRS is to discover and characterize Earth-approaching objects of either type, which might represent a danger for our planet.



Figure 4 Pan -STARRS Facility

The combination of relatively small mirrors with very large digital cameras results in a relatively cheap observing system that can scan the entire available sky several times each month (Institute for Astronomy (Ed.), 2014) .

Figure 5 shows one of the telescopes.



Figure 5 PS2 Telescope

### 2.1.3 LINEAR

Lincoln Near Earth Asteroid Research (LINEAR) is an MIT Lincoln Laboratory program funded by the United States Air Force and NASA. The goal of LINEAR is to demonstrate the application of technology originally developed for the surveillance of Earth orbiting satellites, to the problem of detecting and cataloguing near-Earth asteroids that threaten the Earth.

The project is placed at the White Sands Missile Range in Socorro, New Mexico, and the data collected by the telescopes is processed on-site to generate observations. These are checked in the main Lincoln Laboratory facility and at Hanscom AFB and then are sent to the MPC. The MPC assigns designations to LINEAR's new discoveries of NEOs, comets, unusual objects, and main belt asteroids.

As was shown in Figure 3, the LINEAR was the most important facility in the early 2000s but now the importance of LINEAR in asteroid detection has decreased drastically (LincolnLaboratory(Ed.), 2014).

### 2.1.4 Spacewatch

The Spacewatch project was founded in 1984 under the leadership of Tom Gehrels (Astronomer and Planetary Science teacher in the University of Arizona). The project started with a 0.9-meter telescope, which was the first to scan automatically the sky in search for NEOs.

As can be seen in Figure 3, Spacewatch has been collecting data since its foundation and, being the oldest project in this category, it has several records: it was the first to

discover NEOs with CCDs, the first to discover comets with a CCD, the first to discover a NEO with automated image processing software.

In Figure 6 it is shown the current facility in Tucson, Arizona, with the 1.8-meter telescope that was incorporated in 2001.



Figure 6 Spacewatch facility in Tucson, Arizona

### 2.1.5 NOEWISE

The NEOWISE project is the most recent and, unlike the other projects, it is the only space-based facility. Its name comes from Wide-field Infrared Survey Explorer (WISE) mission. Funded by the NASA's Planetary Science Division, NEOWISE harvests measurements of asteroids and comets from the WISE images and provides a rich archive for searching WISE data for Solar System objects.

WISE was launched in December 2009, and surveyed the full sky in four infrared wavelength bands (centered at 3.4, 4.6, 12 and 22  $\mu\text{m}$ ) until depletion of the liquid hydrogen ( NASA (Ed.), 2014) used to cool the telescope (September 2010). The survey continued as NEOWISE for an additional four months using the two shortest wavelength detectors. The spacecraft was placed into hibernation in February 2011, after completing its search through the inner Solar System.



Figure 7 NEOWISE spacecraft

NEOWISE operations were resumed in December 2013. Just six days after the new start, NEOWISE discovered its first potentially hazardous near-Earth asteroid, 2013 YP139.

The idea is that NEOWISE can help learn more about the population of near-Earth objects and comets that could pose an impact hazard to the Earth. This spacecraft is equally sensitive to both light-coloured asteroids and optically dark objects that are difficult to be discovered and characterized by ground-based observers. The shape and components of WISE can be seen in Figure 8:

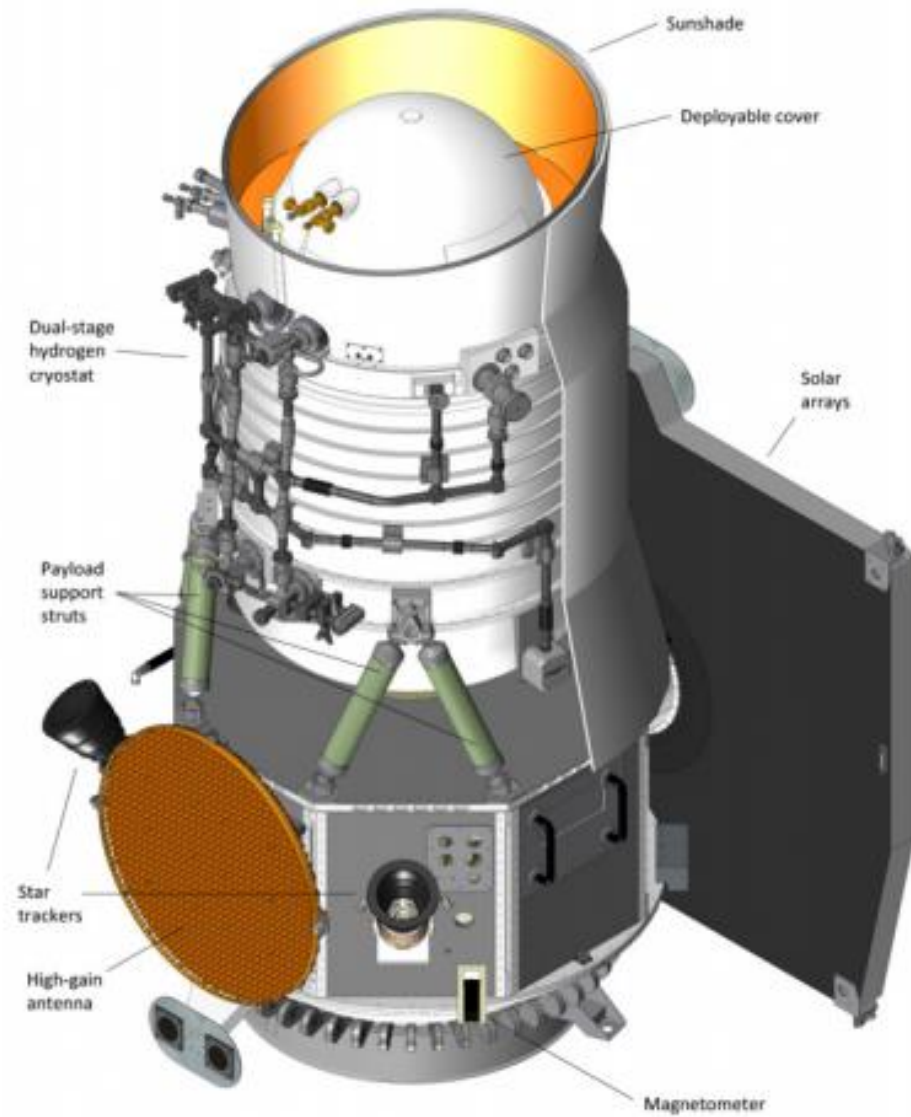


Figure 8 NEOWISE Spacecraft detailed view

As of mid-August 2014, NEOWISE has carried out more than one-third of its second survey of the sky. Over 111,000 infrared measurements have been taken of over 7200 Solar System objects, including 157 NEOs and 38 comets (Mainzer, et al., 2011).

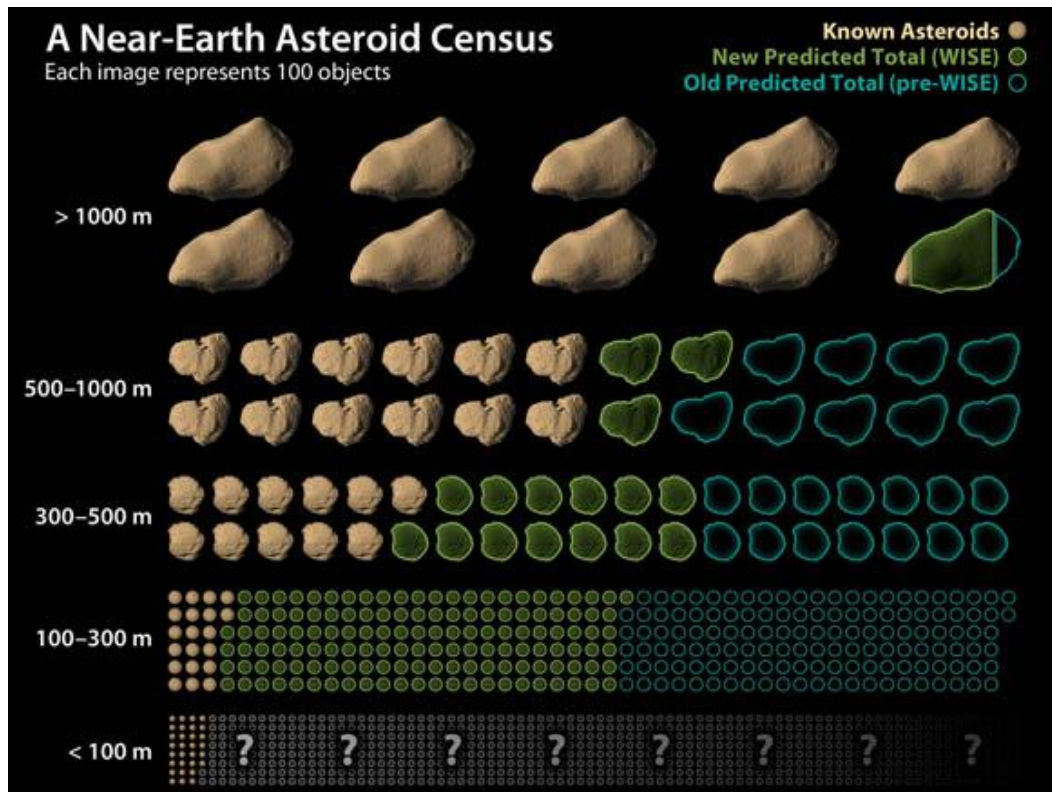


Figure 9 NEA census prediction by NEOWISE

## 2.2 Asteroid deviation

An asteroid impact is a real threat, and the space agencies need to establish a plan to fight against this hazard.

As was introduced at the beginning of the chapter, there are a lot of asteroids that every year hit the Earth. Most of them are not large enough to cause serious damages, some fall in non-populated areas, but some could hit the Earth provoking enormous disasters (as for example the collision mentioned before, that occurred in Russia) or devastate the Earth by causing temporary winters due to the dust accumulated in the stratosphere.

Both ESA and NASA are developing programmes to assess some possible strategies to deflect the asteroid trajectory. Two such initiatives are described here below.

### 2.2.1 NEOShield

The NeoShield programme was created by the European Union to protect the Earth against impacts by NEOs. NeoShield will include the participation of institutions and companies from across Europe, the United States and Russia (NeoShield (Ed.), 2014).

The main purpose of this programme is to assess and develop technologies to deflect the asteroids trajectories. In particular the goal of the organization is to launch a mission to demonstrate that current technologies allows to deviate an asteroid.

One of the most promising concepts for such a mission is the so-called “kinetic impactor”: a spacecraft slams into the NEO at very high speed, giving it a nudge and causing it to change its orbit so that it deviates from its original collisional course (Hernandez, W. Barbee, Bhaskaran, & Getzandanner, 2013).

Two other asteroid deviation concepts will be assessed. The first is based on the gravitational pull between an object in space and a spacecraft. This concept is known as a gravity tractor (Lu & Love, 2005) and consists in using the gravitational pull of a spacecraft in the vicinity of an object, such as an asteroid, over a long time to make the object change its orbit. The gravity tractor concept will be investigated by the Carl Sagan Institute in Palo Alto, California, which also carries out similar work for NASA. The other concept is deflection (and not destruction) by an explosion close to the asteroid’s surface. This ‘blast deflection’ concept will be investigated by TsNIIMash, a Russian institution also working for the Russian space agency Roscosmos (Airbus (Ed.), 2014) (Harris & Drube, 2010).

### 2.2.2 Asteroid Impact and Deflection Assessment (AIDA) Study

The AIDA study is another example of the cooperation between countries to develop a common project. In this case, the AIDA mission is a joint effort of ESA, JHU/APL, NASA, OCA and DLR.

The mission goal, as its name suggests, is to study the deflection of an asteroid by impacting on it. For this reason, two different spacecraft are used: impactor (DART), and a rendezvous probe (AIM). The target of the mission is the binary asteroid system Didymos.

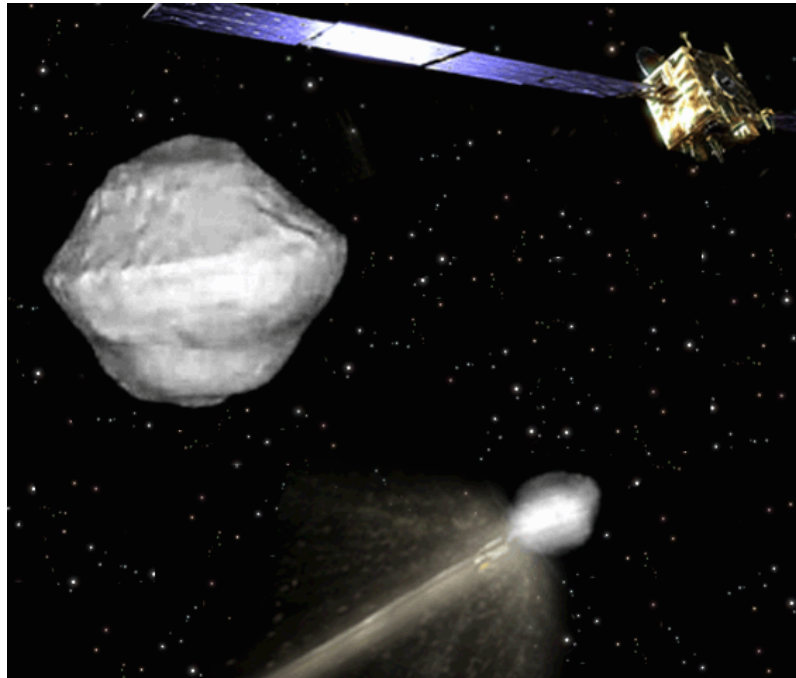


Figure 10 AIDA mission concept

The idea is that DART will impact the secondary of the Didymos binary system while AIM will observe and measure the impact effects on the asteroid orbit.

For this joint project, an equal timing of the experiment is set for both missions (additionally maximum proximity of the target to Earth allows ground-based characterisation of the experiment). Despite the joint procedure, the two spacecraft are still able to pursue their missions fully independently. Therefore if, for some reason, one of the spacecraft cannot contribute to the joint campaign, the other will be able to achieve the individual mission goals.

The AIDA rendezvous spacecraft (AIM) will be under the responsibility of ESA. This spacecraft will arrive before DART in order to characterise the binary asteroid and to observe the impact and the resulting ejecta and craters.

The target asteroid Didymos (1996 GT) is an Apollo asteroid discovered on 1996 by Spacewatch. It has a satellite orbiting it with a period of 11.9 hours, hence the appellation "Didymos", meaning "twin". Table 1 lists some parameters that will be included in the models developed in further sections.

Semi-major axis: 1.644 AU	Geometric albedo: 0.147
Orbital Period: 770.14 days	Diameter primary: 800 m
Eccentricity: 0.384	Diameter secondary: 150 m
Inclination: 3.4 deg	Separation: 1050 m

Table 1 Didymos characteristics

Table 2 summarizes the AIM propulsion data. It is possible to observe each mission phase (Launch, Earth swing-by and arrival) and the main parameters related to each phase.

<b>Launch</b>	<b>19/08/2019</b>
Escape velocity [km/s]	1.0
Declination [deg]	-14.46
Escape mass [kg]	400
<b>Earth swing-by</b>	<b>07/11/2020</b>
Infinite velocity at SB [km/s]	5.44
Vel. at pericentre [km/s]	10.8
Pericentre altitude [km]	2854
<b>Arrival</b>	<b>01/08/2022</b>
Final mass [kg]	324
SEP delta-v [km/s]	2.9
Xenon consumption [kg]:	73
Hydrazine consumption [kg]:	5
Thruster on time [d]:	213
Total Impulse[10 <sup>6</sup> kg m/s]:	1.05

Table 2 AIM Propulsion Data

### 2.3 Asteroid sampling

Missions to asteroids are becoming popular. At present time, Rosetta's lander Philae is close to land on comet 67P/Churyumov-Gerasimenko (ESA (Ed.), 2014). One of the goals of this mission is to drill the comet and collect some sample in order to determine the comet's composition. This is very interesting from a scientific point of view because, as was introduced before, the comets and asteroids contain a lot of information about the formation of our Solar System.

For the near future the challenge is to capture an entire asteroid. As can be imagined, the dimensions of a target asteroid in this case will be quite smaller compared to the targets of other missions to asteroids.

The idea of a spacecraft capturing an asteroid could seem close to science fiction but NASA's FY2014 budget proposal includes a plan to robotically capture a small near-Earth asteroid and redirect it safely to a stable orbit in the Earth-Moon system where the astronauts can visit and explore it.

The NASA Extreme Environment Mission Operations (NEEMO) 15 and 16 missions in 2011 and 2012, respectively, simulated several challenges that the explorers will face when visiting an asteroid, including how to anchor to and move around the surface of a near-Earth object and how to collect samples of it. The mission will consist in sending a spacecraft that will collect a small NEO. The spacecraft would use a kind of bag to safely transport the asteroid and move it to the desired orbit.



Figure 11 Spacecraft capturing the target asteroid

Once the asteroid is placed in the desired orbit (accessible, around the Moon, etc.), a second spacecraft carrying the astronauts will dock with it and the astronauts will be able to perform all sort of experiments on the asteroid, sampling the best zones and sending back the samples to the terrestrial laboratories.

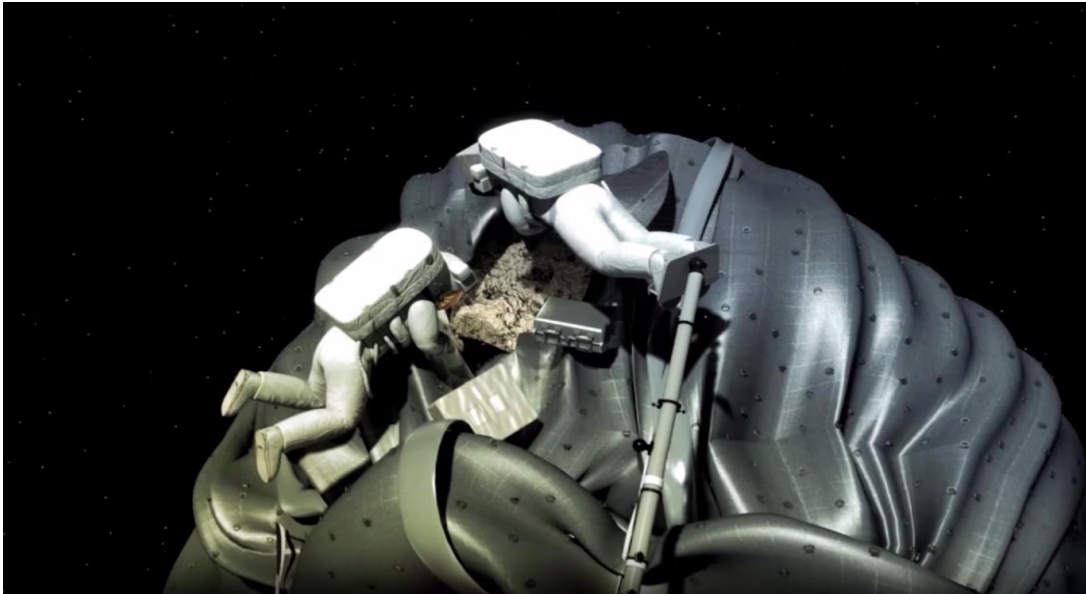


Figure 12 Astronauts studying the captured asteroid

Apart from the technology required to perform this kind of mission, the target asteroid is key and this project will deal with how to select and reach it properly (NASA, 2014).

## 3. Models

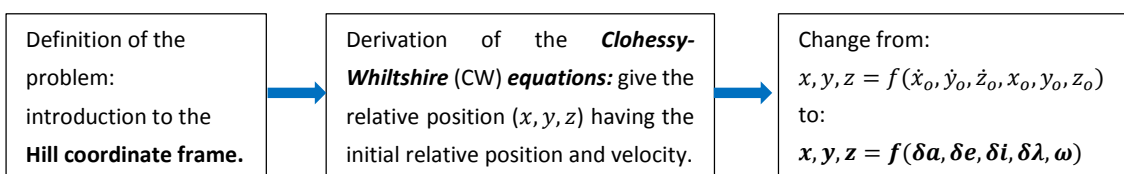
The aim of this section is to present the models that have been developed along the study. In general, each model is implemented as an independent Matlab function and the simulations presented in section 4 make use of the models (call the Matlab function) when required. Four models are presented:

- *Relative Orbit Description*: set of equations that describes the relative orbit between two bodies (the chief and the deputy satellites). The objective is to fix the chief satellite (placed where the asteroid is supposed to be) and to obtain the position of a second body (could be the spacecraft or the real asteroid considering the simulated orbital elements) using the difference on their orbital elements.
- *OCC and semi-major axis uncertainty*: the concept of “orbit quality” is introduced and it is presented a model that calculates the semi-major axis uncertainty in the asteroid orbit based on the “Orbit Condition Code” (OCC) of such orbit.
- *Regression model for the uncertainties*: all small asteroid cases are studied in order to find out the relation between the uncertainty in the semi-major axis and the uncertainty in other two orbital elements as the eccentricity and the inclination. A linear regression is presented to relate the three parameters.
- *Asteroid detection model*: given the relative position of the asteroid, the spacecraft and the Sun, this model evaluates if the spacecraft is able to detect the asteroid based on the positions and the technology used in the on-board camera.

At the end of each model it will be summarized the inputs and outputs related to the Matlab function. In addition, in ANNEX I: Matlab Functions the summary of all functions used along the project is presented.

### 3.1 Relative Orbit Description

This section shows the derivation of the equations that are used in the study. The development is based on the relative motion equations presented in the book “Analytical Mechanics of Space Systems” by Hanspeter Schaub and John L. Junkins. The idea is to show the transformations required in order to have the relative position of two bodies (in  $x, y$  and  $z$  coordinates) given the orbital element differences  $\delta a, \delta e, \delta i, \delta \lambda$  and  $\omega$  that will be introduced along the section. The steps that will be performed in this subsection are:



### 3.1.1 Hill coordinate frame

The next figure illustrates the starting point of the development. Two satellites are considered. The satellite about which all other satellites are orbiting is referred to as the chief satellite. The remaining satellites, referred to as the deputy satellites, are to fly in formation with the chief. It is important to note that it is not necessary that the chief position actually be occupied by a physical satellite. In this study, the chief position will serve as a reference point about which the deputy satellites orbit.

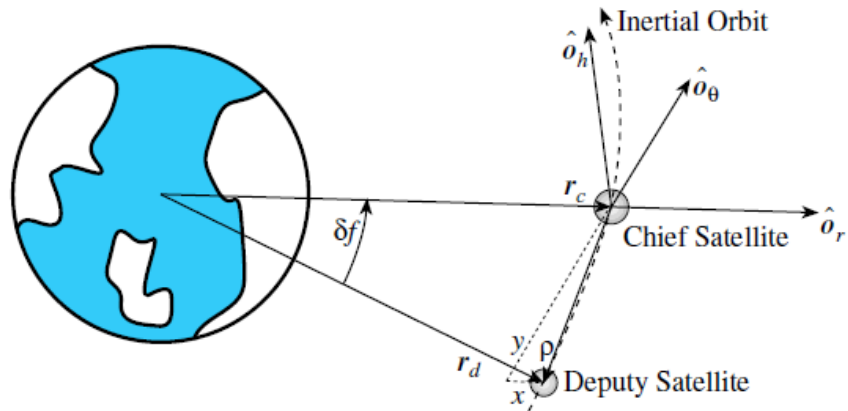


Figure 13 Hill reference frame definition

The inertial chief position is expressed through the vector  $\mathbf{r}_c(t)$  and the deputy position is given by  $\mathbf{r}_d(t)$ . In order to express the movement from the chief point of view, the Hill coordinate frame is introduced. Its origin is at the chief position and its orientation is given by the vector triad  $\{\hat{\mathbf{o}}_r, \hat{\mathbf{o}}_\theta, \hat{\mathbf{o}}_h\}$  as can be shown in Figure 13. The  $\hat{\mathbf{o}}_r$  vector is in the orbit radius direction.  $\hat{\mathbf{o}}_h$  is parallel to the orbit momentum vector in the orbit normal direction. Finally, the  $\hat{\mathbf{o}}_\theta$  vector completes the right-handed coordinates system. In other words:

$$\hat{\mathbf{o}}_r = \frac{\mathbf{r}_c}{r_c}, \quad \text{Eq. 1}$$

$$\hat{\mathbf{o}}_\theta = \hat{\mathbf{o}}_h \times \hat{\mathbf{o}}_r, \quad \text{Eq. 2}$$

$$\hat{\mathbf{o}}_h = \frac{\mathbf{h}}{h}, \quad \text{Eq. 3}$$

with  $\mathbf{h} = \mathbf{r}_c \times \dot{\mathbf{r}}_c$ . This rotating reference frame is referred to as the Hill frame.

Note that if the inertial chief orbit is circular, then  $\hat{\mathbf{o}}_\theta$  is parallel to the satellite velocity vector.

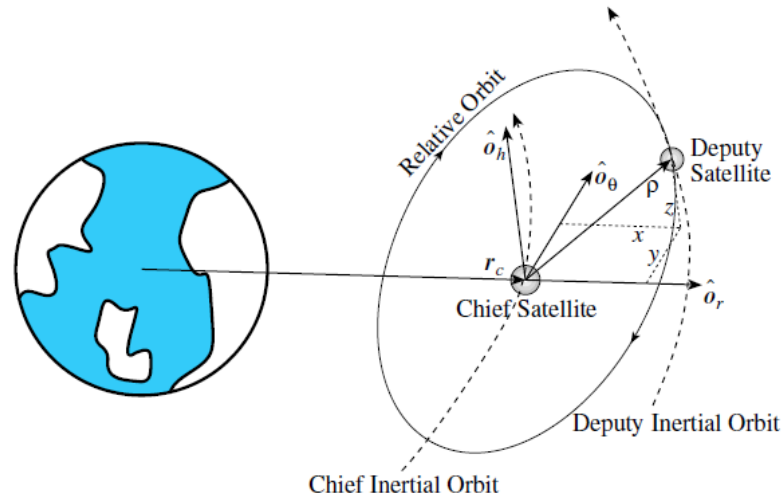


Figure 14 Relative orbit definition

As can be seen in Figure 14, the vector  $\boldsymbol{\rho}$  can be used to define the position of the deputy satellite in the Hill coordinate frame:

$$\boldsymbol{\rho} = (x, y, z)^T .$$

Eq. 4

The advantage of using the rotating chief Hill frame is that the physical relative orbit dimensions are immediately apparent from these coordinates. The  $(x, y)$  coordinates define the relative motion in the chief orbit plane while the  $z$  coordinate defines any motion out of the chief orbit plane.

### 3.1.2 Clohessy-Wiltshire Equations

As was introduced before the aim of this subsection is to obtain the relative movement equations that give the relative position in Hill frame coordinates  $(x, y, z)$ . To derive the relative equations of motion using Cartesian coordinates in the rotating Hill frame, we write the deputy satellite position vector as:

$$\mathbf{r}_d = \mathbf{r}_c + \boldsymbol{\rho} = (r_c + x) \hat{\mathbf{o}}_r + y \hat{\mathbf{o}}_\theta + z \hat{\mathbf{o}}_h ,$$

Eq. 5

where  $r_c$  is the current orbit radius of the chief satellite.

The angular velocity vector of the rotating Hill frame  $\mathcal{O}$  relative to the inertial  $\mathcal{N}$  frame is given by:

$$\omega_{\mathcal{O}/\mathcal{N}} = \dot{f} \hat{\omega}_h , \quad \text{Eq. 6}$$

$f$  being the chief frame true anomaly. Taking two derivatives with respect to the inertial frame provides the deputy satellite acceleration vector:

$$\begin{aligned} \ddot{\mathbf{r}}_d = & \left( \ddot{r}_c + \ddot{x} - 2\dot{y}\dot{f} - \ddot{f}y - \dot{f}^2(r_c + x) \right) \hat{\mathbf{o}}_r \\ & + \left( \ddot{y} + 2\dot{f}(\dot{r}_c + \dot{x}) + \ddot{f}(r_c + x) - \dot{f}^2y \right) \hat{\mathbf{o}}_\theta + \ddot{z} \hat{\mathbf{o}}_h . \end{aligned} \quad \text{Eq. 7}$$

This kinematic expression can be simplified by making use of the following identities. The chief orbit angular momentum magnitude is given by  $h = r_c^2 \dot{f}$ . Since  $h$  is constant for Keplerian motion, taking the first time derivative of  $h$  yields

$$\dot{h} = 0 = 2 r_c \dot{r}_c \dot{f} + r_c^2 \ddot{f} . \quad \text{Eq. 8}$$

This constrain can be used to solve for the true anomaly acceleration:

$$\ddot{f} = -2 \frac{\dot{r}_c}{r_c} \dot{f} . \quad \text{Eq. 9}$$

Furthermore, we write the chief satellite position as  $\mathbf{r}_c = r_c \hat{\mathbf{o}}_r$ . Taking two time derivatives with respect to the inertial frame and using the orbit equations of motion gives the following expression for the chief acceleration vector:

$$\ddot{\mathbf{r}}_c = (\ddot{r}_c - r_c \dot{f}^2) \hat{\mathbf{o}}_r = - \frac{\mu}{r_c^3} \mathbf{r}_c = - \frac{\mu}{r_c^2} \hat{\mathbf{o}}_r . \quad \text{Eq. 10}$$

Equating vector components in the previous equation allows to obtain the chief orbit radius acceleration is expressed as

$$\ddot{r}_c = r_c \dot{f}^2 - \frac{\mu}{r_c^2} = r_c \dot{f}^2 \left( 1 - \frac{r_c}{p} \right) , \quad \text{Eq. 11}$$

being  $p$  the semi-latus rectum, that can be expressed as  $p = \frac{h^2}{\mu}$ . Substituting Eq. 11 and Eq. 9 into Eq. 7, the deputy acceleration vector expression is reduced to

$$\begin{aligned} \ddot{\mathbf{r}}_d = & \left( \ddot{x} - 2\dot{f} \left( \dot{y} - y \frac{\dot{r}_c}{r_c} \right) - x f^2 - \frac{\mu}{r_c^2} \right) \hat{\mathbf{o}}_r \\ & + \left( \ddot{y} + 2\dot{f} \left( \dot{x} - x \frac{\dot{r}_c}{r_c} \right) - f^2 y \right) \hat{\mathbf{o}}_\theta + \ddot{z} \hat{\mathbf{o}}_n . \end{aligned} \quad \text{Eq. 12}$$

Next, we substitute the kinematic acceleration expression in Eq. 12 into the orbit equations of motion. The deputy satellite orbital equations of motion are given by

$$\ddot{\mathbf{r}}_d = -\frac{\mu}{r_d^3} \mathbf{r}_d = -\frac{\mu}{r_d^3} \begin{pmatrix} r_c + x \\ y \\ z \end{pmatrix} , \quad \text{Eq. 13}$$

with the index  $O$  specifying the Hill rotating frame and  $r_d = \sqrt{(r_c + x)^2 + y^2 + z^2}$ . Equating Eq. 12 and Eq. 13 yields relative equations of motion:

$$\ddot{x} - 2\dot{f} \left( \dot{y} - y \frac{\dot{r}_c}{r_c} \right) - x f^2 - \frac{\mu}{r_c^2} = -\frac{\mu}{r_d^3} (r_c + x) , \quad \text{Eq. 14}$$

$$\ddot{y} + 2\dot{f} \left( \dot{x} - x \frac{\dot{r}_c}{r_c} \right) - f^2 y = -\frac{\mu}{r_d^3} y , \quad \text{Eq. 15}$$

$$\ddot{z} = -\frac{\mu}{r_d^3} z . \quad \text{Eq. 16}$$

The only assumption which has been made is that no disturbances are acting on the satellites and thus the Keplerian motion assumption in the orbital equation of motion in Eq. 13 are correct. The relative equations of motion are valid for arbitrarily large relative orbits and also when the chief orbit is be eccentric. If the relative orbit coordinates  $(x, y, z)$  are small compared to the chief radius  $r_c$ , then the equations can be simplified as follows. The deputy orbit radius  $r_d$  is approximated as

$$r_d = r_c \sqrt{1 + 2 \frac{x}{r_c} + \frac{x^2 + y^2 + z^2}{r_c^2}} \approx r_c \sqrt{1 + 2 \frac{x}{r_c}} , \quad \text{Eq. 17}$$

where second order terms have been neglected. This allows us to write

$$\frac{\mu}{r_d^3} \approx \frac{\mu}{r_c^3} \left( 1 - 3 \frac{x}{r_c} \right) . \quad \text{Eq. 18}$$

The term  $\frac{\mu}{r_c^3}$  can also be written in the following useful forms:

$$\frac{\mu}{r_c^3} = \frac{r_c}{p} f^2 = \frac{f^2}{1 + e \cos f} . \quad \text{Eq. 19}$$

Note that the orbit parameters shown in Eq. 19 are chief orbit elements. Neglecting second order terms, we are able to simplify the right hand side of Eq. 13:

$$-\frac{\mu}{r_d^3} \begin{pmatrix} r_c + x \\ y \\ z \end{pmatrix} \approx -\frac{\mu}{r_c^3} \left(1 - 3\frac{x}{r_c}\right) \begin{pmatrix} r_c + x \\ y \\ z \end{pmatrix} \approx -\frac{\mu}{r_c^3} \begin{pmatrix} r_c - 2x \\ y \\ z \end{pmatrix} . \quad \text{Eq. 20}$$

Substituting Eq. 20 in Eq. 14, Eq. 15 and Eq. 16 and simplifying the resulting expressions yields the relative orbit equations of motion:

$$\ddot{x} - x f^2 \left(1 + 2\frac{r_c}{p}\right) - 2f \left(\dot{y} - y \frac{\dot{r}_c}{r_c}\right) = 0 , \quad \text{Eq. 21}$$

$$\ddot{y} + 2f \left(\dot{x} - x \frac{\dot{r}_c}{r_c}\right) - y f^2 \left(1 - \frac{r_c}{p}\right) = 0 , \quad \text{Eq. 22}$$

$$\ddot{z} + \frac{r_c}{p} f^2 z = 0 . \quad \text{Eq. 23}$$

Using Eq. 9 and Eq. 19, along with the true latitude  $\theta = \omega + f$ , the general relative equations of motion (Melton, 2000):

$$\ddot{x} - x \left(\dot{\theta}^2 + 2\frac{\mu}{r_c^3}\right) - y \ddot{\theta} - 2\dot{y} \dot{\theta} = 0 , \quad \text{Eq. 24}$$

$$\ddot{y} + x \ddot{\theta} + 2\dot{x} \dot{\theta} - y \left(\dot{\theta}^2 - \frac{\mu}{r_c^3}\right) = 0 , \quad \text{Eq. 25}$$

$$\ddot{z} + \frac{\mu}{r_c^3} z = 0 . \quad \text{Eq. 26}$$

If the chief satellite orbit is circular, then  $e = 0$ ,  $p = r_c$ , and the chief orbit radius  $r_c$  is constant. Since for a circular orbit the mean orbital rate  $n$  is equal to the true anomaly rate  $\dot{f}$ , the relative equations of motion reduce to the simple known as the **Clohessy-Whitshire** (CW) **equations** (Wiltshire, Sept 1960).

$$\ddot{x} - 2n\dot{y} - 3n^2x = 0 , \quad \text{Eq. 27}$$

$$\ddot{y} + 2n\dot{x} = 0 , \quad \text{Eq. 28}$$

$$\ddot{z} + n^2z = 0 . \quad \text{Eq. 29}$$

### 3.1.3 Orbit Element Difference Description

The Hill reference coordinates system  $(x, y, z)$  is a common method to describe a relative orbit but it has the disadvantage that the differential equations of motion must be solved in order to obtain the relative orbit geometry. To do so, initial conditions are required:

$$\mathbf{X} = (x_0, y_0, z_0, \dot{x}_0, \dot{y}_0, \dot{z}_0) . \quad \text{Eq. 30}$$

At this point an alternative is proposed. An orbit can be defined by its orbital elements:

$$\mathbf{e} = (a, e, i, \Omega, \omega, M_0) , \quad \text{Eq. 31}$$

where  $a$  is the semi-major axis,  $e$  is the eccentricity,  $i$  is the orbit inclination,  $\Omega$  is the longitude of the ascending Node,  $\omega$  is the argument of the pericenter and  $M_0$  is the initial mean anomaly.

Using the orbit elements simplifies the orbit description and the satellite position computation. Instead of solving a differential equation to find the current satellite states, the algebraic Kepler's equation must be numerically solved to find the current mean anomaly angle. With the CW equations both velocity and position were fast variables while with the orbit element difference the only quantity that varies is the mean anomaly.

Then, the relative orbit will be defined in terms of the orbit element difference vector  $\delta\mathbf{e}$ :

$$\delta\mathbf{e} = \mathbf{e}_d - \mathbf{e}_c = (\delta a, \delta e, \delta i, \delta \Omega, \delta \omega, \delta M_0) , \quad \text{Eq. 32}$$

where  $\mathbf{e}_d$  is the deputy satellite orbit element vector and  $\mathbf{e}_c$  is the chief orbit element vector. To avoid some numerical difficulties for near circular orbits, the vector  $\mathbf{e}$  is defined through:

$$\mathbf{e} = (a, \theta, i, q_1, q_2, \Omega) .$$

Eq. 33

At this point  $M_0$  will not be used anymore. Instead of  $M_0$ ,  $\theta$  will be used, which is defined as the true latitude angle (sum of argument of perigee and true anomaly),  $q_1$  and  $q_2$  being defined through:

$$q_1 = e \cos \omega ,$$

Eq. 34

$$q_2 = e \sin \omega .$$

Eq. 35

Now it is required to obtain the equations that give the position of the deputy satellite with respect to the chief satellite in the Hill reference frame. In order to do so, we define the following three coordinate systems: Let  $\mathcal{C}$  and  $\mathcal{D}$  be the Hill coordinate frames of the chief and deputy satellites, respectively, and let  $\mathcal{N}$  be the inertial frame. Then  $[\mathcal{CN}] = [\mathcal{CN}(\Omega_e, i_e, \theta_e)]$  is the direction cosine matrix mapping vector components in the inertial frame to components in the chief Hill frame. To relate the orbit element difference vector  $\delta \mathbf{e}$  to the corresponding LVLH (Local-Vertical-Local-Horizon) Cartesian coordinate vector  $\mathbf{X}$ , we write the deputy spacecraft inertial position vector  $\mathbf{r}_d$  in chief and deputy Hill frame component as:

$${}^c r_d = {}^c (r_c + x, y, z) ,$$

Eq. 36

$${}^d r_d = {}^d (r_d, 0, 0) .$$

Eq. 37

The deputy position vector  $r_d$  is now mapped from the deputy Hill frame to the chief Hill frame using

$${}^c r_d = [\mathcal{CN}][\mathcal{ND}] {}^d r_d .$$

Eq. 38

To simplify the notation from here on, the subscript c is dropped and any parameter without subscript is implicitly meant to be a chief orbit parameter. Taking the first variation  $[\mathcal{ND}]$  and  $r_d$  about the chief satellite motion leads to the first-order approximation:

$$[\mathcal{ND}] \approx [\mathcal{NC}] + [\delta \mathcal{NC}] ,$$

Eq. 39

$$r_d \approx r + \delta r .$$

Eq. 40

With the previous equation it is possible to write:

$${}^c r_d = ([I_{3 \times 3}] + [CN][\delta NC]) \begin{pmatrix} r + \delta r \\ 0 \\ 0 \end{pmatrix}. \quad \text{Eq. 41}$$

Dropping second-order terms, the deputy position vector is written as

$${}^c r_d = \begin{pmatrix} r + \delta r \\ 0 \\ 0 \end{pmatrix} + r [CN] \begin{pmatrix} \delta NC_{11} \\ \delta NC_{21} \\ \delta NC_{31} \end{pmatrix}, \quad \text{Eq. 42}$$

with the matrix components  $\delta NC_{i1}$  given by

$$\delta NC_{11} = NC_{12} \delta \theta - NC_{21} \delta \Omega + NC_{31} \sin \Omega \delta i, \quad \text{Eq. 43}$$

$$\delta NC_{21} = NC_{22} \delta \theta + NC_{11} \delta \Omega - NC_{31} \cos \Omega \delta i, \quad \text{Eq. 44}$$

$$\delta NC_{31} = NC_{32} \delta \theta + \sin \theta \cos i \delta i. \quad \text{Eq. 45}$$

Substituting Eq. 43, Eq. 44 and Eq. 45 into Eq. 42, the deputy position vector is written in terms of orbit element differences as

$${}^c r_d = \begin{pmatrix} r + \delta r \\ 0 \\ 0 \end{pmatrix} + r \begin{pmatrix} 0 \\ \delta \theta + \delta \Omega \cos i \\ -\cos \theta \sin i \delta \Omega + \sin \theta \delta i \end{pmatrix}. \quad \text{Eq. 46}$$

To be able to write this equation in terms of the desired orbit elements and their differences, the orbit radius  $r$  must be expressed in terms of the elements given in Eq. 33:

$$\delta r = \frac{r}{a} \delta a + \frac{V_r}{V_t} r \delta \theta - \frac{r}{p} (2aq_1 + r \cos \theta) \delta q_1 - \frac{r}{p} (2aq_2 + r \sin \theta) \delta q_2 \quad \text{Eq. 47}$$

where the chief radial and transverse velocity components  $V_r$  and  $V_t$  are defined as

$$V_r = \dot{r} = \frac{h}{p} (q_1 \sin \theta - q_2 \cos \theta), \quad \text{Eq. 48}$$

$$V_t = r \dot{\theta} = \frac{h}{p} (1 + q_1 \cos \theta + q_2 \sin \theta), \quad \text{Eq. 49}$$

with  $h$  being the magnitude of the chief orbit angular momentum.

By comparing the chief Hill frame components of the deputy position vector descriptions, we can express the local Cartesian hill frame coordinates  $x$ ,  $y$  and  $z$  in terms of the orbit element differences as (reference page 502):

$$x = \delta r , \quad \text{Eq. 50}$$

$$y = r(\delta\theta + \delta\Omega \cos i) , \quad \text{Eq. 51}$$

$$z = r(\sin\theta \delta i - \cos\theta \sin i \delta\Omega) . \quad \text{Eq. 52}$$

When describing a relative orbit through the orbit element differences, it is not convenient to describe the anomaly difference through  $\delta\theta$  or  $\delta f$ . For elliptic chief orbits, the difference between two orbits will vary with throughout the orbit. To avoid this inconvenience, the desired anomaly difference between two orbits is typically expressed in terms of a mean anomaly difference  $\delta M$ . This anomaly difference will remain constant, assuming unperturbed Keplerian motion, even if the chief orbit is elliptic. Differences in true anomaly are written in terms of differences in mean anomaly and differences in eccentricity as:

$$\delta f = \frac{(1 + e \cos f)^2}{\eta^3} \delta M + \frac{\sin f}{\eta^2} (2 + e \cos f) \delta e . \quad \text{Eq. 53}$$

In a first approach, it is studied the case where the eccentricity  $e$  is a small quantity but greater than  $\rho/r$ , while powers of  $e$  are smaller than  $\rho/r$ . In this case the terms which are linear in  $e$  are retained and the higher-order terms are dropped. The orbit radius is now approximated as:

$$r = \frac{a\eta^2}{1 + e \cos f} \approx a(1 - e \cos f) , \quad \text{Eq. 54}$$

while  $\eta^2 \approx 1$ . If we use Eq. 53, together with Eq. 54 and we differentiate to have  $\delta r$ , we obtain the linearized dimensional relative motion for the small eccentricity case:

$$x(f) \approx (1 - e \cos f) \delta a + \frac{a e \sin f}{\eta} \delta M - a \cos f \delta e , \quad \text{Eq. 55}$$

$$y(f) \approx \frac{a}{\eta} (1 + e \cos f) \delta M + a(1 - e \cos f) \delta\omega + a \sin f (2 - e \cos f) \delta e + a(1 - e \cos f) \cos i \delta\Omega , \quad \text{Eq. 56}$$

$$z(f) \approx a(1 - e \cos f) (\sin\theta \delta i - \cos\theta \sin i \delta\Omega) . \quad \text{Eq. 57}$$

In this study, the chief satellite has a circular orbit with no inclination,  $e = i = 0$  which simplifies the equations as follows:

$$x(f) \approx \delta a - a \cos f \delta e , \quad \text{Eq. 58}$$

$$y(f) \approx a\delta M_{end} + a\delta\omega + 2a\sin f\delta e + a\delta\Omega, \quad \text{Eq. 59}$$

$$z(f) \approx a\sin\omega\delta i. \quad \text{Eq. 60}$$

Since the chief is in a circular motion the start of the Early encounter phase can be defined as the periapsis passage of the chief orbit, by convention:  $f = 0$ :

$$x(t_o) \approx \delta a - a\delta e, \quad \text{Eq. 61}$$

$$y(t_o) \approx a(\delta M_{end} + \delta\omega + \delta\Omega), \quad \text{Eq. 62}$$

$$z(t_o) \approx a\sin\omega\delta i. \quad \text{Eq. 63}$$

Recall that:  $\delta M_{end} = \delta M + \delta n(t_{end} - t_o).$  Eq. 64

Here,  $\delta n$  is found using:

$$\delta n = \sqrt{\frac{\mu}{(a + \delta a)^3}}. \quad \text{Eq. 65}$$

It has been checked that the result obtained is the same if the derivative is used:

$$\delta n = -\frac{3}{2}\sqrt{\frac{\mu}{a^5}}\delta a. \quad \text{Eq. 66}$$

By convention we can define  $t_o = 0$ . In addition, the initial displacement in the transversal direction can be easily defined by an initial angular displacement  $\delta\lambda_0$  that is the sum of  $\delta M + \delta\omega + \delta\Omega$ . It is known that as mean longitude  $\lambda$  the sum of  $M + \omega + \Omega$ , and so  $\delta\lambda_0$  simply defines the difference of mean longitude at the start of the early encounter phase:

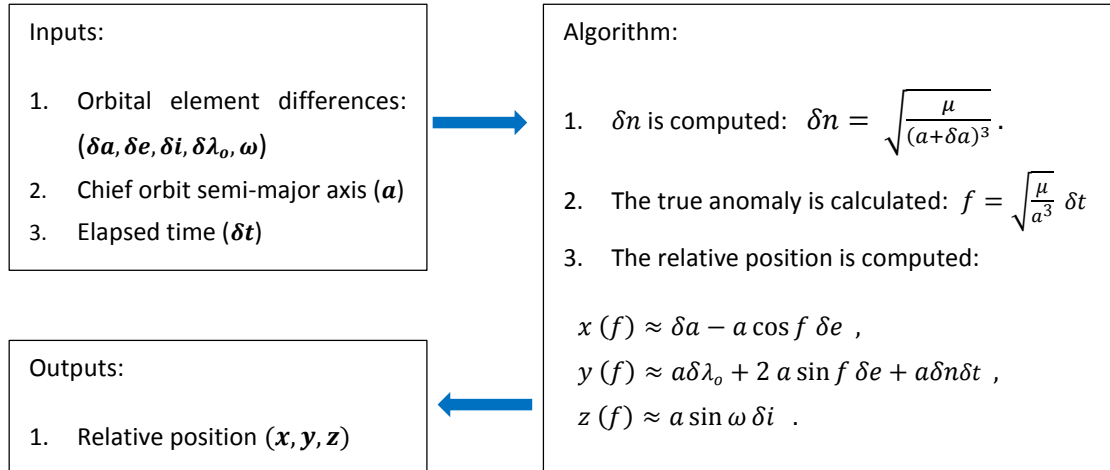
$$x(t_o) \approx \delta a - a\delta e, \quad \text{Eq. 67}$$

$$y(t_o) \approx a\delta\lambda_0, \quad \text{Eq. 68}$$

$$z(t_o) \approx a\sin\omega\delta i. \quad \text{Eq. 69}$$

Note that these equations will be used to establish the starting position of the asteroid. It is also important to keep in mind that for a circular orbit, as that of our chief asteroid, the argument of the periapsis is not defined. For that reason, this parameter will have random values between  $-\pi$  and  $+\pi$ .

In conclusion, by defining the 5 parameters ( $\delta a, \delta e, \delta i, \delta \lambda, \omega$ ) involved in Eq. 58, Eq. 59 and Eq. 60 the relative position is computed. The algorithm implemented is the following:



In order to simplify the simulations along the study, the asteroid orbit will be assumed circular with a semi-major axis ( $a$ ) of 1 AU and 0 degrees of inclination.

In further studies the relative movement between the spacecraft and the asteroid will be analysed. In this case, the trajectory is also defined by these 5 parameters ( $\delta a, \delta e, \delta i, \delta \lambda_0, \omega$ ) that will be referred to as “design variables”, so the aim of the optimization is to find out which values for these variables maximize the probability to detect the target asteroid.

### 3.2 OCC and semi-major axis uncertainty

In the subsection 3.1 it was concluded that the 5 design variables ( $\delta a, \delta e, \delta i, \delta \lambda_0, \omega$ ) were required in order to calculate the relative position ( $x, y, z$ ). In this section, the difference in semi-major axis ( $\delta a$ ) will be obtained.

During the study, the cases will be differentiated according the asteroid OCC. The OCC is an indicator of the ephemerides quality and it is directly related with the semi-major axis uncertainty. The uncertainty will be used as semi-major axis difference  $\delta a$ . In other words, if the asteroid had a very accurate ephemerides it would be placed at the “chief satellite” position (or equivalently in the  $(0, 0, 0)$  position). Unfortunately, as there exist an uncertainty in the semi-major axis, the asteroid will be placed in a position  $(x_i, y_i, z_i)$ , that will depend on  $\delta a$  and the other design variables that will be discussed in the subsequent sections.

#### 3.2.1 Orbit Condition Code

The quality of the orbit ephemerides is evaluated regarding the uncertainty in the orbit semi-major axis. As the semi-major axis determine the orbit period, this element is used in order to compute an intermediate parameter, the *RunOff*:

$$RunOff = 3600 \cdot 3 \cdot \frac{k_0}{P} \left( d\tau \cdot e + 10 \cdot \frac{dP}{P} \right), \quad \text{Eq. 70}$$

where:

$d\tau$  is the uncertainty in the perihelion time (in days).

$e$  is the eccentricity.

$P$  is the orbital period (in years).

$dP$  is the uncertainty in the orbital period (in days).

$k_0$  is the Gaussian constant in degrees  $k_0 = \frac{180}{\pi} \cdot 0.01720209895$ .

The 3600 factor converts to seconds of arc and the 3 factor is an empirical factor that is applied in order to make the formal errors closer to reality.

The *RunOff* is the in-orbit longitude runoff in seconds of arc per decade and is directly related to the “uncertainty parameter” (denoted by “*U*”) in the range from 0 to 9. The “uncertainty parameter” can be referred to as the “Orbit Condition Code” (OCC) too, so the conversion can be made as shown in Table 3:

<i>OCC</i>	<i>RunOff</i>	<i>OCC</i>	<i>RunOff</i>
0	< 1.0	5	< 1692
1	< 4.4	6	< 7488
2	< 19.6	7	< 33121
3	< 86.5	8	< 146502
4	< 382	9	> 146502

Table 3 *OCC* and *RunOff* values

It is important to note that for each *OCC* there is a maximum *RunOff* value. That means that for a specific *OCC* there exists a range of *RunOff* values.

### 3.2.2 Uncertainty in the semi-major axis

Usually, the *RunOff* is computed given the other data presented in 3.2.1. Then the *OCC* is calculated with the help of Table 3. In this case, the problem starts with the *OCC*, then the  $dP$  is calculated, which will give the  $\delta a$ . In order to develop an accurate and feasible model, the worst case is considered. That means that if an orbit with an *OCC* of 3 has to be evaluated, the worst value for the *RunOff* parameter is considered, in this case  $RunOff = 86.5$  even if it sure that for an orbit with this *OCC* value the *RunOff* will be lower.

Then, the uncertainty in the orbit period is calculated using Eq. 70. Since the scenario consider a chief orbit with  $e=0$  and  $d\tau$  is the error on the periapsis time, a value of  $d\tau = 0$  is used. As can be seen, in the following equation the  $dP$  has been deduced:

$$dP = \left( \frac{RunOff \cdot P}{3600 \cdot 3 \cdot k_0} - e \cdot d\tau \right) \frac{P}{10} . \quad \text{Eq. 71}$$

Once the uncertainty in the period is obtained, the uncertainty in the semi-major axis is computed by the following equation:

$$a + da = \sqrt[3]{\mu \left( \frac{P + dP}{2\pi} \right)^2} , \quad \text{Eq. 72}$$

$$da = \sqrt[3]{\mu \left( \frac{P + dP}{2\pi} \right)^2} - a . \quad \text{Eq. 73}$$

### 3.3 Regression model for the uncertainties

This model establishes a relation between the uncertainty in the semi-major axis  $\delta a$  and the uncertainties in the eccentricity  $\delta e$  and the inclination  $\delta i$  of the relative orbit. For that, the NASA near earth objects database (NASA (Ed.), 2014)<sup>1</sup> is used. This database allows to filter the NEOs according the following parameters:

- “Total dV”: required velocity variation to reach the object.
- “Total dur”: duration of the mission.
- “Stay”: minimum time that the mission will stay at the asteroid.
- “Launch”: available date to start the mission.
- “H”: asteroid’s absolute magnitude.
- “OCC”: Orbit Condition Code.

In order to find a feasible model, the filter parameters in Figure 15 have been selected:

Figure 15 Filter selection

From each asteroid the data that will be used are:

- “OCC”.
- The semi major axis of the orbit “a” and the uncertainty of this value “error”.
- The eccentricity of the orbit “e” and the uncertainty of this value “error”.
- The inclination of the orbit “i” and the uncertainty of this value “error”.

In Table 4 the data corresponding to the asteroids with OCC=1 are shown:

Object Designation	(2002 XY38)	(2003 SM84)	(2006 RH120)	(2006 WB)	(2009 UY19)	(2012 UV136)
Orbit ID	26	15	47	18	23	19
OCC	1	1	1	1	1	1
a	0,910584828	1,125486683	0,987302287	0,849282015	1,02360672	1,006210949
error	5,68E-08	2,93E-08	2,58E-08	1,63E-08	5,53E-08	7,96E-08
e	0,217518532	0,082079172	0,019145262	0,180406383	0,03079387	0,13898906
error	1,83E-06	4,39E-06	4,61E-09	1,12E-07	7,62E-08	1,74E-06
i	2,102977803	2,795180298	0,797447122	4,880543628	9,05358023	2,221036211
error	2,50E-05	2,94E-05	1,26E-06	1,01E-05	3,79E-05	1,74E-06

Table 4 Parameters for asteroids with OCC=1

<sup>1</sup> <http://neo.jpl.nasa.gov/nhats/>

If the uncertainty in the eccentricity and the inclination are plotted against the uncertainty in the semi-major axis it can be noted that there exists a linear dependency in logarithmic. For this reason the next model is proposed:

$$\log_{10} y = \log_{10} a + b \cdot \log_{10} x \quad , \quad \text{Eq. 74}$$

where:

$x = \text{semi} - \text{major axis uncertainty}$  ,

$y = \text{eccentricity (or inclination) uncertainty}$  ,

$a, b$ : parameters to be computed .

In order to use the linear regression, the logarithm is applied to the data. Then, by making use of the linear regression formulas, it is easy to calculate  $\log_{10} a$  and  $b$ . For the linear regression, the mean value is used in order to calculate  $\log_{10} a$  (the y-intercept value), consequently, the plotted line passes through the mean value. In contrast, in this study, the median value (instead of the mean value) will be used to calculate the y-intercept value, the reason is that we want to have the half of the points above the line and the other half below it. So, the following method is applied:

1. Calculate the mean of  $x$  and  $y$ :  $\bar{x}$  and  $\bar{y}$  using

$$\bar{x} = \frac{x_1 + x_2 + \dots + x_n}{n} \quad . \quad \text{Eq. 75}$$

2. Calculate the median of  $x$  and  $y$  (numerical value separating the higher half of a data sample, a population, or a probability distribution, from the lower half).
3. Calculate  $b$ :

$$b = \frac{\sum_{i=1}^n (x_i - \bar{x})(y_i - \bar{y})}{\sum_{i=1}^n (x_i - \bar{x})^2} \quad . \quad \text{Eq. 76}$$

4. At this point, the  $\log_{10} a$  is computed but, as it has been introduced before, the median is used:

$$\log_{10} a = \log_{10} y_{\text{median}} - b \cdot \log_{10} x_{\text{median}} \quad . \quad \text{Eq. 77}$$

5. The value of  $a$  is computed:

$$a = 10^{\log_{10} a} \quad . \quad \text{Eq. 78}$$

6. In order to obtain a value of  $y$  for a given  $x$  the next expression can be used:

$$y = a x^b . \tag{Eq. 79}$$

Table 5 shows the values that have been obtained for the two uncertainties:

Parameter	Eccentricity	inclination
$\bar{x}$	-5,7253023	
$x_{median}$	-5,3240684	
$\bar{y}$	-4,3517711	-4,2282992
$y_{median}$	-4,0699763	-4,0580319
$b$	0,76591414	0,67193149
$\log_{10} a$	0,007803	-0,4806227
$a$	1,0181294	0,33065667

Table 5 Regression parameters summary

For the eccentricity the formula in Eq. 80 yields Figure 16:

$$e \text{ uncertainty} = 1,0181294 (\text{sma uncertainty})^{0,76591414} . \tag{Eq. 80}$$

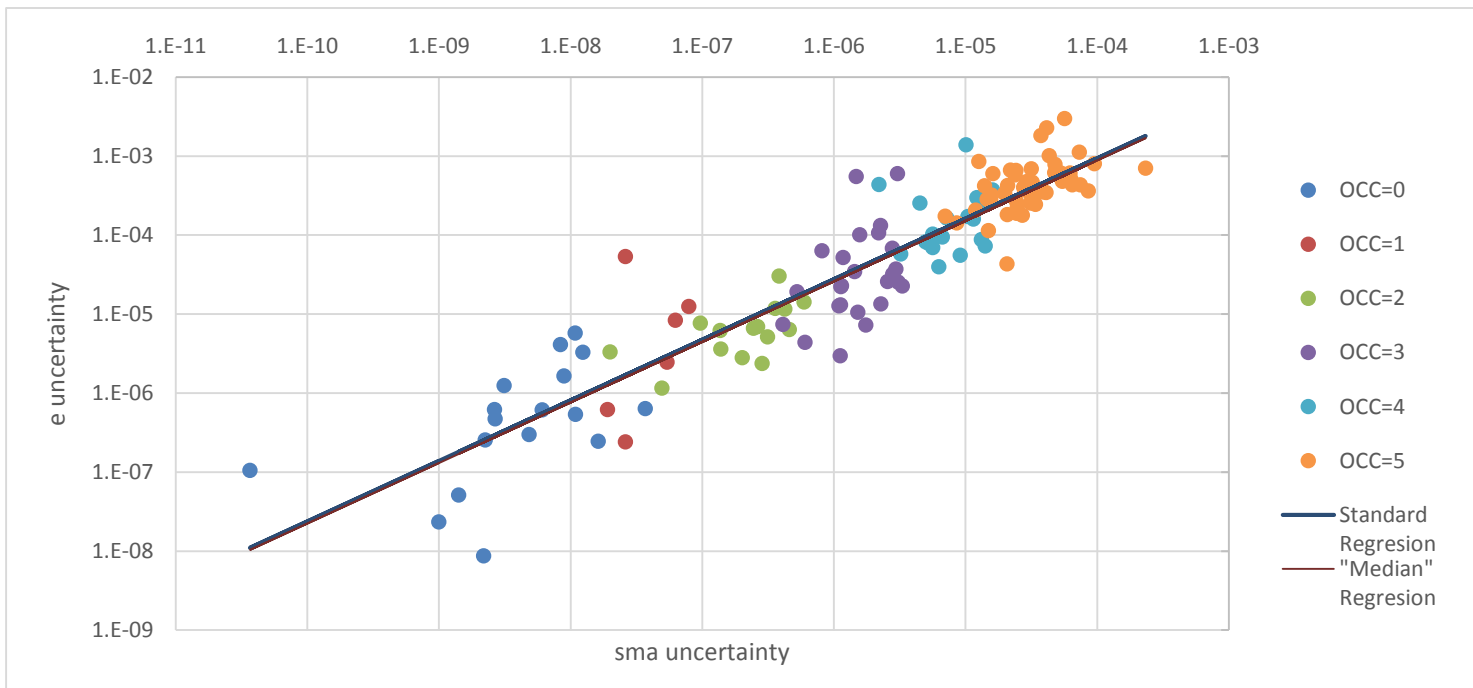


Figure 16 Eccentricity uncertainty vs sma uncertainty

while for the inclination uncertainty the formula in Eq. 81 yields Figure 17:

$$i \text{ uncertainty} = 0,33065667(\text{sma uncertainty})^{0,67193149} . \quad \text{Eq. 81}$$

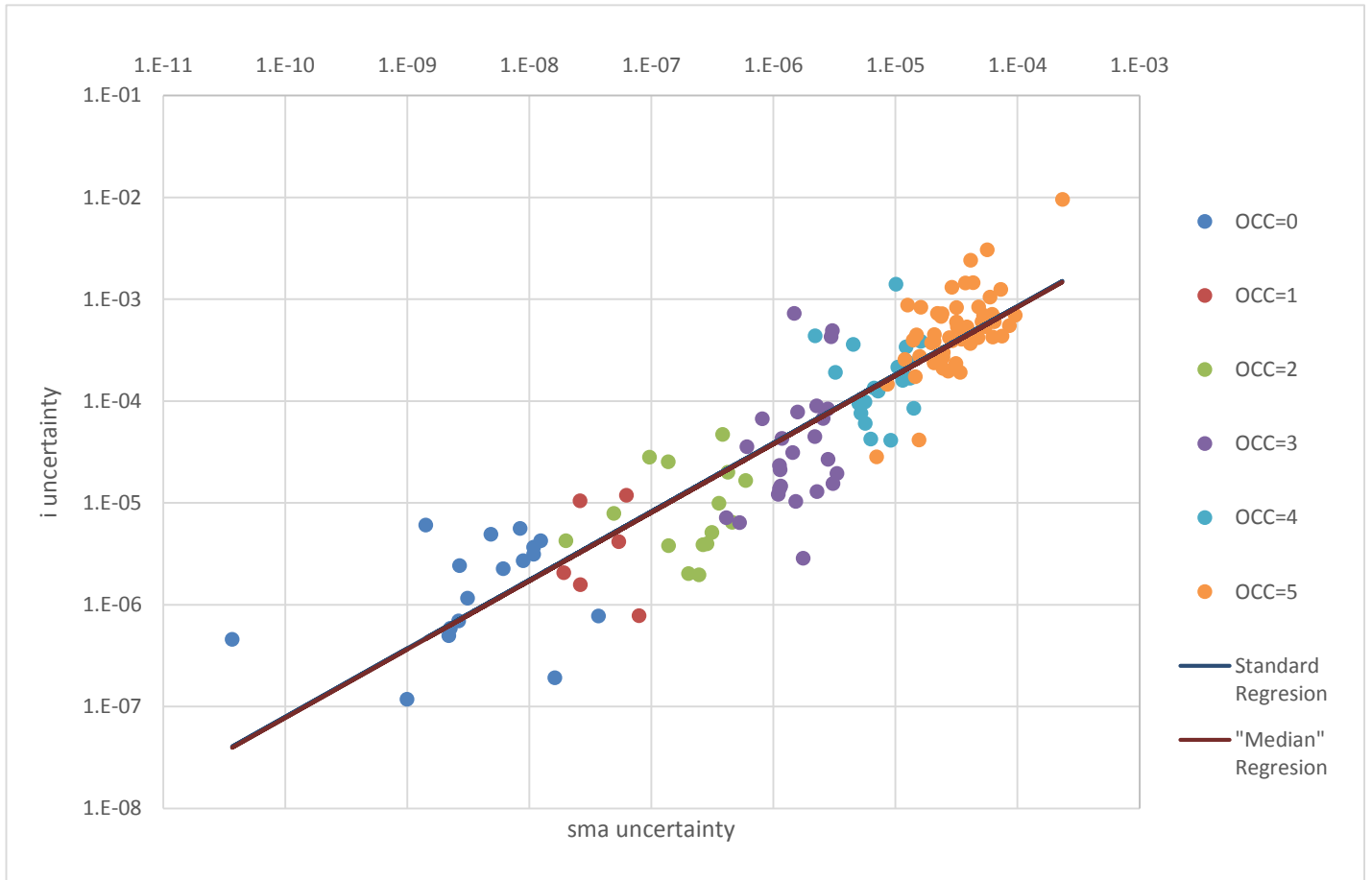


Figure 17 Inclination uncertainty vs semi-major axis uncertainty

### 3.3.1 Model Validation

In order to assess if the obtained equation satisfies our expectations the function can be plotted in the same frame as the data analysed. The result are Figure 16 and Figure 17 where can be seen that functions obtained fits satisfactorily the cloud of points.

The aim was to have the half of the uncertainty values (points plotted) above the line that represents Eq. 80 and Eq. 81 and the other half below. A Matlab function has been developed in order to evaluate check for every uncertainty value if it is higher or lower than the value given by the equations. After evaluating all the points it is ensured that one half of the data is in the upper part and the other half is in the lower.

### 3.4 Asteroid Detection Model

The asteroid detection model is proposed in order to evaluate if the asteroid can be detected by the spacecraft given the relative position between both. The result of the function is a binary: it has a value of 1 if the asteroid is visible, 0 otherwise.

The model is based on the apparent magnitude  $V$  (Bowell, 1989):

$$V = H + 5 \cdot \log_{10}(R_{sc} \cdot R_{ast}) - 2.5 \cdot \log_{10}((1 - G) \cdot \phi_1(k) + G \cdot \phi_2(k)) , \quad \text{Eq. 82}$$

where the absolute magnitude  $H$  of the object is given by:

$$D = 1329km \cdot 10^{\frac{-H}{5}} \cdot p_v^{-\frac{1}{2}} , \quad \text{Eq. 83}$$

where  $p_v$  represents the asteroid's albedo, or:

$$H = -5 \cdot \log_{10} \left( \frac{D \cdot \sqrt{p_v}}{1329} \right) . \quad \text{Eq. 84}$$

$R_{sc}$  and  $R_{ast}$  are the distances from the asteroid to the spacecraft and to the Sun respectively,  $k$  is the solar phase angle and  $G$  is the phase slope parameter, which describes how the asteroid brightness falls with increasing solar phase angle. The phase slope parameter  $G$  has generally a value between 0 and 1, usually decreasing with decreasing albedo of the asteroid. A constant  $G$  parameter equal to 0.15 is assumed (Stuart, 2003).

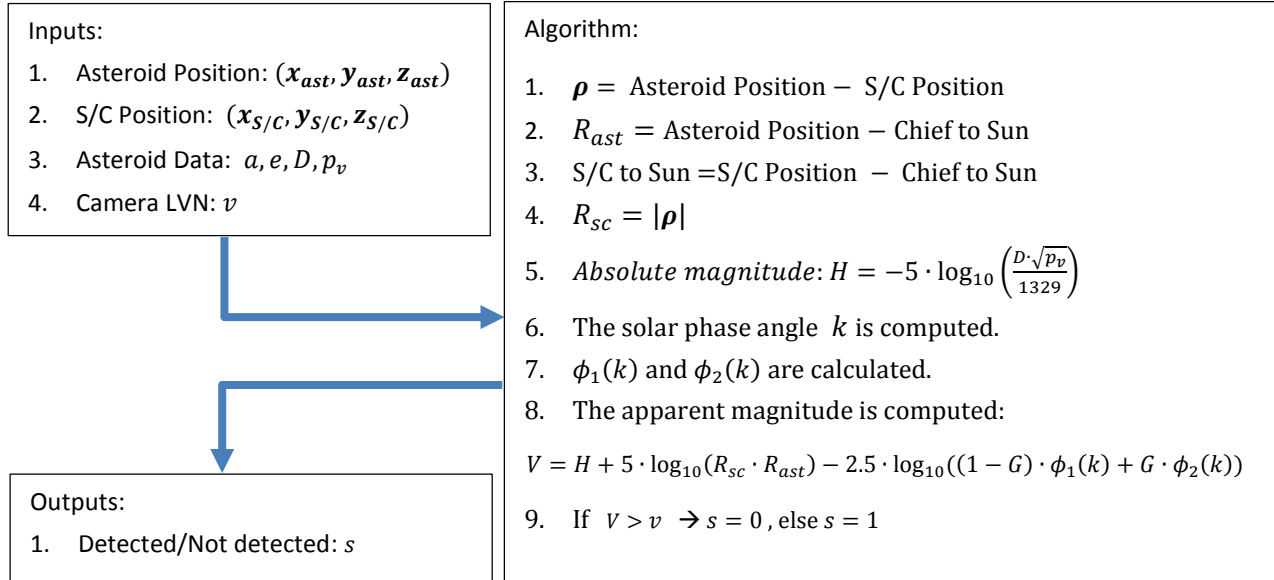
The expressions for  $\phi_1(k)$  and  $\phi_2(k)$  are:

$$\phi_1(k) = \exp \left( -3.33 \left( \tan \left( \frac{k}{2} \right) \right)^{0.63} \right) , \quad \text{Eq. 85}$$

$$\phi_2(k) = \exp \left( -1.87 \left( \tan \left( \frac{k}{2} \right) \right)^{1.22} \right) . \quad \text{Eq. 86}$$

It is important to notice that the higher the apparent magnitude the more difficult it is to see the asteroid. So, taking into account the expressions for  $\phi_1(k)$  and  $\phi_2(k)$  it is easy to see that the apparent magnitude is maximized for  $k = 180^\circ$  and the minimum value is found for  $k = 0^\circ$ .

In Figure 18 the situation to be analysed is shown. The inputs for this model are the *Asteroid position*, the *S/C position*, the *camera LVM* (defined in page 59) and the *Asteroid data*.



As can be seen in Figure 18, the *Asteroid position* and the *S/C position* are the distances from the chief position to both objects in the Hill reference frame. The *Asteroid data* includes the values for the asteroid's semi-major axis, eccentricity, diameter and albedo. The first two parameters are used to calculate the vector *Chief to Sun*, the diameter and the albedo are used to calculate the absolute magnitude  $H$ .

Once we have the three vectors that were mentioned above, the next step is to obtain the distances from the *Asteroid to Sun* and from the *S/C to Sun*. Then, the  $\rho$  vector is computed and the angle  $k$  is found. As introduced in the previous paragraph, we can see that the best configuration to see the asteroid from the spacecraft is when the S/C is placed between the Asteroid and the Sun. In this situation the light that comes from the Sun is reflected in the asteroid and directed to the S/C.

That argument is equivalent to say that the function is minimized for  $k = 0^\circ$ . As the angle  $k$  increases, less light is reflected to the S/C and consequently it becomes more difficult to see the asteroid:

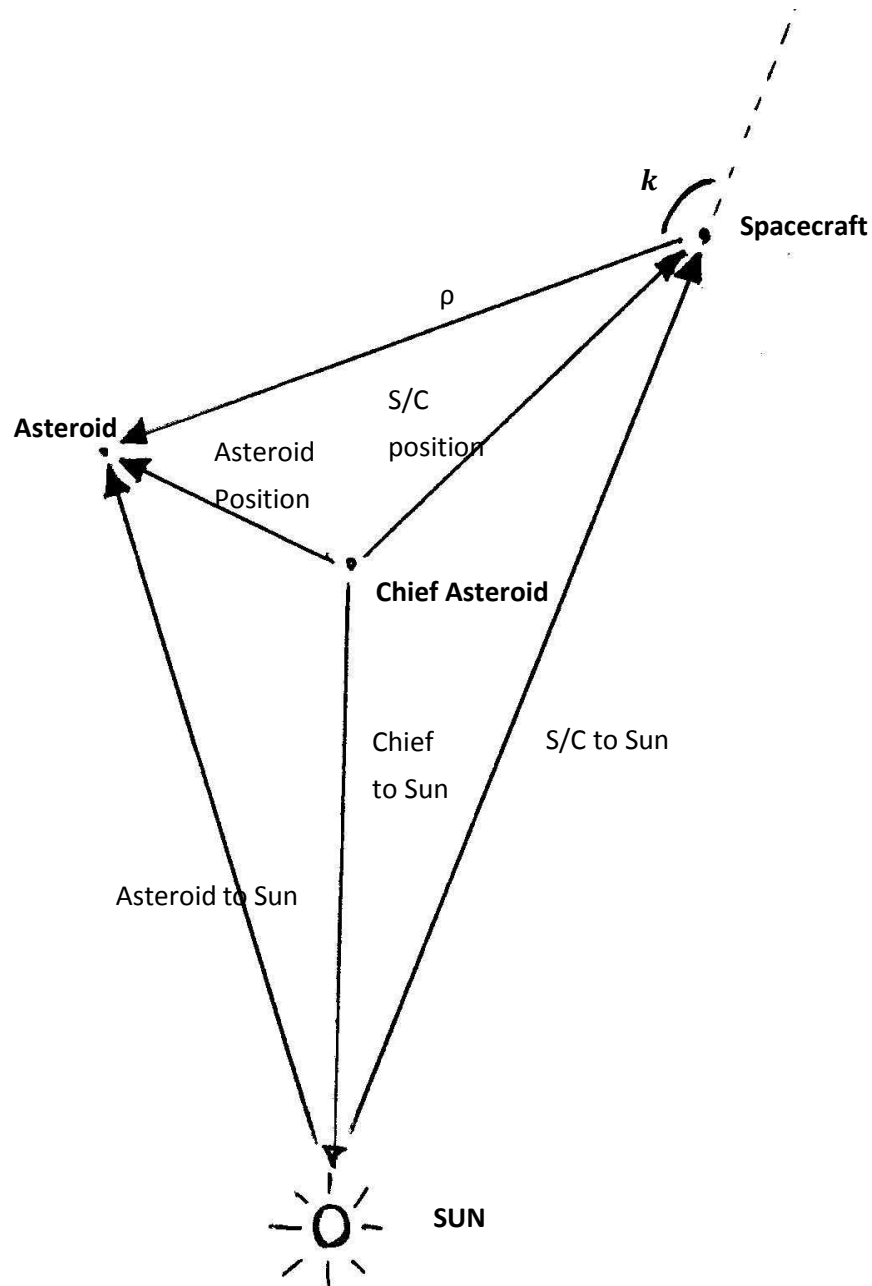


Figure 18 Asteroid detection definitions and configuration

### 3.4.1 Additional constraints

In order to have an accurate model there is another consideration to be done: if in the configuration that is being analysed the angle  $k$  is larger than 320 degrees, it means that the asteroid lies in the “No detection zone” shown in Figure 19:

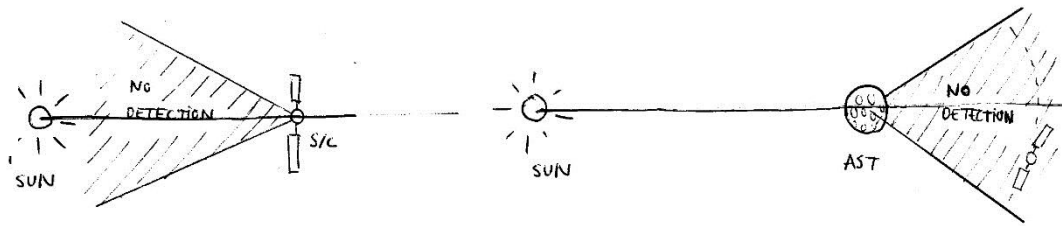


Figure 19 "No detection" zone

This fact is a consequence of the SNR (Signal to Noise Ratio) that the camera can accept. In this situation, the sunlight blinds the S/C camera, introducing a SNR that makes the asteroid undetectable, even if it is relatively close to the spacecraft.

In the Matlab function, the angle  $k$  is evaluated and if the value is above 320 degrees the apparent magnitude is set to a value higher than the camera's threshold.

### 3.4.2 Camera performance

The value set to the camera is one of the keys of the model and the study itself. In a first approach a value between 15 and 17 is selected following real mission data. (Massimiliano Vasile, 2013). However, this value will be increased in the next years as new technology and methods are applied.

### 3.4.3 Model validation

The next step is to test the model, for that reason the function is run, placing the S/C or the asteroid in the centre and evaluating the apparent magnitude in the surrounding area.

In this case the model is modified to test two different situations. In the first one, the asteroid is placed in the middle of the bi-dimensional domain. With a discretization of the domain it is possible to see in which areas the value of the apparent magnitude is bigger and where it is lower.

As it has been stated before, if the S/C is placed in the areas where the apparent magnitude is lower than the camera LMV, the asteroid will be visible. In that case, the S/C has to be placed between the Sun and the asteroid.

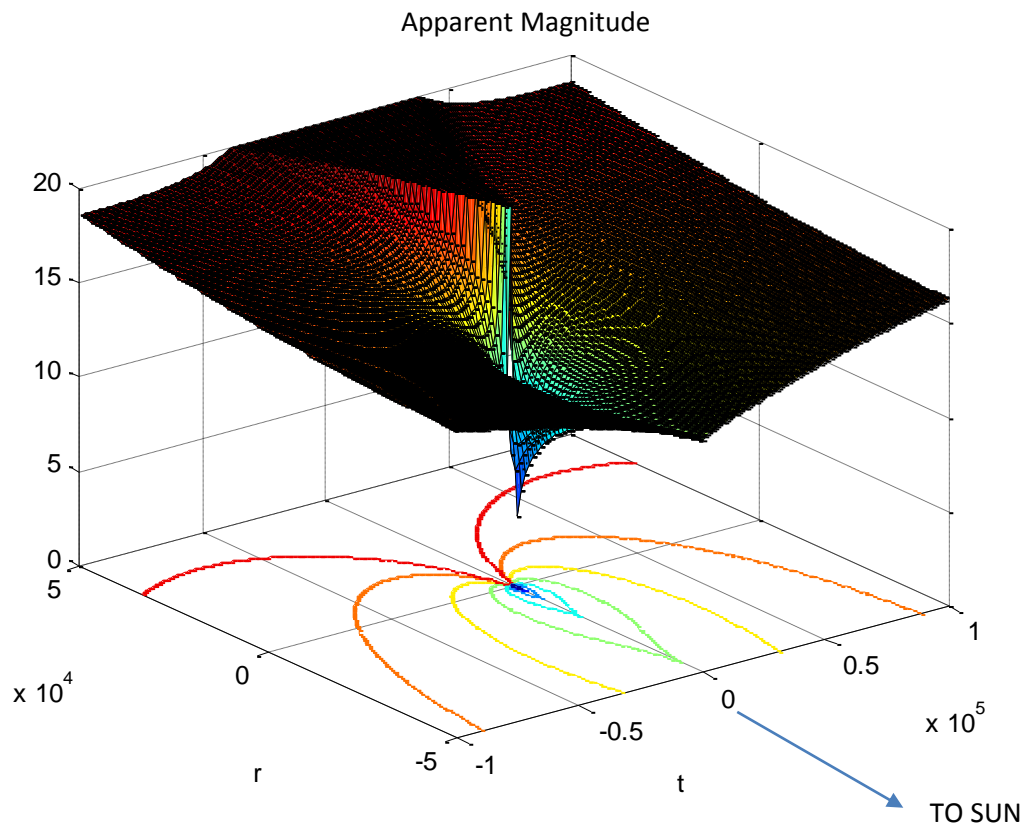


Figure 20 Apparent magnitude (Asteroid in the centre)

If a particular value is applied to the camera, for example 15, Figure 21 is obtained. If the S/C is placed in the inner section, the asteroid will be detected, but if the S/C is orbiting in the outer section the asteroid won't be visible:

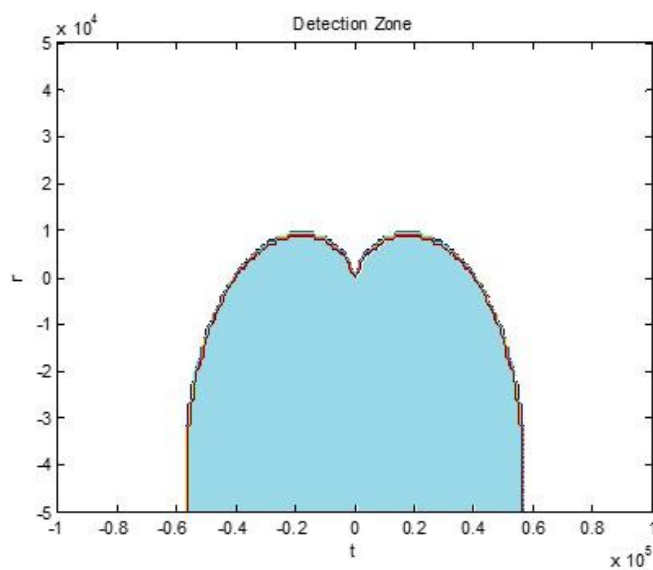


Figure 21 Detection Zone for camera=15 and asteroid in the centre

In Figure 21 we can appreciate the importance of the angle  $k$ . Even if the distance increases, if the angle is low enough the asteroid is visible.

Then, a second situation has been tested: the S/C stays in the center of the domain and the asteroid is orbiting around. As expected, Figure 22 is exactly the same but tuned by 180 degrees. In that case, the lower (and better) values for the apparent magnitude are found if the asteroid is orbiting close to the S/C but in the opposite side of the Sun.

Note that this is exactly the same that happened in the previous model where the best values were obtained if the S/C was placed between the asteroid and the Sun.

Figure 22 illustrates the second case.

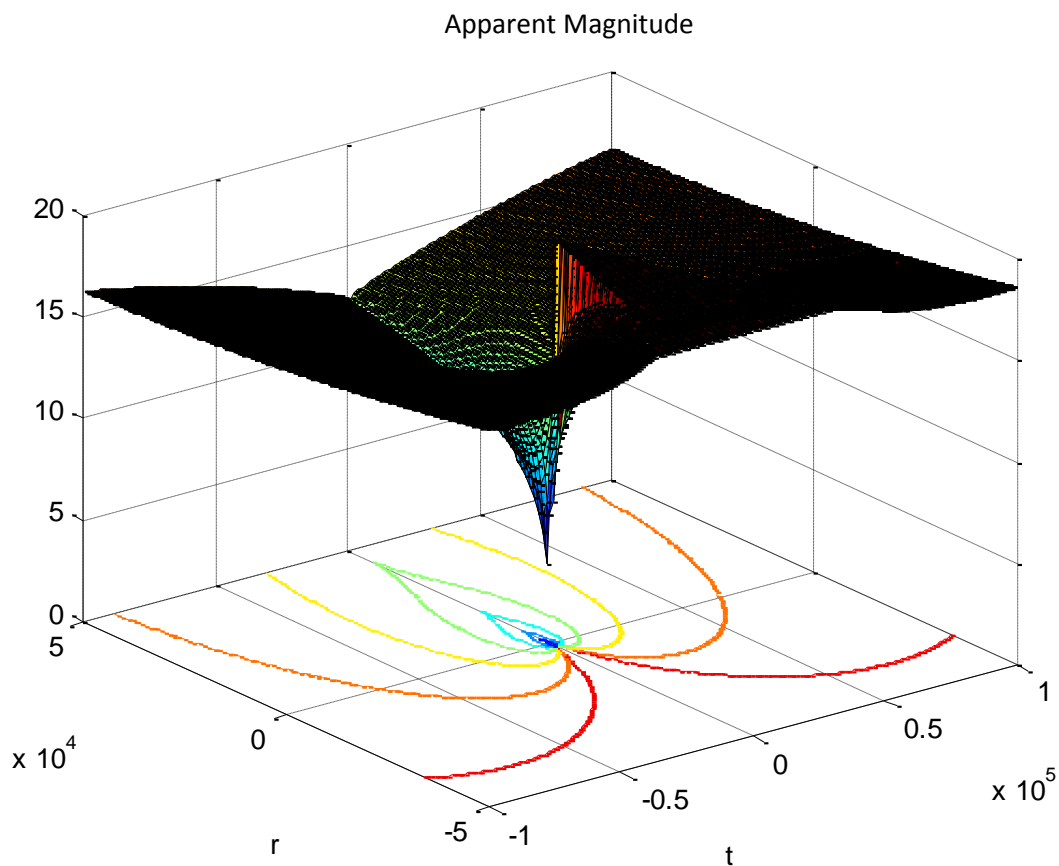


Figure 22 Apparent magnitude (S/C in the centre)

As in the previous case, it is possible to fix a value for the camera. In this case, the shape is the same but, instead of being oriented to the Sun, it is oriented in the opposite direction.

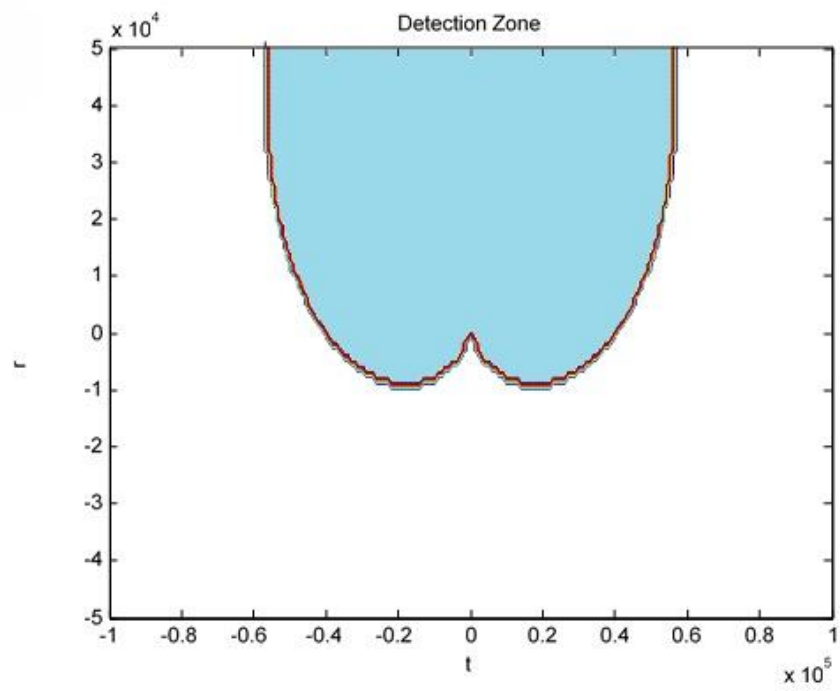


Figure 23 Detection Zone for camera=15 and S/C in the centre

### 3.5 Virtual Uncertain Population

This section will serve to understand why the previous models have been developed and what paper have each of them in the general problem that will be studied. The main idea of the project is to find out which is the best trajectory to approach and detect a small asteroid. In addition, as was seen in section 3.2, the small asteroid ephemerides are not very accurate and the asteroid may not lie at the exact place where it is supposed to. So, how can we simulate the probability to detect the small asteroid?

First of all, a domain is created. In this domain, the origin  $(0, 0, 0)$  is where the asteroid would be if the trajectory was exactly known. Then the OCC corresponding to the small asteroid to be studied is selected. With that OCC the  $\delta a$  is computed.

The second step consists on generating a random population of asteroids. The uncertainty in the semi-major axis of the generated asteroids will vary from 0 to  $\delta a$ . Then, the other parameters that define the orbit are calculated for each asteroid ( $\delta e$  and  $\delta i$  are calculated with the linear regression in section 3.3 and  $\delta \lambda_0$  and  $\omega$  are initialized randomly with values between  $-\pi$  and  $\pi$ ).

Having the orbital parameters defined for each asteroid generated, the relative position to the real asteroid (the one that lies on the origin) is computed as per equations deduced in section 3.1. Consequently a random cloud of asteroids is generated around the origin representing the places where the real asteroid could be. In Figure 24 the cloud is represented together with the ellipsoid that contains the 99.5% of the randomly generated asteroids. This shape will be analyzed in section 4.6.3.

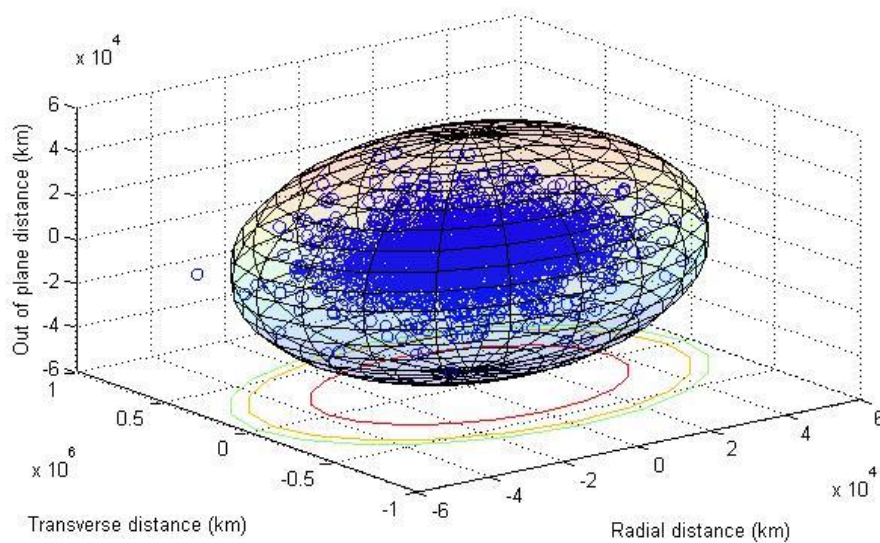
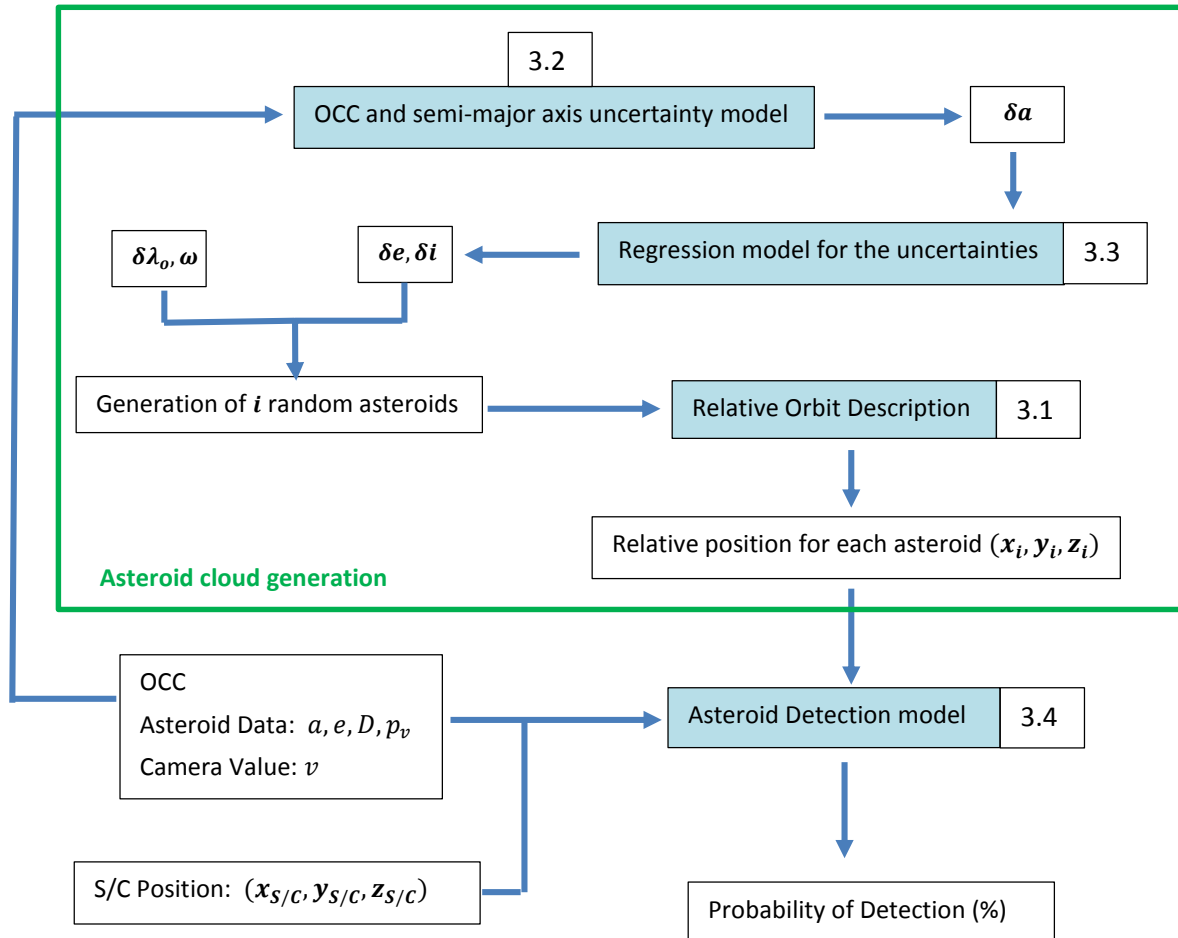


Figure 24 Cloud of asteroids

Once the cloud of simulated asteroids has been generated, the spacecraft trajectory is simulated. It will be checked how many asteroids the spacecraft is able to detect along the path making use of the model developed in section 3.4. Then, a simple calculus is performed: if 1000 asteroids have been generated and the spacecraft has detected 950 along the trajectory, the probability to detect the real asteroid is 95%.

To sum up, the models (highlighted in blue) are related in the following way:



During the study the asteroid cloud that is generated randomly will be used to model the uncertainty that exist in the asteroid real position. Even though both concepts represent the same, they has to be differentiated. To avoid misunderstanding the asteroid to be studied will be referred to as “target asteroid” and the cloud of asteroids that has been generated to simulate the potential positions will be referred to as “virtual uncertain population”.

## 4. Simulations

---

In this chapter the simulations performed are presented together with the results obtained for each case of study.

### 4.1 Study 0: Genetic algorithm

First, it is necessary to test the simulation that will be performed to adjust the parameters in order to obtain optimal results. Along the following studies the Genetic Algorithm (GA) is used to optimize the design variables that define the spacecraft's proximal motion and, consequently, to obtain the maximum possible probability of detection.

#### 4.1.1 Description

The Genetic Algorithm, as its name indicates, is based on the evolution of a population. At the beginning, an initial population of random members is created. In our case each member represents one spacecraft with its design variables  $(\delta a, \delta e, \delta i, \delta \lambda, \omega)$ . Next, each member is evaluated, which means that the detection probability is computed for each spacecraft.

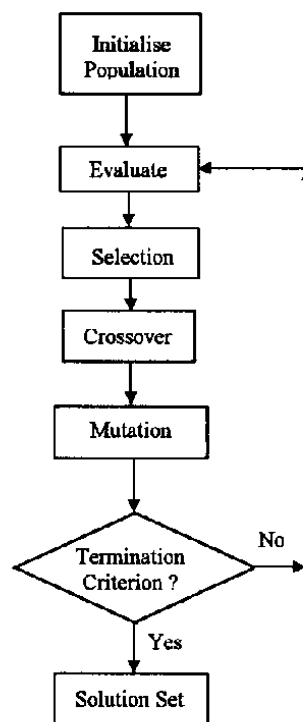


Figure 25 Genetic Algorithm

The members who have obtained the best punctuation in the previous evaluation are selected and mixed to create the next generation. As in nature, where best members of a community are those that reproduce. After that, a factor of mutation is introduced. This is done because by changing just a part of the individual (for example changing the  $\delta\lambda_0$  of the spacecraft) the result may be improved, making it possible to find the absolute maximum (or minimum) value of the simulation, not just a local extreme.

Last but not least, there is the termination criterion, which needs to be evaluated to terminate the genetic algorithm or to continue with a new generation. In order to set this criterion, there are a lot of options and Matlab allows to choose several ones. Figure 26 shows a genetic algorithm executing that can be stopped by Stall generations (generations that can be evaluated without obtaining an improvement in the optimal value), Time (total elapsed time for computation) and Generations (maximum generations that can be created in each execution). Matlab not also allows the user to see the percentage met for each criteria (to know what will cause the execution stop), but also allows to see the mean value of the population and the best one. In this case the Matlab function is trying to minimize the chances of missing the asteroid:

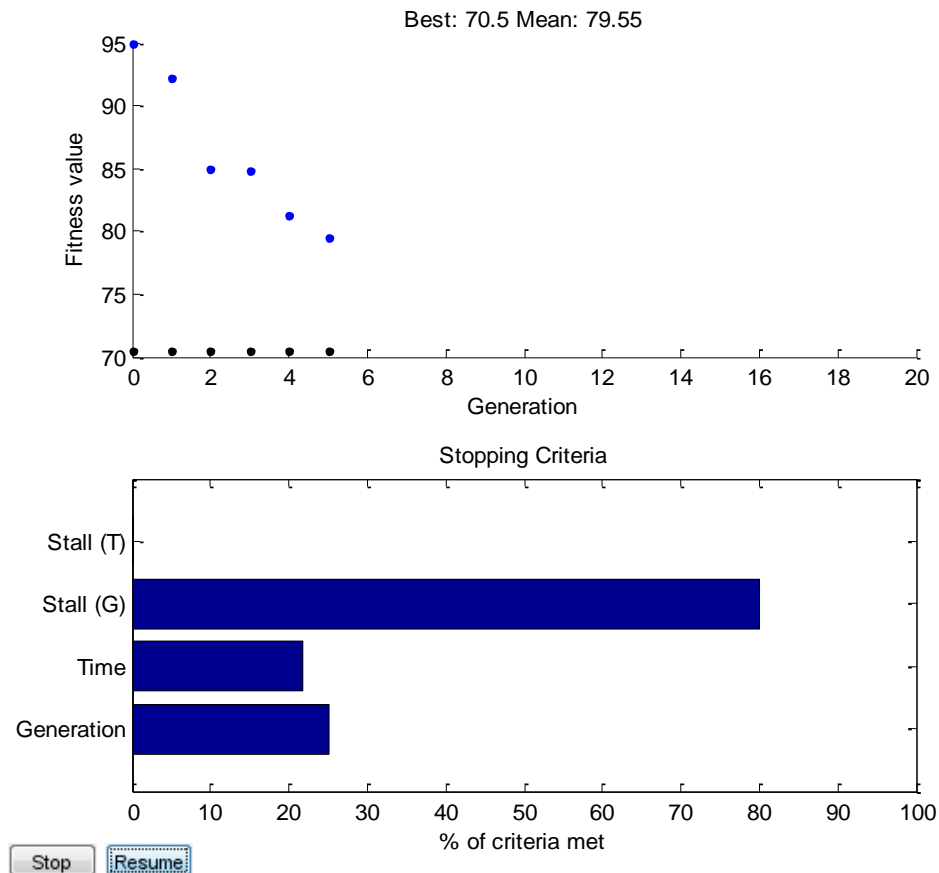


Figure 26 Termination criteria example

If the stopping criteria are not set correctly, the execution can waste a huge amount of time making unnecessary calculations, so the execution time can be reduced substantially if these parameters are set correctly.

#### 4.1.2 Parameter evaluation

As was discussed in the previous subsection, there are some parameters that need to be adjusted to reduce the computational time. Besides, there are other parameters that not only affect the calculation time, but also can have consequences on the results.

##### *Number of asteroids generated*

The first value to be analysed is the number of asteroids that compose the virtual uncertain population. Previously it has been introduced that a random population of asteroids need to be generated to assess the probability of detection (Montecarlo simulation) but, how many asteroids have to be generated? The answer is obvious, a sufficiently large number to have a reliable result (not enough asteroids will result in variable and unreliable results, in the extreme, if only one asteroid was generated, the result could vary from 0 to 100%) but sufficiently small so that the computational time does not increase unnecessarily.

In order to establish a suitable number of asteroids to generate, the next expression is used:

$$\sigma_x^2 = \frac{p \cdot q}{n} , \quad \text{Eq. 87}$$

where  $q = 1 - p$ .  $p$  is the probability to achieve,  $n$  the number elements generated. So,  $\sigma_x = \sqrt{\frac{p \cdot q}{n}}$ .

In most of the simulations the probability of detection wanted would be  $p = 99.5\%$ . Then, if 2000 asteroids are used, the variance will be:

$$\sigma_x = \sqrt{\frac{0.995 \cdot (1 - 0.995)}{2000}} = 0.00158 . \quad \text{Eq. 88}$$

If the  $3\sigma_x$  is computed,

$$3\sigma_x = 0.0047 . \quad \text{Eq. 89}$$

That means that once the simulation has been performed, if it is repeated again the result will vary about 0.5% in the 99.5% (due to the use of  $3\sigma_x$ ) of the cases. So, 2000 is considered a suitable number of asteroids for the simulations.

### *Upper and Lower bounds*

The upper and lower bounds (maximum and minimum values for design variables  $\delta a, \delta e, \delta i, \omega$  and  $\delta \lambda$ ) are set in order to define the space where the possible solutions can be found. Before making any try it is necessary to observe that the ellipsoid of uncertainty dimensions increase proportionally with the OCC considered and the time since discovery, so the upper and lower values will be referred to the ellipsoid of uncertainty values.

First, in order to ensure that the limits allow to find every solution the limits criteria were set as follows:

	$\delta a$	$\delta e$	$\delta i$	$\delta \lambda_0$	$\omega$
Lower bound	$-10 \cdot \max(\delta a)$	$-10 \cdot \max(\delta e)$	$-10 \cdot \max(\delta i)$	$\min(\delta M)$	$-\pi$
Upper bound	$10 \cdot \max(\delta a)$	$10 \cdot \max(\delta e)$	$10 \cdot \max(\delta i)$	$\max(\delta M)$	$\pi$

With that method the space allowed for the solution was 10 times the maximum and minimum values for the semi major axis, eccentricity and inclination. For the argument of perigee the entire interval between  $-\pi$  and  $\pi$  pi is considered while for the initial mean longitude the bound depend on the  $\delta t$  (that is considered 20 years) and the  $\delta n$  (which is function of  $\delta a$ ):  $\delta M = \delta n \cdot \delta t$

After performing some validations it was observed that all values where far enough from the limits with the exception of the semi-major axis, which sometimes appeared close to the upper bound. In order to avoid to be restrictive with possible results the bound for the semi-major axis were extended (now the upper and lower values are 20 times the maximum or minimum values found in the asteroid population).

This configuration was checked and confirmed to be sufficient.

#### 4.2 Study 1: probability of detection (OCC and CAD)

In this first study the probability of detection is assessed depending on the close approach duration (CAD, defined as the trajectory that the spacecraft performs before the rendezvous with the target asteroid) and the OCC. The result obtained provides a quick reference that will be confirmed when further studies are performed.

Simulation parameters	
Number of asteroids considered	2000
Asteroid diameter	20 meters
OCC range	From 0 to 5
Close Approach Duration	From 1 to 14 months
Camera LMV	15

Table 6 Simulation 1 parameters (study 1)

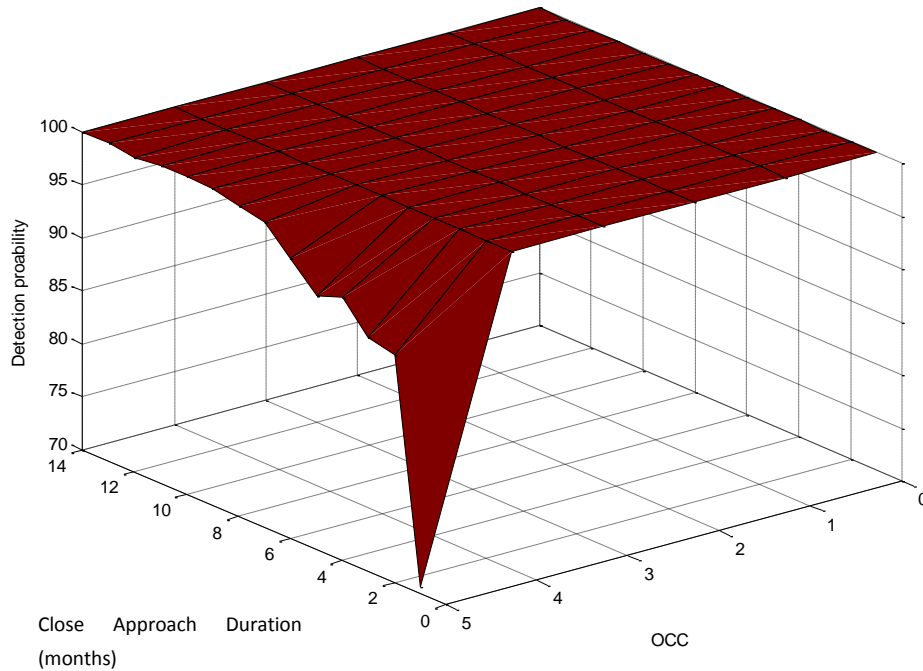


Figure 27 Detection Probability for Diameter=20 m (STUDY 1)

Figure 27 shows the probability of detecting an asteroid with a diameter of 20 meters. Observing the figure it is possible to conclude that for all OCC except 5 the result is close to 100%. In the case of OCC=5, the value decreases for the simulations where less months are considered but the value of the probability quickly reaches the 100% after a few months.

Due to the little variation of the probability obtained it was decided to repeat the simulation but now considering an asteroid with a diameter of 5 meters.

Simulation parameters	
Number of asteroids considered	1000
Asteroid diameter	<b>5 meters</b>
OCC range	From 0 to 5
Close Approach Duration	From 1 to 14 months
Camera LMV	15

Table 7 Simulation 2 parameters (study 1)

In Figure 28, it is possible to see that a similar result is obtained for diameter of 5m. However, in this case the detection probability starts to decrease for OCC=4 and the 100% is reached after few months as in the previous example.

Besides, a significant descent is found for OCC=5 where the probability decreases to 14% for the first two months and then it smoothly increases until it stabilizes near a value of 50%.

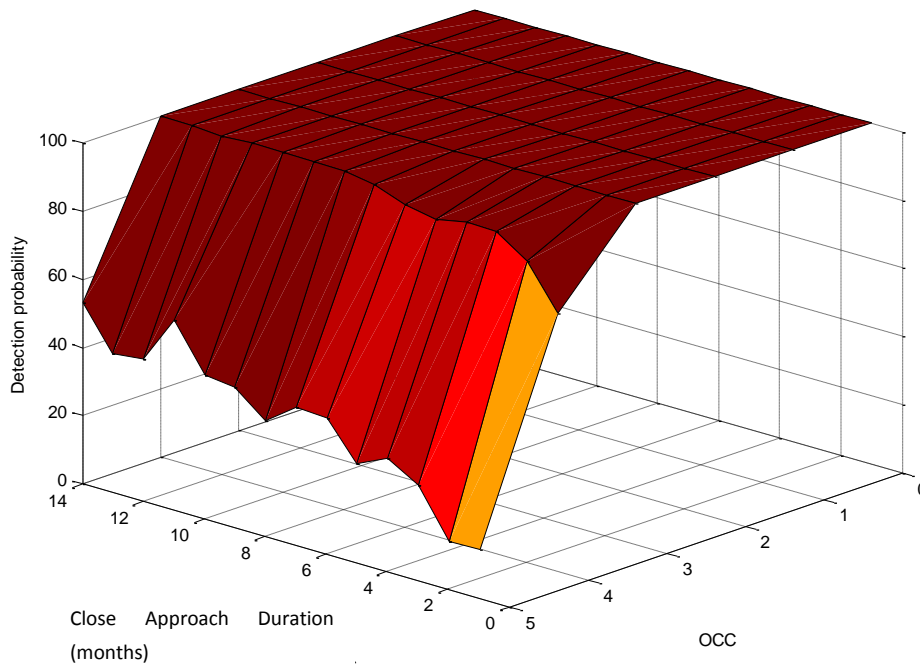


Figure 28 Detection Probability for Diameter=5 m (STUDY 1)

The first conclusions that can be deduced are that the OCC and the asteroid diameter values have a strong influence on the probability of detecting the asteroid and the number of months has a significant influence when short close approach is considered but after a certain number of months the probability of detection may not be improved.

### 4.3 Study 2: probability of detection (OCC and asteroid diameter)

In the previous study it was seen that the OCC and the diameter were key factors while the duration of the close approach phase had a less significant influence depending on the simulation performed. For that reason, in this second study, the asteroid diameter is introduced as a variable to confirm its influence and assess which can be the range that is more interesting to study.

Table 8 shows the parameters used in the simulation:

Simulation parameters	
Number of asteroids considered	2000
Asteroid diameter	From 5 to 25 meters
OCC range	From 0 to 5
Close approach duration	10 months
Camera LMV	15

Table 8 Simulation 1 parameters (study 2)

With this combination of parameters Figure 29 is obtained.

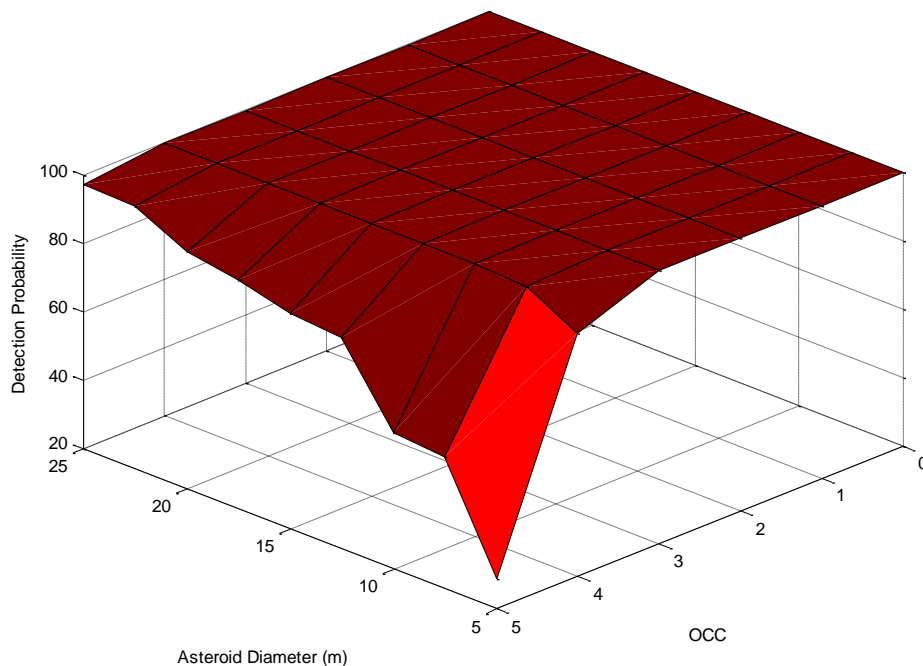


Figure 29 Detection probability CAD = 10 months (study 2)

As in the previous study, the simulation is not as revealing for lower OCC values due to the fact that the probability of detection saturates at 100% in all the domain considered, even if asteroids with diameters around 5 meters are considered.

The zone that seems more interesting begins for OCC=4 and asteroid diameter between 5 and 10 meters. So, further studies will be focused in that direction. Before, it would be useful to see the variation if 5 months are considered instead of 10:

Simulation parameters	
Number of asteroids considered	2000
Asteroid diameter	From 5 to 25 meters
OCC range	From 0 to 5
Close Approach Duration	5 months
Camera LMV	15

Table 9 Simulation 2 parameters (study 2)

With a close approach duration of 5 months the following figure is obtained:

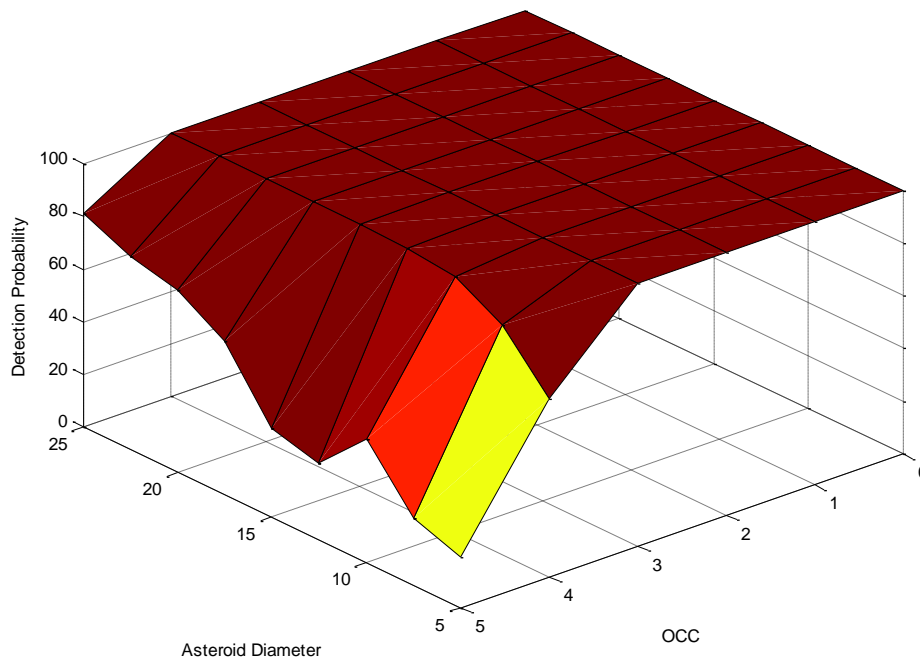


Figure 30 Detection probability for CAD = 5 Months (study 2)

With that it is confirmed that the OCC and the asteroid diameter define the results obtained and the number of months can vary it sharply if a short time is considered but if a considerable number of months is studied, the variation will be very smooth.

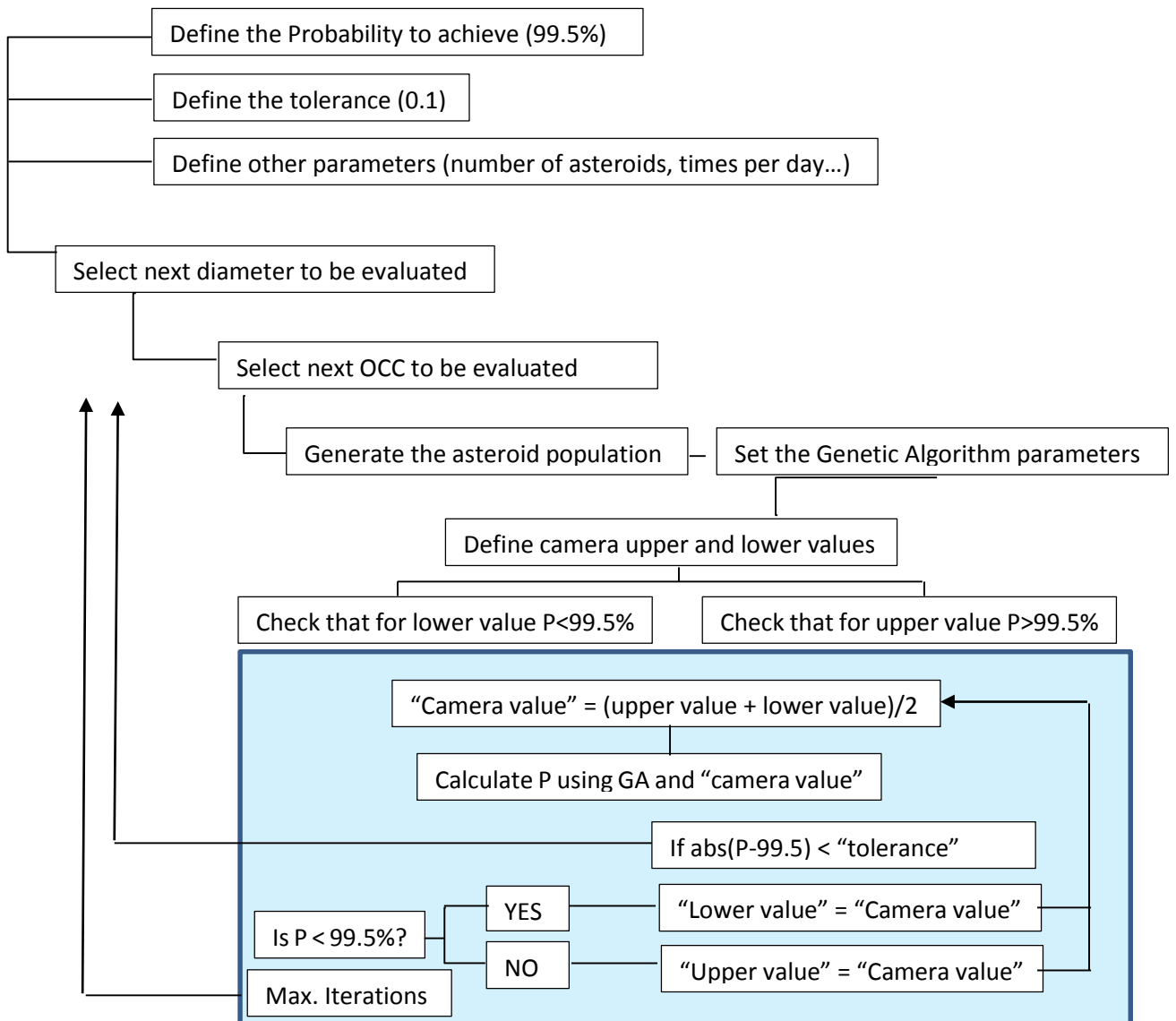
It has been confirmed too that OCC 4 and 5 have to be studied deeply to find out which trajectories can maximize the probability of detection for asteroids with small diameter.

#### 4.4 Study 3: Camera value

The aim of this study is to assess the limiting visual magnitude of the camera, “camera LVM”, (which indeed means the technology applied to the camera) required to reach a set probability. The idea is to find out the camera LVM required for a selected diameter values and for each OCC. In the case that is shown the probability that will be achieved is 99.5% and the diameters that will be evaluated are 5, 10, 15 and 20 meters.

In this study, the OCC value from 0 to 5 is considered. As in the previous studies, it is important to keep in mind that when an OCC is considered (for example OCC=1), the Matlab creates a virtual uncertain population within the maximum uncertainties values, which means that some of the asteroids are very close to OCC=2.

The algorithm used to find the results is shown next:



The simulations parameters:

Simulation parameters	
Number of asteroids considered	2000
Asteroid diameter	5, 10, 15 and 20 meters
OCC range	From 0 to 5
Close Approach Duration	5 months
Probability to achieve	99.5%

Table 10 Simulations parameters study 3

With the previous algorithm Figure 31 is obtained.

In Figure 31 two values are set:

- the value of LMV = 15 corresponds to the current cameras that are on board spacecraft.
- The value of LMV = 20 is close to the cameras used in terrestrial telescopes.

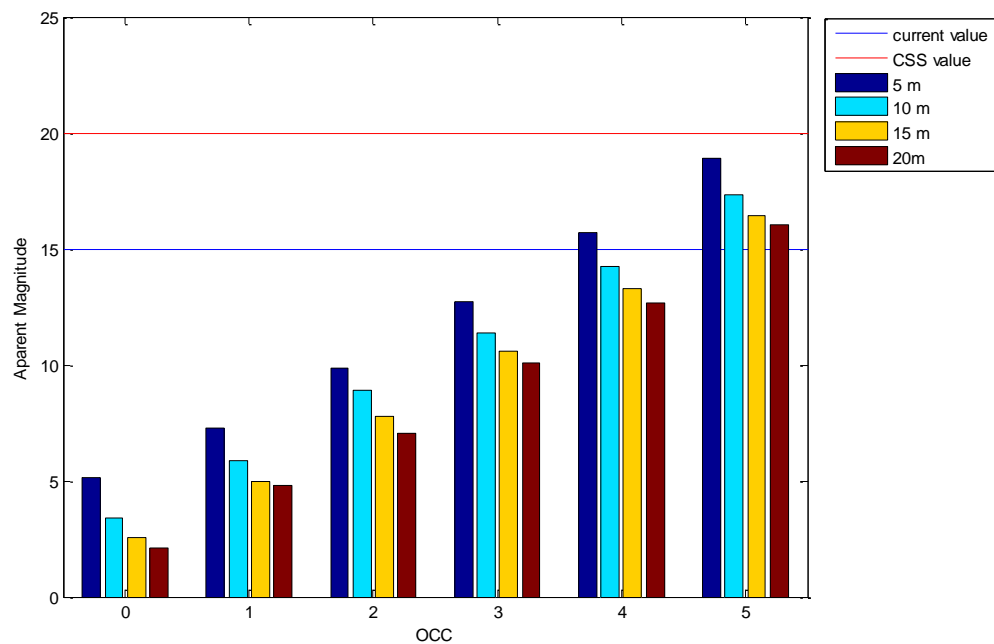


Figure 31 Camera LMV required for different asteroid diameter and OCC

It is possible to conclude that, with current technology, it is possible to launch missions to:

- OCC 1, 2 and 3.
- OCC 4 and diameter around 7 meters (or high).

In addition, the required technology for a mission to an asteroid of OCC 0 and diameter 5 meters is similar to that required for an asteroid of OCC 1 and diameter 20 meter.

If, in the near future, the camera LMV reaches 20 the amount of possible missions is increased and all asteroids between OCC 0 and 5 and diameter larger than 5 would be accessible.

#### 4.5 Study 4: CAD influence on detectable asteroid dimensions

In previous studies it has been observed the influence of four parameters: the OCC, the CAD, the asteroid diameter and the camera used in the mission.

For all of them, the impact on the probability of detection has been assessed and it has been proved the strong influence of each one except for the “Close Approach Duration” parameter, which seems to have less importance than the other three. On the other hand, it has been observed that the influence of the close approach duration depends on the case that is being studied. For that reason this fourth study is performed. In this case, a deeper analysis of the number of months used is developed.

Before starting any simulation, the expected result is to find a particular relation between the duration of the close approach phase and the asteroid diameter. It seems obvious that for asteroids with smaller diameter the close approach will last more time due to the fact that the amount of area that will be swept is larger (in order to approach the asteroid the required distance to detect it). So, Figure 32 shows an example of the expected result:

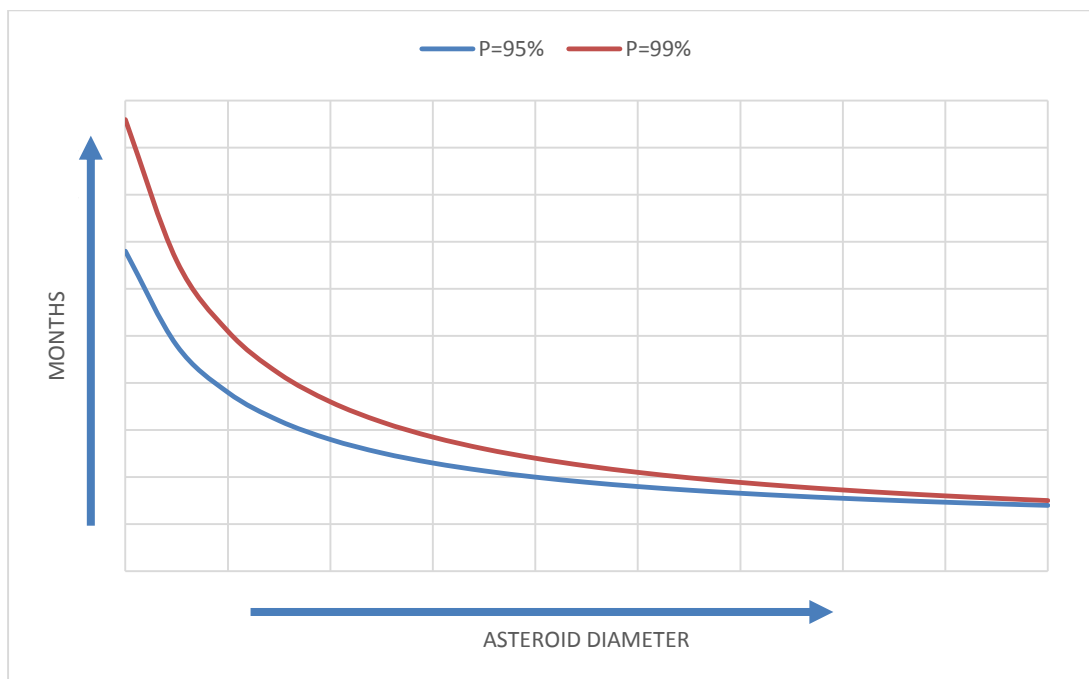


Figure 32 Expected results study 4

The number of months is also a very important factor to assess the mission feasibility: even if it is possible to launch a mission to a specific asteroid with a probability

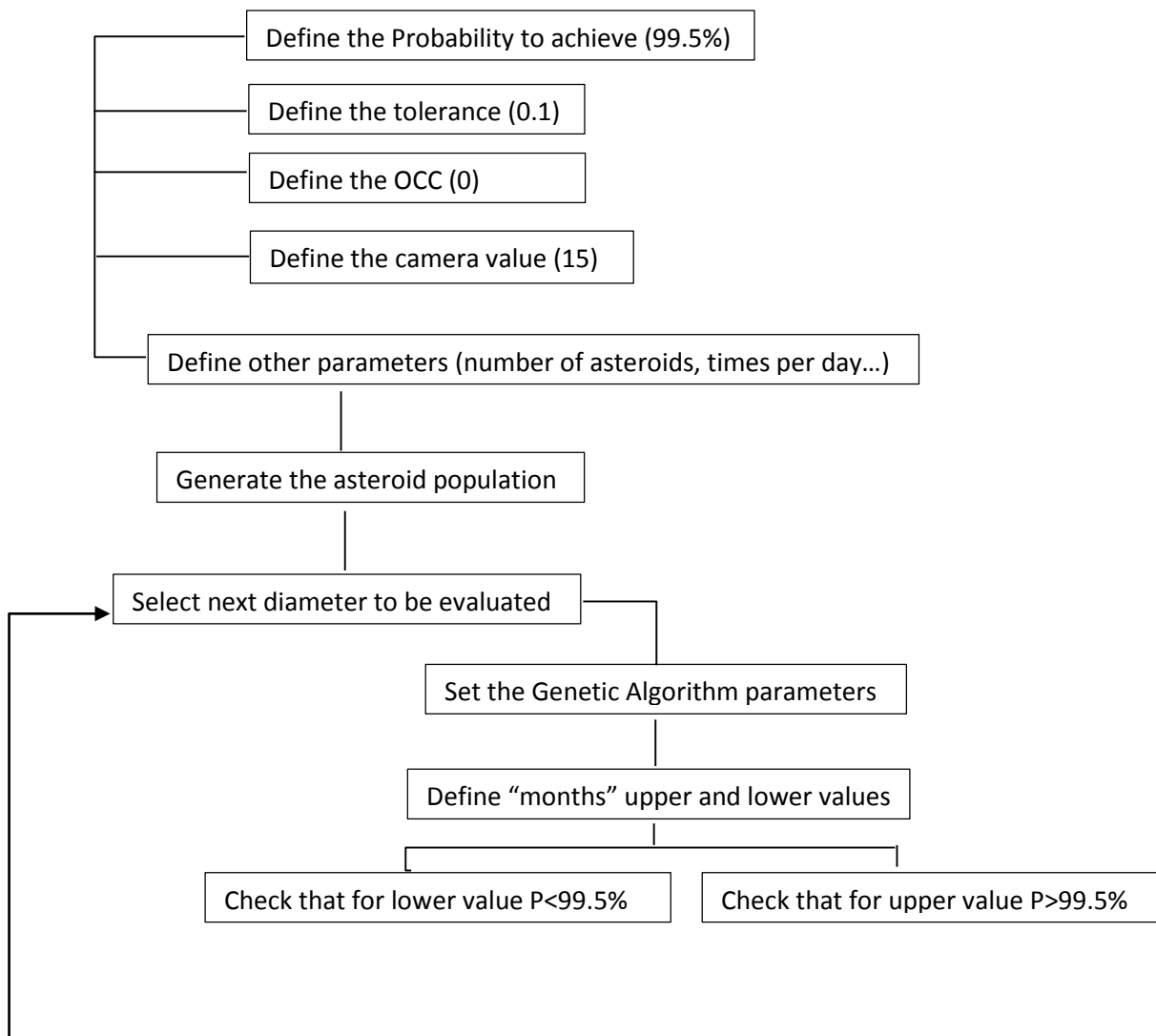
of detection acceptable, the duration of the close approach could be very long and that could cause the mission to be rejected.

The parameters used in the simulation are shown in Table 11:

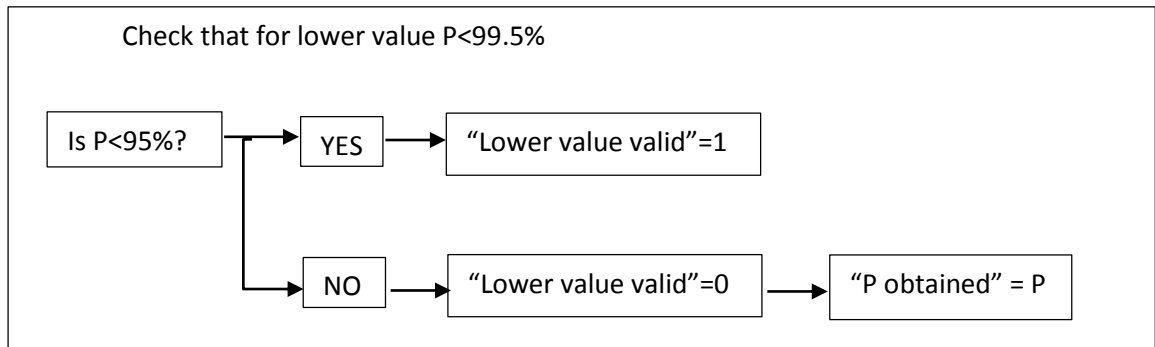
Simulation parameters	
Number of asteroids considered	2000
Asteroid diameter	10, 20, 50 and 100meters
OCC range	-
Probability to achieve	99,5%

Table 11 Simulation parameters study 4a

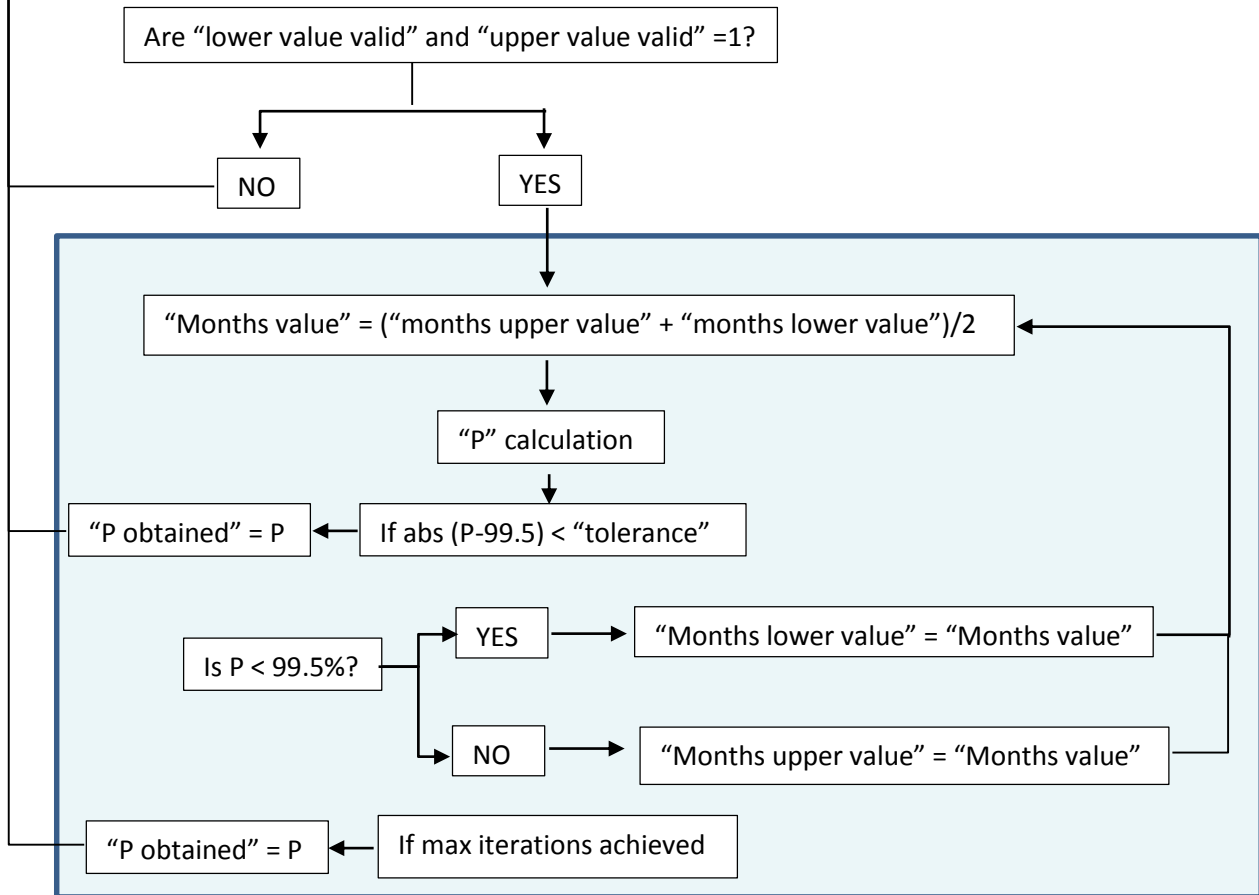
The algorithm used in this case is similar to the one utilized in the previous study. In this case, because of the complexity of the results obtained and in order to make easier the post simulation analysis, some control variables have been added. The algorithm is shown to understand the function of this variables:



In 4.4 we were sure that the upper and lower camera values provide a probability value higher and lower than 99.5% respectively. Unfortunately, we can make the same assumption in this study. For that reason two new variables are introduced, which will help us to better understand the final results obtained in the simulation. These two variables are called “lower (upper) value valid” and have the same length than the array of asteroid diameters. For each diameter, every time that the lower or upper value are checked the result of this verification is stored in this variable. It is shown the example for the lower value but it is extendible to the upper one:

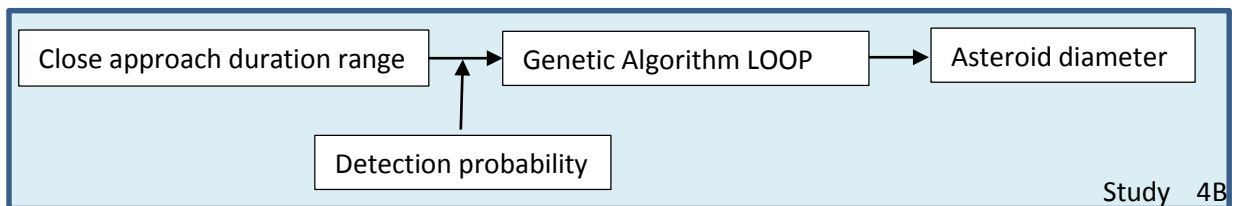
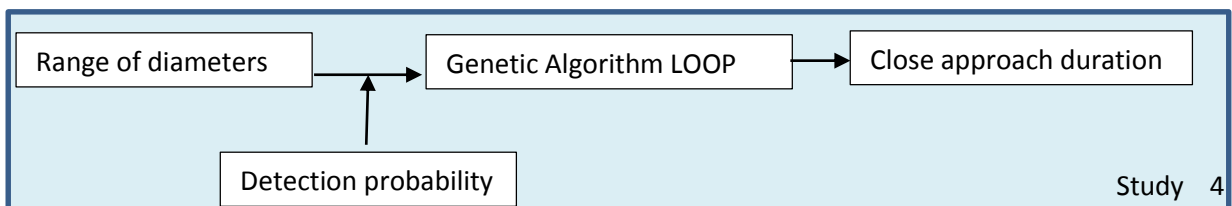


Then, before starting the loop to find the exact number of months that corresponds to a probability of 99.5%, a previous check is performed:



After performing the simulation it was observed that either the “Months lower value” or the “Months upper value” are not suitable for the simulation and it is very difficult to establish the upper and lower limits correctly. As the dependency between the diameter and the close approach duration has not been shown, the strategy has been changed to find out correct results.

The algorithm is the same that was used in the previous simulation but now the close approach duration range is selected and genetic algorithm is used to find the diameter that allows the required probability of detection.



In this simulation not only the asteroid diameter is shown. In addition, some extra data is stored to make a further analysis.

As was shown in page 62 where the algorithm is presented, in each loop the probability “P” is calculated and then compared to the reference (99.5%). If the difference is less than the tolerance, the loop is stopped and the “number of months” (“Asteroid diameter” in case of 4B) is stored.

Now, the results of the last population used in the GA is also stored together with the scores of each individual. Every time the target probability is reached, a new structure is added to the “Result” variable. The structure contains two fields, one containing the 5 design variables required for each member of the population and other field containing the score of the individual. This structure of information will be very helpful to analyse the different orbits obtained in the next study.

After performing the corrected simulation, the following values are obtained. The asteroid diameter is shown in meters:

		Close approach duration (months)							
		1	2	3	4	5	6	7	8
OCC	0	1	1	1	1	1	1	1	1
	1	1	1	1	1	1	1	1	1
	2	1,14	1	1	1	1,08	1	1	1
	3	5,5	3,56	3,48	3,25	4,01	3,16	2,41	2,13
	4	25,47	14,59	13,23	13,8	12,78	13,14	9,61	8,02
	5	105,12	71,66	60,5	60,5	60,5	49,34	40,86	32,61

Table 12 Asteroid diameter for P=99.5% (From 1 to 8 months)

		Close approach duration (months)							
		9	10	11	12	13	14	15	
OCC	0	1	1	1	1	1	1	1	
	1	1	1	1	1	1	1	1	
	2	1	1	1	1	1	1	1	
	3	2,07	2,13	2,03	2,13	2,13	2,13	1,75	
	4	8,25	7,57	8,11	8,36	7,85	8,25	7,5	
	5	30,75	32,61	31,68	30,75	30,75	31,64	30,75	

Table 13 Asteroid diameter for P=99.5% (From 9 to 15 months)

Table 12 and Table 13 show the minimum diameter in order to obtain a probability of detection of 99.5%. That means that if an asteroid with OCC=4 has to be detected with a close approach duration of 1 month, the asteroid diameter must be larger than 25.47 meters. If the close approach duration is increased to 9 months the asteroid diameter can be reduced to 8.25 meters.

In 4.5 it has been confirmed that the close approach duration has a strong influence if the next conditions are satisfied:

- OCC value is higher than 2.
- The close approach duration in months is less than 8 months approximately.

It can be observed to that there are small but significant variations in the asteroid diameter. Probable due to the difficulty in the genetic optimization.

In order to understand why both previous conditions are required to note the influence of the close approach duration, the next study is performed, where the results are analysed case per case.

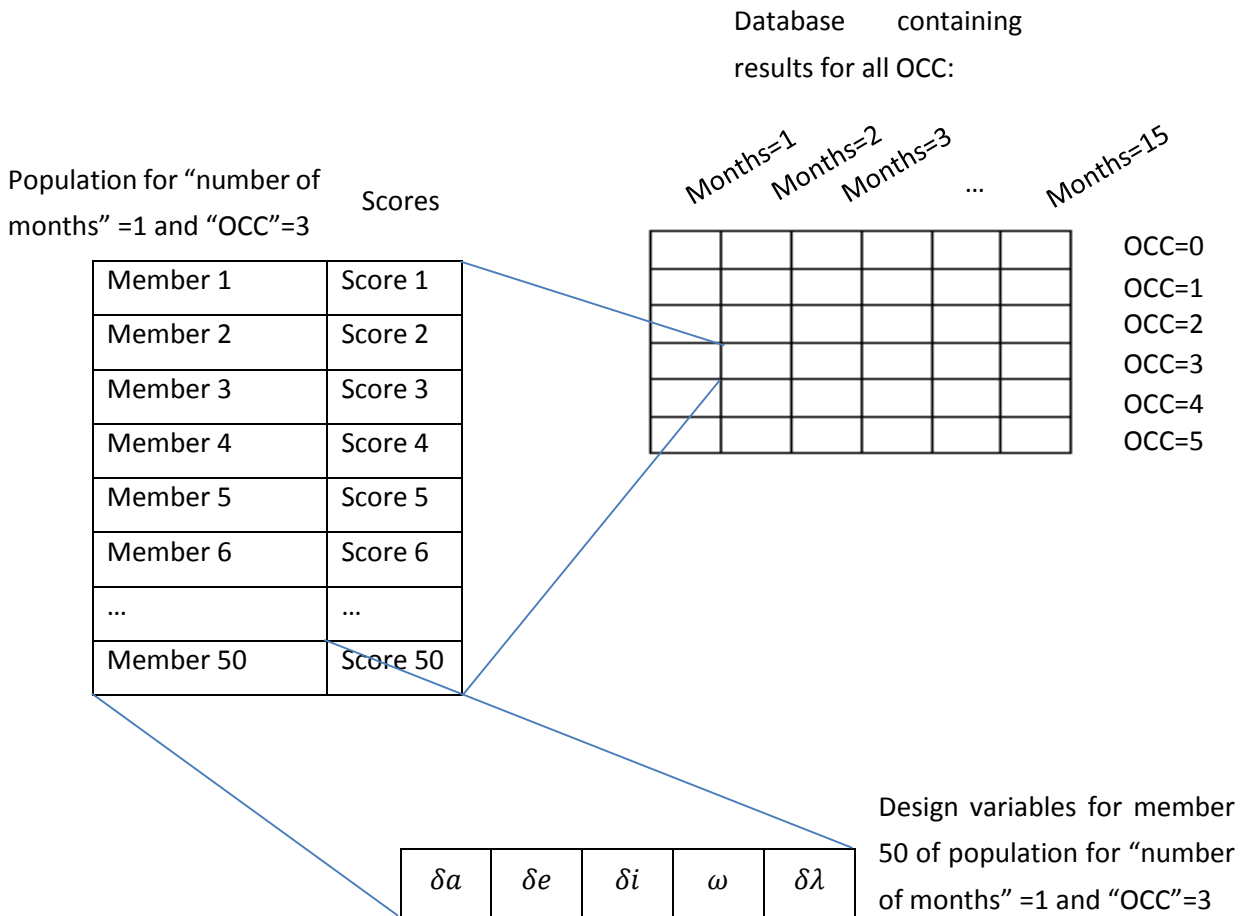
### 4.6 Study 5: Results analysis

This study shows the analysis of the results obtained in the study 4, so study 5 target represents the main goal of the project, i.e. to assess feasible missions and show the best trajectory in each case.

4.6 is divided in 5 different parts, each part can be used separately but they are interconnected due to the fact that each part creates variables that are used in the others.

#### 4.6.1 Part 1: Data loading

The simulation performed in 4.5 is so heavy that the required time to perform it is close to one week. In order to avoid the long waiting, the code was subdivided in six different parts (one for each OCC) and the simulation has been run in parallel. So, for each simulation a vector is generated containing the data for every CAD (from 1 to 15 months). Every vector component contains the final Population obtained in the genetic algorithm and the scores for each member of the population. The six vectors (one for each OCC) are placed together in a global array that will be used as a database and will be accessed during the next parts.



Before adding the vector to the database it is checked if the upper limit or the maximum number of iterations have been achieved using the control variables in order to avoid the loading of non-correct results.

#### 4.6.2 Part 2: Parameters selection

Once the database is completed, the selection of the parameters is performed. In this part, the code allows to select:

- Orbit Condition Code (OCC).
- Close approach duration (CAD).

These two parameters are available because the idea is that the engineer that wants to select a trajectory can easily introduce the OCC of the target asteroid and the close approach duration that can be assumed in the mission.

#### 4.6.3 Part 3: Ellipsoid of uncertainty

Before analysing the spacecraft trajectory, it is key to know the ellipsoid of uncertainty, this ellipsoid represent the potential area where the asteroid could be placed.

In a first attempt to draw the ellipsoid the following measures were used:

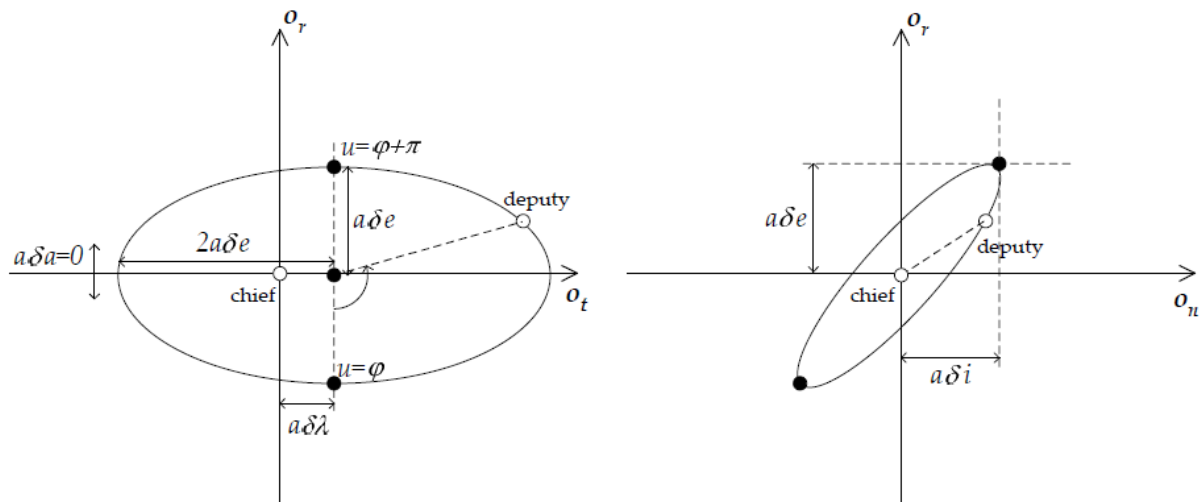


Figure 33 Ellipsoid of uncertainty measures

Note that the axis are presented with the Hill reference frame coordinates. The  $o_r$  stands for the radial component,  $o_t$  stands for the tangential component (direction of motion) and  $o_n$  represents the out of plane component.

However, due to the randomly generated values that have been used along the study it was found that the best way to plot the ellipsoid was using the maximum values obtained after the random generation of the virtual uncertain population. With that method, the 99.5% of the asteroid virtual population should be inside the ellipsoid, with a higher concentration in the centre.

In the drawing, the ellipsoid is plot with a determined grade of transparency in order to make easier the visualization of the virtual uncertain population (note it was shown in section 3.5):

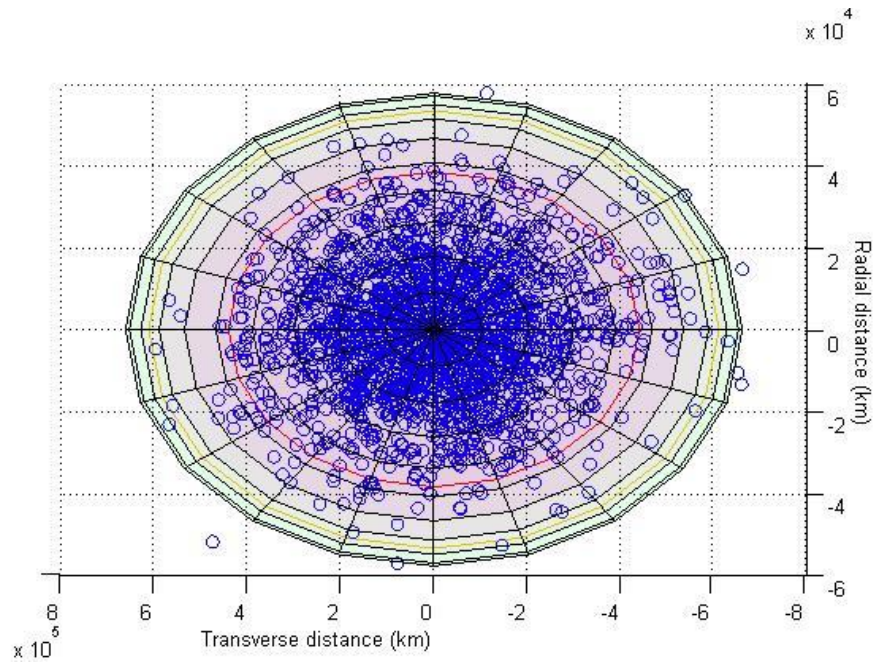


Figure 34 Ellipsoid plot (top view)

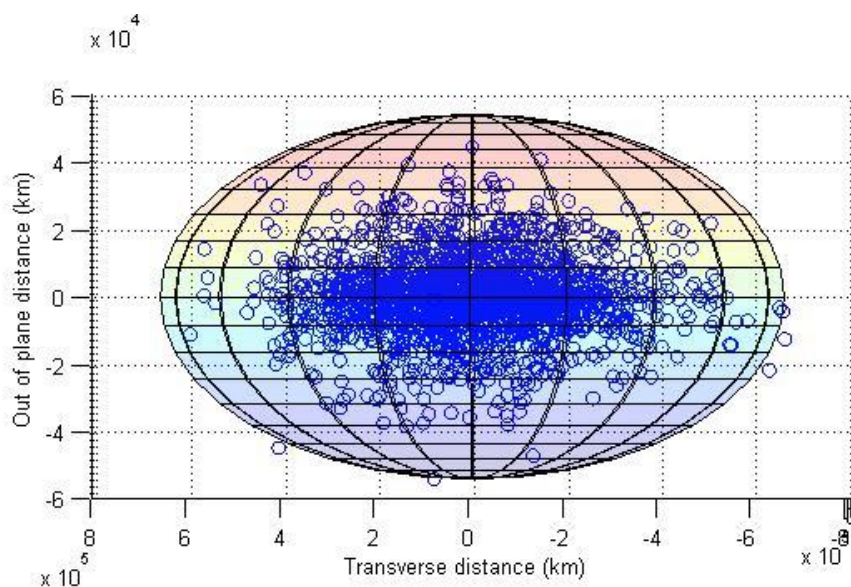


Figure 35 Ellipsoid plot (front view)

#### 4.6.4 Part 4: Optimum spacecraft and orbit analysis

Before analysing a specific case, it can be helpful to see the result from a global point of view. Doing that, it can be observed the validity of the results obtained.

The first step is to assess if the optimization is satisfactory. That means to observe the spacecraft population composition at the last generation of each case. In section 4.6.1 it was shown the structure of data that was generated after performing the simulations. It was explained that the entire spacecraft population and the members score was stored for each case. At this point, this data is used in order to know how many different members of the last generations have reached the best score:

		Close approach duration (months)														
		1	2	3	4	5	6	7	8	9	10	11	12	13	14	15
OCC	0	35	39	43	41	48	46	45	48	48	47	47	47	48	44	47
	1	19	19	25	22	21	28	34	30	33	37	42	38	40	36	37
	2	1	4	2	1	4	1	1	3	4	3	2	5	5	6	4
	3	5	2	2	4	1	1	3	3	1	3	1	1	2	2	3
	4	5	3	4	3	2	5	1	3	6	4	2	2	2	5	1
	5	1	10	6	8	1	2	1	8	1	2	4	1	1	4	3

Table 14 Number of different members into the final population that have reached the maximum score

It is important to take into account that the population size is 50 members. For that reason, if more than 15 different members have achieved the maximum score (shown in red), it is considered that reaching the maximum score is relatively easy. This fact appears for OCC 1 and 2 and means that due to the small size (compared to higher OCC) of the uncertainty ellipsoid, multiple solutions are possible. The cases where more than 5 members reach the maximum score are shown in yellow. For these cases an optimization may be required, but the number of solutions available is relatively high. Finally, the green colour is used for the cases where less than 5 members reach the maximum score. These cases shows that an optimization is required. Despite this analysis, it can be observed that the yellow distribution is scattered along all the table. In order to better understand the results, Table 15 is included.

To make a further analysis it is checked for each case how many different members reach the maximum score but, in this case, only the members that represent more than 10% of the population are included. That means that, in Table 15, only the members that are repeated more than 5 times are included. This analysis is made to distinguish if there are predominant or random solutions.

Cases where no members are found indicate that the solutions are randomly found (shown in red). In contrast, for the cases where 1 or 2 members are found indicate that it exists a predominant solution (shown in green).

		Close approach duration (months)														
		1	2	3	4	5	6	7	8	9	10	11	12	13	14	15
OCC	0	0	0	0	0	0	0	0	0	0	0	0	0	0	0	0
	1	0	0	0	0	0	0	0	0	0	0	0	0	0	0	0
	2	1	1	0	0	1	1	0	0	0	0	0	0	0	0	0
	3	1	1	1	1	1	0	1	0	0	1	0	0	1	1	2
	4	1	1	1	1	1	1	0	2	2	1	1	1	2	1	1
	5	1	1	1	1	1	1	0	1	1	0	2	0	1	1	1

Table 15 Number of different members into the final population that have reached the maximum score and represents more than 10% of the total population

In a first approach, it can be observed that the blue highlighted zone is especially interesting due to availability of valid solutions. In order to know the reason, it will be very helpful to analyse the different trajectories obtained for each case.

#### 4.6.5 Part 5: Trajectory representation and analysis

In this section the most representative trajectories are plotted and a further analysis is performed in order to understand the limited validity of the results obtained in the simulations.

First of all, the plot format is introduced. Four views are represented: one isometric view that covers the general orbit, one front view that shows the orbit in the out-of-plane and transverse coordinates (z-y plane), one lateral view that includes the out-of-plane and radial coordinates (z-x plane), and one top view composed by the radial and transverse coordinates (x-y plane). The ellipsoid transparency allows to see the entire trajectory.

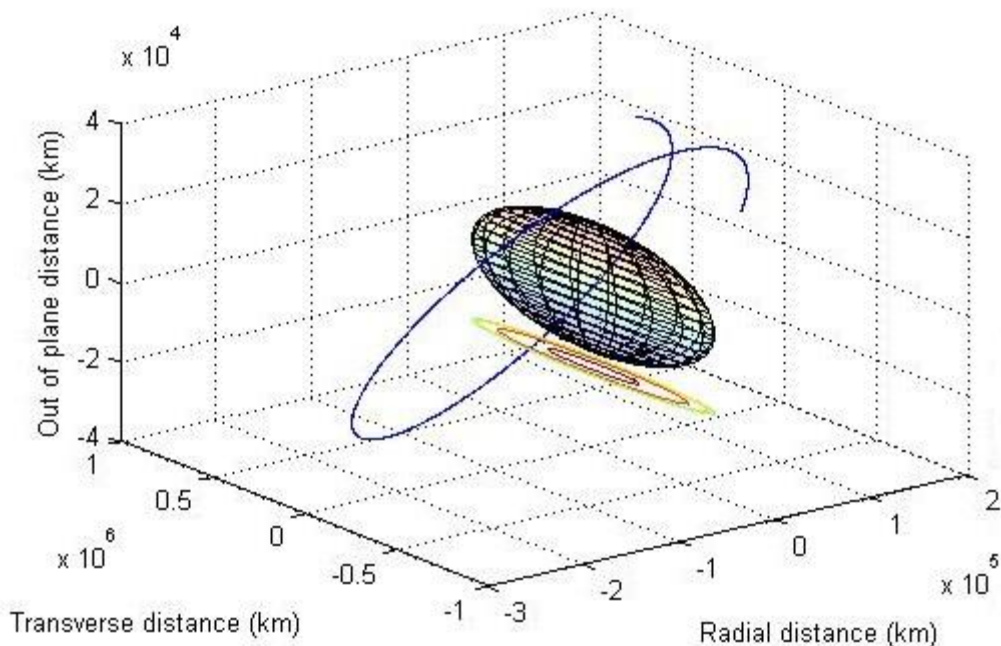


Figure 36 Trajectory plot for OCC=4 and CAD = 14 months (Isometric view)

The first conclusion that can be extracted is that the uncertainty ellipsoid is actually closer to a cylinder. It can be noticed that, due to the drift caused by the asteroid  $\delta t$ , the transversal distance is one order of magnitude larger than the radial distance, and the latter is also one order of magnitude larger than the out of plane distance. So, the uncertainty region is almost flat and larger in the transversal direction.

The three projected views in Figure 37 allow to see the spacecraft movement in each axis. It can be seen that in a first approach, the spacecraft sweeps the uncertainty zone in the three coordinates:

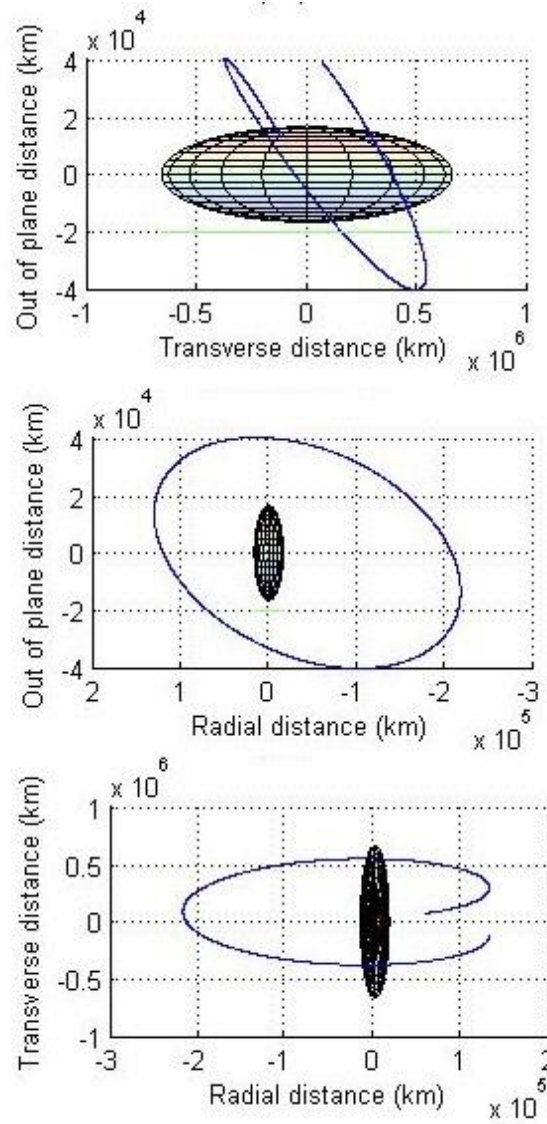


Figure 37 Front, lateral and top view for OCC=4 and CAD = 14 months

Once we have the entire trajectory view another question arises: Which are the most important parts of the trajectory? It is obvious that all positions on the trajectory are not equally interesting, there will be points where the spacecraft has a higher likelihood to detect the asteroid and there will be points where the uncertainty ellipsoid is not visible to the spacecraft.

#### *Accumulated probability*

In 3.4 it was introduced the idea that the best area to detect the asteroid is when the spacecraft is placed between the Sun and the asteroid but the goal of this subsection is to show exactly in which zones the probability is increased and which zones are not relevant for the asteroid detection. For this reason a new variable is introduced: the accumulated probability.

Now, while plotting the spacecraft trajectory, the number of asteroids in the virtual uncertain population that have been detected is computed and stored in the new variable. Dividing the number of virtual asteroids detected by the total virtual population it is possible to compute the probability to detect the target asteroid. The accumulated probability is represented together with the trajectory in Figure 38.

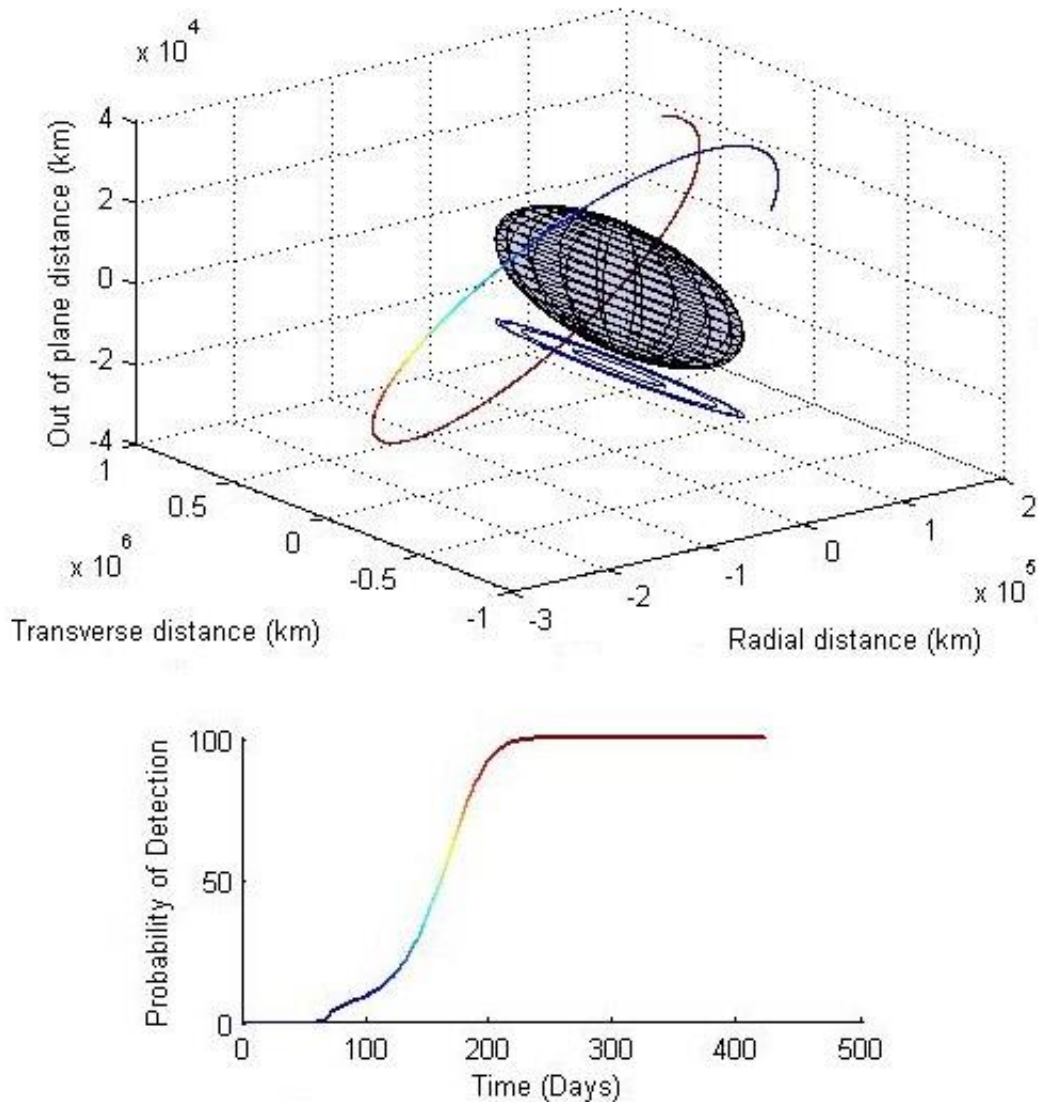


Figure 38 Accumulated probability for OCC=4 and CAD = 14 months

The same case as before has been used to show the importance of knowing the accumulated probability along the track. Thanks to this tool it can be concluded that in the first (from day 1 to 70) and the last (from day 250 to 420) sections of the trajectory the spacecraft is not detecting any new asteroid from the virtual uncertain population. In addition, the period when the spacecraft is detecting new virtual asteroids lasts only about 6 months ( $250 - 70 = 180 \text{ days} = 6 \text{ months}$ ). The three additional views are used in

order to confirm that these 6 months correspond to the part of the trajectory when the spacecraft is placed between the Sun and the uncertainty ellipsoid:

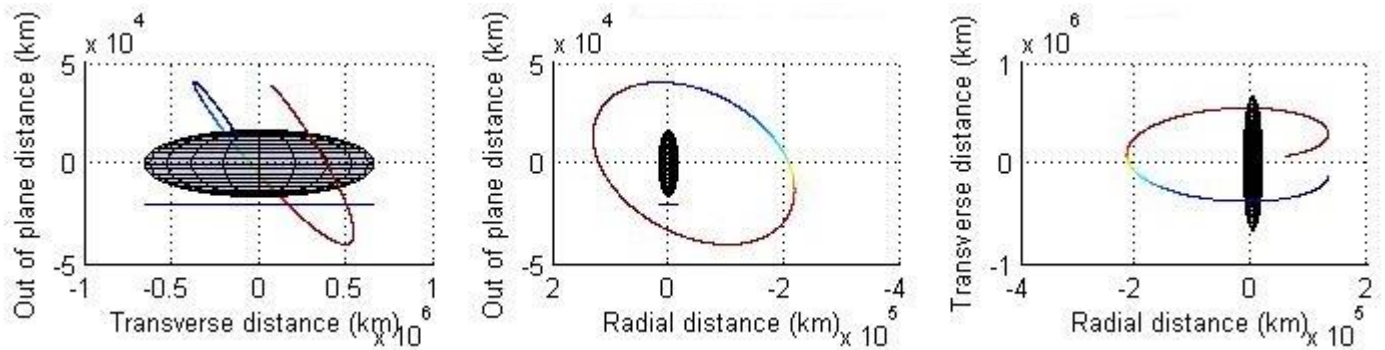


Figure 39 Front, lateral and top views with accumulated probability for OCC=4 and CAD = 14 months

In this case the most relevant is the top view. It can be observed that the trajectory starts from behind the ellipsoid, where the asteroid is not visible. Then the spacecraft moves until it is placed between the Sun and the ellipsoid. During the next 6 months the spacecraft moves along the transversal coordinate to cover all the ellipsoid and detect the asteroid with 99.5% probability.

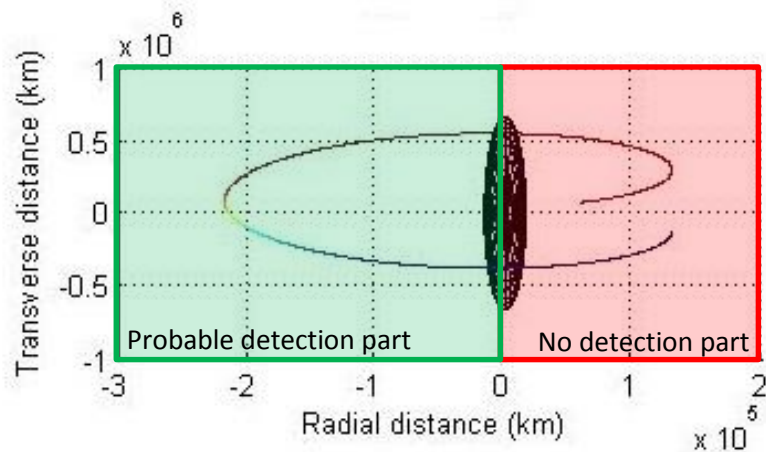


Figure 40 Top view with orbit parts differentiation

To conclude, 6 months are enough to sweep the ellipsoid in the transversal distance, which means detect the 99.5% of the asteroid population. So, it is acceptable that the results are not improved for close approach duration higher than 6 months. In other words, if more than 6 months are used, there will be a part of the trajectory where it is not possible to detect the asteroid.

To gain further insight about how the spacecraft detect the asteroid and to confirm the statement made in this section, it was thought to include also the detection zone that was developed in 3.4 into the trajectory plots.

*Detection zone plot*

The detection zone is the area that represents the field of vision of the spacecraft camera. It is considered that if the asteroid is placed inside this area, it will be detected. As was seen in section 3.4 the detection zone dimension is proportional to the asteroid diameter, so, for each case studied, a different detection zone is used.

The detection zone has been plotted in the three auxiliary views. OCC = 4 and a close approach duration of 2 months has been represented and, for simplicity, it is shown the detection zone at the beginning and at the end of the trajectory:

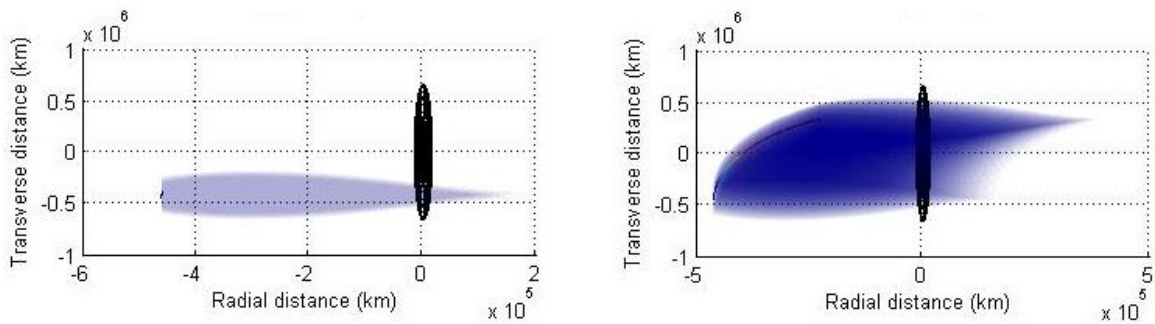


Figure 43 Top view with detection zone plotted

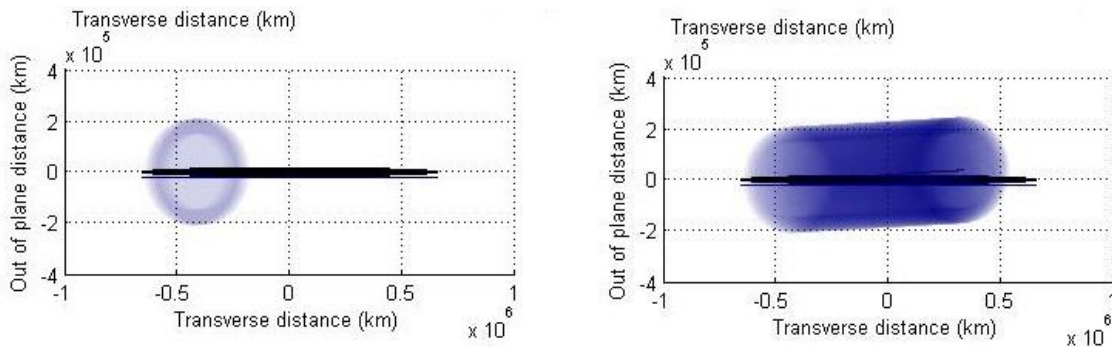


Figure 42 Front view with detection zone plotted

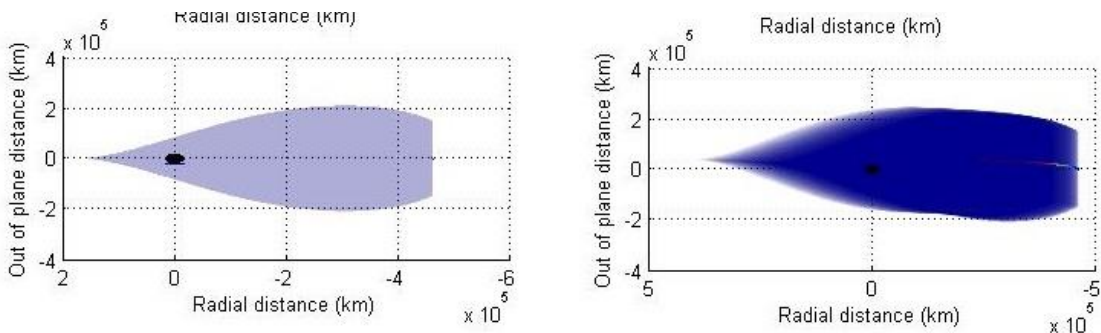


Figure 41 Lateral view with detection zone plotted

It is seen that the ellipsoid is placed inside the detection zone since the first moment in both radial and out of plane coordinates as per Figure 41. In contrast, according Figure 42 and Figure 42, for the transversal coordinate it is required to sweep all the ellipsoid.

To sum up, the previous plots confirm the conclusion obtained with the accumulated probability plot: if high probabilities are desired (i.e. 99.5%) the close approach duration required will last less than 6 months due to the fact that the spacecraft trajectory will sweep the ellipsoid in the transversal direction during this time.

In addition, in reference to the conclusion obtained in 4.6.4 and having confirmed the importance of the shorter CAD the ANNEX III: Study 4b is developed.

#### 4.7 Study 6: Optimal approaches for lower asteroid diameters

At this level of the study the major part of the initial questions have been answered:

- It has been presented the detection probabilities depending on OCC, asteroid diameter and close approach duration (Studies 1 and 2).
- It has been studied the influence of the camera LMV (Study 3).
- It has been presented the minimum diameter that can be achieved for each OCC and close approach duration (Study 4).
- It has been analysed the trajectories that give 99.5% of probability of detection (Study 5).

At section 4.6.5 it was seen that, in order to reach a probability of 99.5%, the trajectories swept the ellipsoid in the transversal direction but, at this point, one question arises: what would happen if smaller asteroids are considered? It is clear that it will not be possible to achieve the 99.5% but, which would be the best strategy to detect the asteroid? 4.7 has been developed to gain further insight about this question.

In 4.5 it was analysed the target asteroid dimensions for CAD from 1 to 15 months. Now, it has been investigated what happens if the close approach duration is increased until 3 years in order to detect asteroid with OCC = 5 and diameter = 4 meters:

Simulation parameters	
Number of asteroids considered	2000
Asteroid diameter	4 meters
OCC	5
Close Approach duration	12, 18, 24, 30 and 36 months
Probability to achieve	-

Table 16 Simulation parameters study 6

Figure 44 shows the probability variation depending on the close approach duration, which covers from 1 to 3 years.

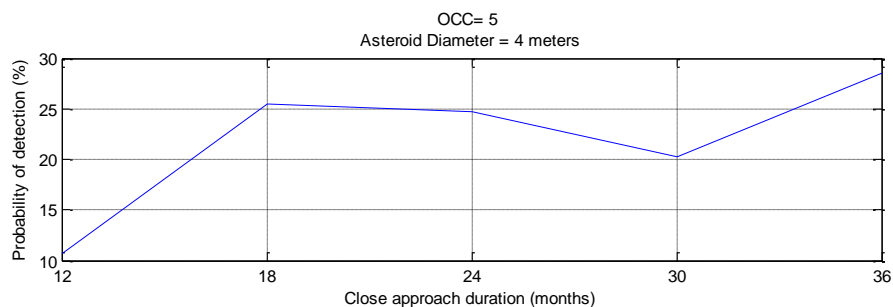


Figure 44 Probability of detection vs CAD for OCC = 5 and diameter = 4 m

Despite the duration can make the mission not feasible, it is important to understand what happens if the close approach is extended to such values. First of all, it is possible to see that the probability of detection increases if the close approach lasts more.

In reference to the trajectory, it was expected to find similar strategies to the previous studies: the spacecraft would sweep the uncertainty region in the transversal coordinate. To confirm so, the plot is made together with the accumulated probability along the track.

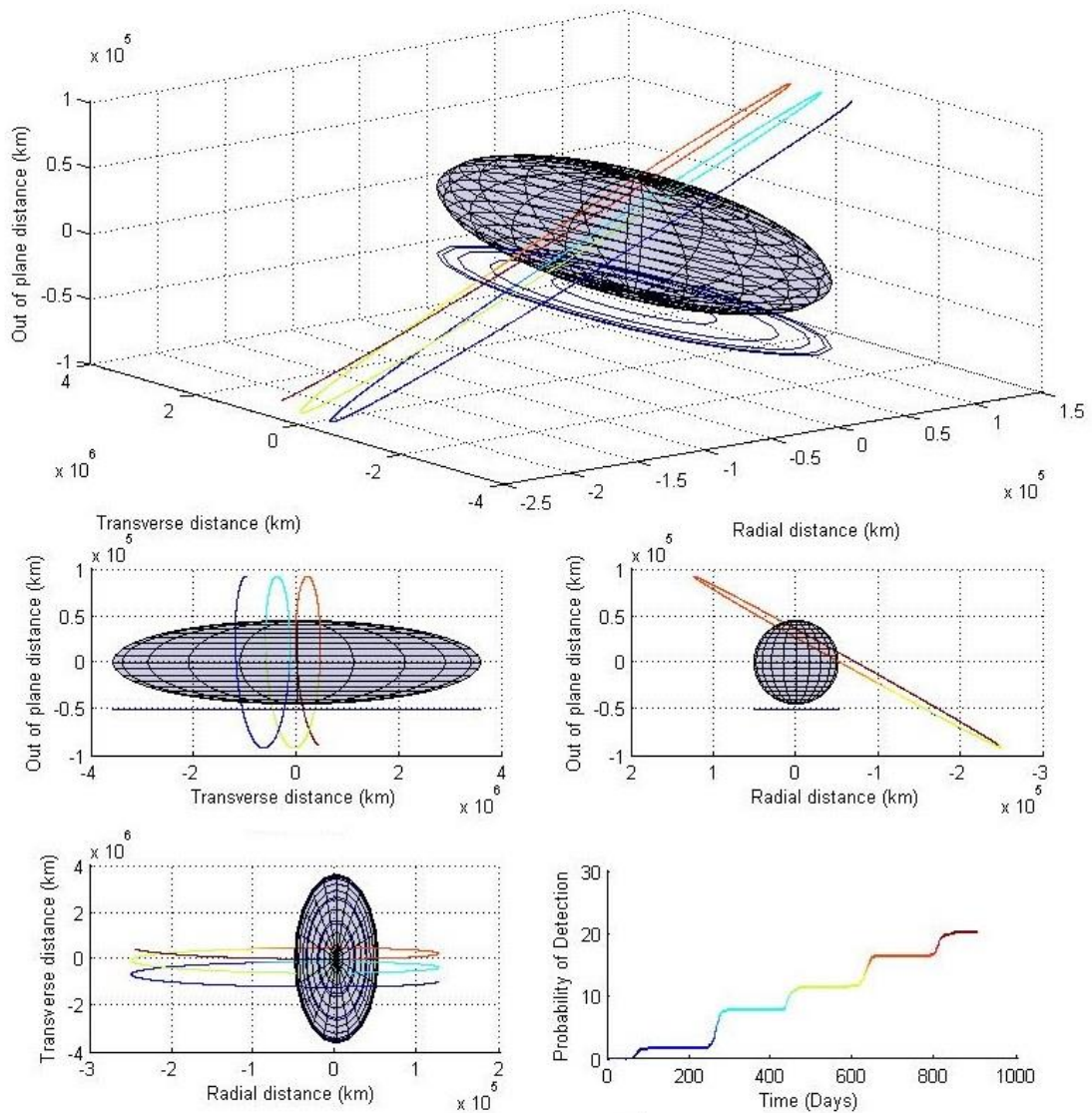


Figure 45 Trajectory plot for OCC = 5, diameter = 4 m and CAD = 30 months

In Figure 45 it can be confirmed that the spacecraft sweeps the transverse distance and every time the spacecraft undergoes the part of the orbit where it is placed between the Sun and the asteroid, the probability of detection is considerably increased. It is key to notice that the transversal distance covered is approximately 2.000.000 Km, almost ten times higher than the radial distance covered.

In conclusion, it can be stated that the uncertainty region is similar to a narrow cylinder and the spacecraft perform a spiral along the transversal coordinate, increasing the chances to detect the asteroid when the spacecraft is placed between the Sun and the asteroid.

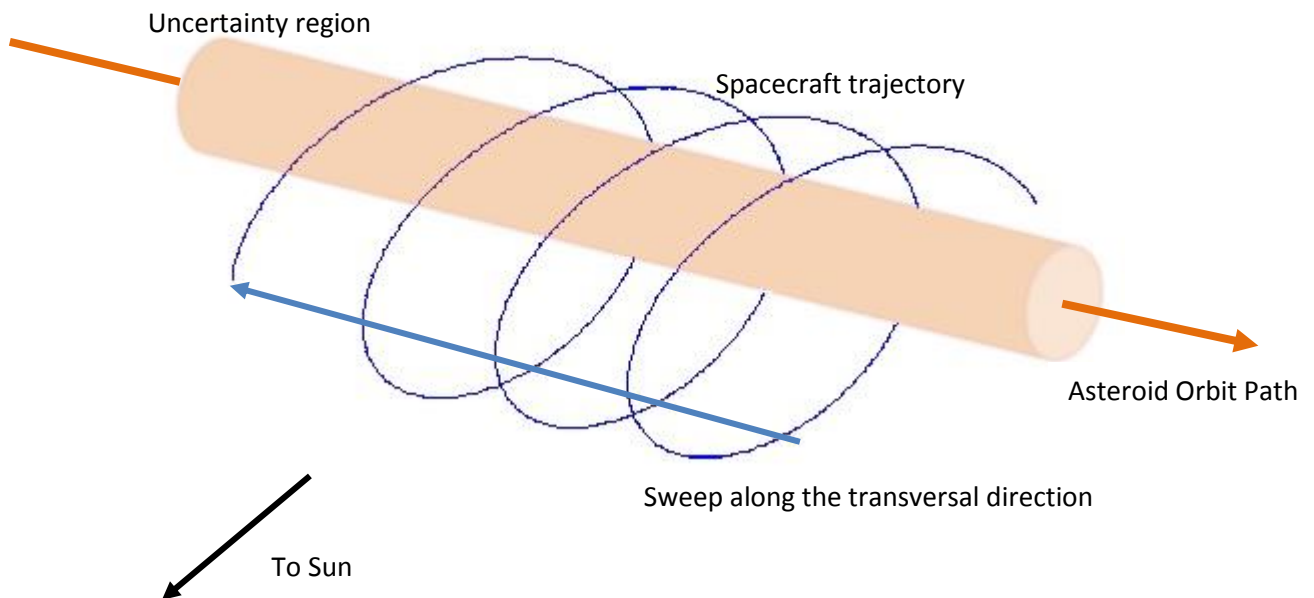


Figure 46 Schematic illustration of the optimal trajectory

## 5. Conclusions

---

Along the project 5 different studies have been performed, using the models that were previously developed.

The main goal was to create a tool to assess the feasibility of a particular mission. The program not only helps to see if a mission can be developed it also allows to know which would be the best trajectory to reach the target asteroid and which are the most important phases of the path. During the development of the project some facts have been highlighted due to the impact observed in the results.

The first conclusion is that the technology regarding the detection camera is a key factor. In 4.4 it was demonstrated that a slightly increase in the camera LVM value can allow to detect a wider range of asteroids (smaller diameters, larger OCC or both). This parameter is related to the level of technology available at the moment of the launch, for that reason, a higher value than current cameras can be selected considering that the spacecraft would be launched in 10 or 20 years.

The second conclusion also remarks the importance of the Orbit Condition Code (OCC). A high value of OCC is equivalent to say that the target asteroid will need to have better known ephemerides to meet an acceptable probability of success.

Another point that has to be emphasized is the importance of the close approach duration. When the project was started the number of months devoted to the close approach was thought to be a very relevant factor, but after performing the last studies it has been proved that the factor is not so outstanding even if it can play a decisive role for lasting missions.

To sum up, the project has established a reference to assess mission feasibility depending on OCC, asteroid diameter and technology used in the camera. Besides, the CAD has been proved to be important in order to improve the detection probability and to understand how the target asteroid has to be approached.

A future study that will help to understand if possible mission to small asteroids with high OCC can be carried out is to perform an assessment of the trajectories that will be required if 2 spacecraft are involved in the mission. The main goal will be knowing if the probability of detection is increased to an acceptable level.

In addition, during the development of this project, the scientific community has made its own studies, highlighting the use of low-thrust manoeuvres. That is, use power to

modify the spacecraft velocity during the trajectory in order to sweep the area of interest (zone between the uncertainty ellipsoid and the Sun) instead of orbiting around the uncertainty region. The strategy presented by other researchers is more time efficient than the ballistic trajectory presented in this study. On the other hand, a low-thrust manoeuvre implies the requirement of carrying out fuel and developing propulsion systems.

## 6. Acknowledgements

---

The acknowledgments are for everyone that has made possible this experience.

First of all, I would like to thank Elena and Joan Pau, the main responsible of the development of the project. Elena has been a reference of professionalism and thoroughness, and has teach me one of the best subjects in the curriculum, opening a window to the science related to Space. I have to thank her also for introducing me to Pau, currently researcher at Cranfield University.

Without any doubt the person most important in this project is Pau. I have worked hard to understand the physics, develop de models and perform the simulations but without his help nothing of this would have been possible. Along the project development Pau has shown a great teacher spirit, solving my doubts whenever I consulted him. Besides, his expertise with Matlab has been very helpful in the key parts of the project.

During the last stage of the Master Degree I have been working in Volotea, a young airline with a great future. It has been very challenging to finish the last subjects while starting such an experience. I would not have done that without the help of my workmates, who has always support me switching shifts and allowing me to assist the required lessons. I would also like to highlight the collaboration of my boss, Sara, who I thank for taking into consideration the stressing situation I have passed through.

Last but not least, I would like to thank all the people and professionals I have met at UPC during the 5 years I have been studying in that University. Along these years I have met extraordinary people who have teach me not only the trickiest lessons but also great values and experiences I will never forget. Sadly, during these years I have also been a privileged spectator of the decline that the Spanish university system is suffering, every year closer to a company and further to the educational centre it should be.

## 7. References

---

- NASA (Ed.). (2014, October). *NASA*. Retrieved from [http://www.nasa.gov/mission\\_pages/WISE/spacecraft/](http://www.nasa.gov/mission_pages/WISE/spacecraft/)
- Airbus (Ed.). (2014, September). *Defense and Space*. Retrieved from <http://www.space-airbusds.com/en/news2/neoshield-protection-against-asteroid-impacts.html>
- Bowell, E. H. (1989). *Asteroids II*. Univ. of Arizona Press, Tucson.
- ESA (Ed.). (2014, October). *ESA/Our Activities/ Space Science*. Retrieved from [http://www.esa.int/Our\\_Activities/Space\\_Science/Rosetta](http://www.esa.int/Our_Activities/Space_Science/Rosetta)
- Hanslmeier, A. (2007). *The Sun and Space Weather*. In A. Hanslmeier. Springer.
- Harris, A., & Drube, L. (2010). *Mitigation of the NEO Impact Threat*. DLR Institute of Planetary Research. DLR Institute of Planetary Research.
- Hernandez, S., W. Barbee, B., Bhaskaran, S., & Getzandanner, K. (2013). *Mission Opportunities for the Flight Validation of the Kinetic Impactor*. *Planetary Defense Conference 2013*.
- Institute for Astronomy (Ed.), U. o. (2014). *Pan-Starrs*. Retrieved from <http://pan-starrs.ifa.hawaii.edu/public/>
- Johnson, L. (2010). *Near Earth Object Observations Program*. *Near Earth Object Observations Program Presentation to Planetary Defense Task Force*, (p. 4).
- Lewis, J. S. (1996). *Mining the Sky: Untold Riches from the Asteroid, Comets, and Planets*. In J. S. Lewis, *Mining the Sky: Untold Riches from the Asteroid, Comets, and Planets*. Addison-Wesley.
- LincolnLaboratory(Ed.). (2014). *Lincoln Laboratory, Massachusetts Institute of Technology*. Retrieved from <http://www.ll.mit.edu/mission/space/linear/>
- Lu, E. T., & Love, S. G. (2005). *A Gravitational Tractor for Towing Asteroids*. NASA Johnson Space Center .
- Mainzer, A., Bauer, J., Grav, T., Masiero, J., Cutri, R. M., Dailey, J., . . . Mar. (2011). *Preliminary Results from NEOWISE: An Enhancement to the Wide-field Infrared Survey Explorer for Solar System Science*. *The Astrophysical Journal*,, Volume 731, Issue 1, article id. 53, 13 ppg.

- Massimiliano Vasile, A. G.-P.-M. (2013). *Light Touch Challenge Analysis Final Report*.
- Melton, R. G. (2000). Time-Explicit Representation of Relative Motion Between Elliptical Orbits. *Journal of Guidance, Control and Dynamics*, 604-610.
- Morbidelli, A. (2005). Origin and Dynamical Evolution of Comets and their Reservoirs. In A. Morbidelli.
- NASA (Ed.). (2014, July 4). *Near Earth Object Program*. Retrieved from [http://neo.jpl.nasa.gov/cgi-bin/nhats?sdir=DESC;show\\_inst=1](http://neo.jpl.nasa.gov/cgi-bin/nhats?sdir=DESC;show_inst=1)
- NASA. (2014, September). <http://www.nasa.gov/>. Retrieved from [http://www.nasa.gov/mission\\_pages/asteroids/news/asteroid\\_initiative.html#.VB76JPI\\_uSo](http://www.nasa.gov/mission_pages/asteroids/news/asteroid_initiative.html#.VB76JPI_uSo)
- NeoShield (Ed.). (2014). *NeoShield*. Retrieved from <http://www.neoshield.net/en/index.htm>
- Sanchez, J. a. (2009). *Multi-criteria comparison among several mitigation strategies for dangerous near Earth objects*. Glasgow: Strathprints Institutional Repository.
- SpaceGuardCentre. (2014, Septiembre 20). Retrieved from <http://spaceguardcentre.com/what-are-neos/faqs/#top>
- Stuart, J. S. (2003). *Observational Constraints on the Number, Albedos, Size, and Impact Hazards of the near-Earth Asteroids*. Massachusetts Institute of Technology.
- Wiltshire, W. H. (Sept 1960). Terminal Guidance System fir Satellite Rendezvous. *Journal of the Aerospace Sciences Vol 27 No 9*, 653-658.

## 8. Project budget

This chapter shows the costs related to the development of the project and offer a reference cost of the whole project. First of all, it is important to know the available resources. The project was started in December 2013. The timing was:

- December and January: Study of relative motion theory.
- February to June: development of models.
- July to September: simulations performed.
- August and September: writing the report.
- October: further simulations performed (study 4b, 5 and 6)
- November: report revision 2 and 3.
- December: report revisions 4 and 5.

During the development of the project other two activities were carried out:

- Finish of the last subjects at UPC (in green can be observed the two peaks corresponding to the final exams period).
- Work at Volotea Airlines, with a previous training in Madrid.

The time available for the project decreases as Volotea work load increases. It is represented a low value corresponding to the final exams of the spring semester and then a raise in the final days due to work load decrease at Volotea.

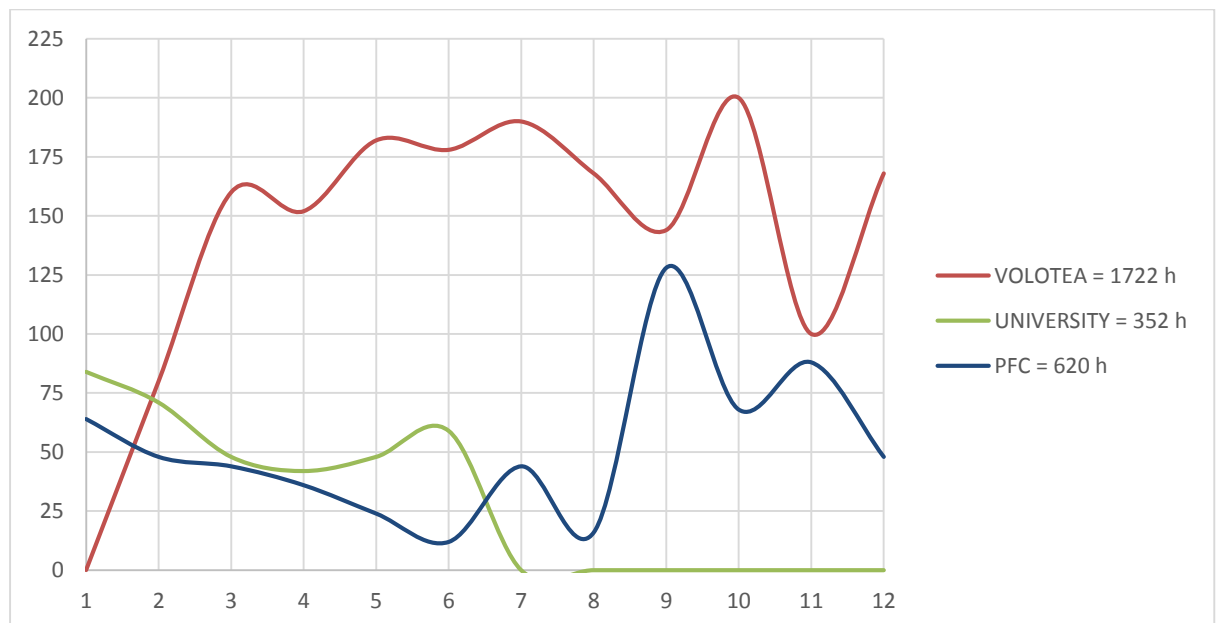


Figure 47 Time distribution along the project (from January to December 2014)

Once resources dedicated to the project are considered, it is easy to provide a project budget based on man power used, hardware and software, and publication costs:

Budget Summary				
General	Concept	Unitary cost	Units	Total
Man power	Full time engineer	10 €/hour	620 hours	6200 €
Software	Matlab licence	2000 €	1 licence	2000 €
	Microsoft Office	200€	1 licence	200 €
Hardware	Computer	1200€	1	1200 €
Power	Electricity	0.14€/kWh	200 W during 1500 h	50 €
Publication	Publication taxes	100 €	1 publication	100 €
			Total	9750 €

Table 17 Budget summary

## 9. Environmental awareness

---

During the conception phase of the project it was considered the environmental consequences that the study may occasion and no special outcome was detected.

After the completion of the study, the previous statement can be confirmed from two points of view. In a first approach it can be considered the consequences of the project development. During this period, two factors can be highlighted: the pollution produced during the transport to the meetings and the power consumption that is required in order to perform the computer simulations. Both factors do not imply an important variation of contamination compared to the usual lifestyle.

On the other hand, it has been considered the consequences of applying the project, that is, to use the trajectories found during the study in real missions. In this case, the environmental consequences assessment can be quite subjective. A space project implies a great amount of pollution and debris: in the spacecraft construction, the launch campaign, etc. but the conclusion of the project is a modification in the final trajectory, so, it is supposed that the mission would be launched independently of the study development. The trajectories that are presented in this study are purely ballistic (the spacecraft trajectory is only modified by the Sun gravity) so no fuel or propulsion system is used (and no debris is generated). In conclusion, comparing the trajectories proposed with other approaches that have been discussed in recent publications (for example low-thrust manoeuvres), it can be stated that pure gravitational relative orbits ensure a lower impact on the space environment.

## 10. ANNEX I: Matlab Functions

---

The Matlab functions used along this project can be divided in three groups:

- Functions to calculate the relative position to the target asteroid:
  - `relativeMotionSimple` (described in section 3.1)
- Functions to generate the asteroid population:
  - `getDelta_a` (described in section 3.2)
  - `getUncert` (described in section 3.3)
- Functions to assess the detection probability (included in the GA):
  - *FitnessFunction*, which includes:
    - `AstDetModelSC` (described in section 3.4)
    - `relativeMotionSimple`
- Functions to analyse the results obtained in the simulations:
  - Orbit Analysis
  - Analyse results

The function that belong to the three first groups have been introduced during the report. However, even if it has been described the results analysis, it has not been described the Matlab functions involved.

The results analysis is performed in a script called with the same name (*Results Analysis*). This script is divided in some sections depending on the purpose of the code:

- Section 1: as was introduced in section 4.6.1 the simulations are performed in parallel for each OCC, so, the first section build up a variable that contain the data for all OCC.
- Section 2: This is the main section, its aim is to process the data. The next steps are followed:
  - The OCC and CAD are selected.
  - The data that match with selected OCC and CAD is stored on a smaller variable called "Results" that contains the spacecraft population and their scores.
  - The "*Analyse results*" function is used. This function access the variable "Results" and returns the design variables corresponding to the spacecraft (or spacecrafts) that has reached the maximum score and appears more than a certain number of times (usually 5) in the population.
  - The asteroid virtual uncertain population is generated.
  - With the asteroid virtual population and the spacecraft the "Orbit Analysis" function is used. This function returns an array containing the information about position (in *x, y and z* coordinates) and accumulated probability of

detection for each time step of the simulation. This array will be used when plotting the trajectory.

- Section 3: In this section the uncertainty ellipsoid is created. This ellipsoid will be plotted together with the trajectory for having a spatial reference about where the target asteroid could be.
- Section 4: Finally, the uncertainty ellipsoid and the array generated in the last point of section 2 are plotted, showing the path followed by the spacecraft in 4 different views (isometric, top, front and lateral) together with the accumulated probability along the orbit.

# 11. ANNEX II: Time reduction

As was introduced in the Genetic Algorithm description (section 4.1), the fitness function is the one that gives back the probability of not detect the asteroid for a given S/C (set of design variables). The fitness function is obviously the function that will be executed more times (it is executed every time the GA perform an evaluation), so it becomes key to reduce the time this function takes to execute.

Making use of the “profile” Matlab function it is possible to analyse the parts of the code that need more time:

Profile Summary				
Generated 26-Jun-2014 13:47:49 using cpu time.				
Function Name	Calls	Total Time	Self Time*	Total Time Plot (dark band = self time)
<a href="#">FitnessFunction_vP</a>	1	24.786 s	1.914 s	
<a href="#">AstDetModelSC</a>	144000	20.195 s	4.990 s	
<a href="#">cross</a>	144000	11.282 s	9.095 s	
<a href="#">dot</a>	144000	3.565 s	3.565 s	
<a href="#">relativeMotionSimple</a>	288000	2.670 s	2.670 s	
<a href="#">ipermute</a>	144000	2.187 s	2.187 s	
<a href="#">deg2rad</a>	288000	0.217 s	0.217 s	
<a href="#">rad2deg</a>	144000	0.141 s	0.141 s	
<a href="#">astroConstants</a>	1	0.006 s	0.006 s	
<a href="#">linspace</a>	1	0 s	0.000 s	

Figure 48 Fitness Function time profile

As the picture shows, the total time required to execute once the Fitness function is almost 25 seconds. Taking into account a GA with 15 generations and a population of 25 individuals it supposes:  $15 \text{ gen} \cdot 25 \text{ ind} \cdot 25 \text{ seconds} = 9375 \text{ seconds} = 2,6 \text{ hours}$

Imagine you need to perform a study with 6 different OCC (from 0 to 5) and 5 different number of diameters. That will represent more than 3 days of simulations. And consider this is the easiest case. Better don't try to estimate the required time for the studies 4 and 5, where an inner loop of GA is used. So this time required is unacceptable.

In this profile is possible to see that the function “AstDetModelSC” is the part inside the fitness function that is consuming more time.

It is also possible visible that the major part is due to the use of “cross” and “dot” functions. If we look inside the function we can see the time value associated to each line:

```

-- * 2018 FEBRUARY 21/04/2018; 18:56:04; 20180221M
28 %
29 %CHANGELOG:
30 %
31 %
0.34 144000 32 rho=Asteroid_Position-Spacecraft_Position;
0.02 144000 33 G=0.15;
0.26 144000 34 ChiefToSun=[-rAst 0 0];
0.18 144000 35 AstToSun=Asteroid_Position-ChiefToSun;
0.11 144000 36 SCtoSun=Spacecraft_Position-ChiefToSun;
0.40 144000 37 rSC=norm(rho);
38
0.14 144000 39 H=-5*log10(Asteroid(1)*sqrt(Asteroid(2))/1329);
40
16.43 144000 41 k= rad2deg(atan2(norm(cross(SCtoSun,rho)),dot(SCtoSun,rho)));
42
0.42 144000 43 F1=exp(-3.33*(tan(deg2rad(k)/2))^0.63);
0.26 144000 44 F2=exp(-1.87*(tan(deg2rad(k)/2))^1.22);
45
46
47
0.54 144000 48 V=H+5*log10(rSC*norm(AstToSun))-2.5*log10((1-G)*F1+G*F2);
49
0.04 144000 50 if V>cam
0.33 143967 51 s=0;
33 52 else
33 53 s=1;
0.01 33 54 end

```

Figure 49 AstDetModelSC time profile

The first action is to replace the “cross” and “dot” functions, because they require 16 seconds to be calculated. It is possible to change it by the mathematic expression itself:

```

31
0.34 144000 32 rho=Asteroid_Position-Spacecraft_Position;
0.05 144000 33 G=0.15;
0.30 144000 34 ChiefToSun=[-rAst 0 0];
0.09 144000 35 AstToSun=Asteroid_Position-ChiefToSun;
0.08 144000 36 SCtoSun=Spacecraft_Position-ChiefToSun;
0.36 144000 37 rSC=norm(rho);
38
0.12 144000 39 H=-5*log10(Asteroid(1)*sqrt(Asteroid(2))/1329);
40
0.05 144000 41 dot_k=SCtoSun(1)*rho(1)+SCtoSun(2)*rho(2)+SCtoSun(3)*rho(3);
0.22 144000 42 cross_k=[SCtoSun(2)*rho(3)-rho(2)*SCtoSun(3),SCtoSun(3)*rho(1)-rho(3)*SCtoSun(1),SCtoSun(1)*rho(2)-rho(1)*SCtoSun(2)];
0.26 144000 43 k=atan2(norm(cross_k),dot_k);
44
0.11 144000 45 F1=exp(-3.33*(tan(k/2))^0.63);
0.10 144000 46 F2=exp(-1.87*(tan(k/2))^1.22);
47
48
49
0.34 144000 50 V=H+5*log10(rSC*norm(AstToSun))-2.5*log10((1-G)*F1+G*F2);
51
0.02 144000 52 if V>cam
0.27 143888 53 s=0;
112 54 else
112 55 s=1;
112 56 end

```

Figure 50 AstDetModelSC time profile after modification of "cross" and "dot" functions

Here the time required for the “AstDetModelSC” has been reduced from 20 seconds to 3.4 seconds. So, the Fitness function only requires 7 seconds to be executed:

### Profile Summary

Generated 26-Jun-2014 19:39:30 using cpu time.

<a href="#">Function Name</a>	<a href="#">Calls</a>	<a href="#">Total Time</a>	<a href="#">Self Time*</a>	Total Time Plot (dark band = self time)
<a href="#">FitnessFunction_vP</a>	1	6.965 s	1.310 s	
<a href="#">AstDetModelSC</a>	144000	3.377 s	3.377 s	
<a href="#">relativeMotionSimple</a>	288000	2.278 s	2.278 s	
<a href="#">astroConstants</a>	1	0 s	0.000 s	
<a href="#">linspace</a>	1	0 s	0.000 s	

Figure 51 Fitness Function time profile after "AstDetModelSC" modification

Once all the functions have been modified to take the less time possible it is time to make use of the “secret weapon”. In order to reduce more the total time, the Fitness Function will be compiled in C++ language using the tools available in Matlab.

Creating a project and then building the function as “mex” file the time is reduced spectacularly:

### Profile Summary

Generated 26-Jun-2014 20:40:11 using cpu time.

<a href="#">Function Name</a>	<a href="#">Calls</a>	<a href="#">Total Time</a>	<a href="#">Self Time*</a>	Total Time Plot (dark band = self time)
<a href="#">FitnessFunction_vP_mex</a> (MEX-file)	1	0.355 s	0.355 s	

Figure 52 Fitness Function time profile after conversion to MEX-file

The time has been reduced to 0.355 seconds. That means that for the same example shown before where 3.25 days were required, now it is possible to have the results within:

$$15 \text{ gen} \cdot 25 \text{ ind} \cdot 0,355 \text{ seconds} = 133 \text{ seconds}$$

For the same example that means 66 minutes in front of the 3.25 days required before the time optimization. That is very powerful tool that allows us to perform complex simulations in small time periods.

## 12. ANNEX III: Study 4b

In 4.6.4 it was observed that the cases that presented a major interest were for OCC 4 and 5 and Close Approaches with a few number of months. In Table 12 and Table 13 the asteroid diameter is shown depending on the close approach duration. In this section, the data is plotted in order to analyse the values from a graphical point of view.

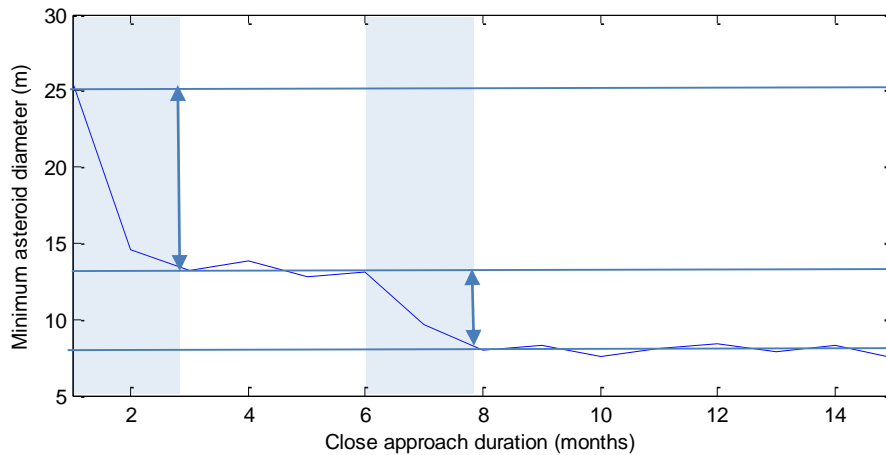


Figure 53 Asteroid diameter vs CAD for OCC = 4 (1 to 15 months)

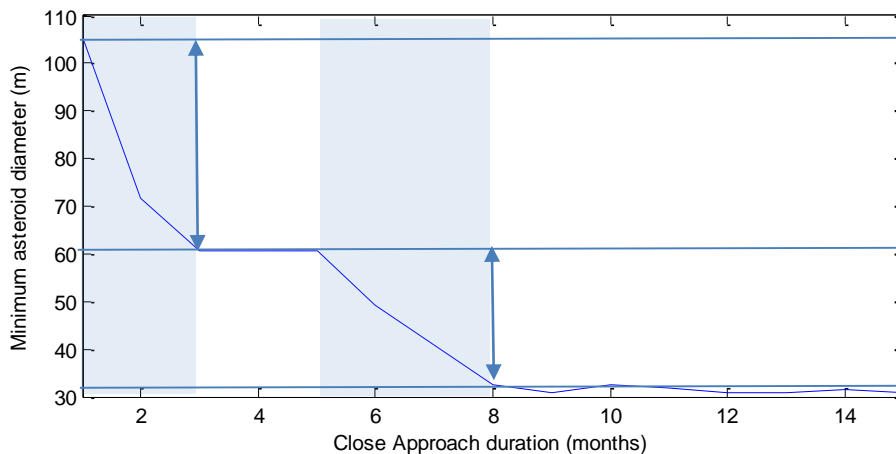


Figure 54 Asteroid diameter vs CAD for OCC = 5 (1 to 15 months)

Both figures show two “hot” zones where the asteroid diameter decreases considerably. These zones have been highlighted and only in a few months represent a reduction of:

- 50% in the first months and 60% in the 6<sup>th</sup> month for OCC = 4.
- 57% in the first months and 52% in the 5<sup>th</sup> month for OCC = 5.

To gain more insight about what happens for shorter close approach duration, the study 4b has been developed. It consist on repeating the same simulation but considering durations from 1 to 42 days.

Figure 55 and Figure 56 shows the diameter reduction along the first month and a half of close approach duration. It has been found that the reduction in the asteroid diameter is very important, in 40 days, the diameter is reduced to almost 50% in both cases and the figure shape is smoother due to the enhanced sampling that has been applied in this case.

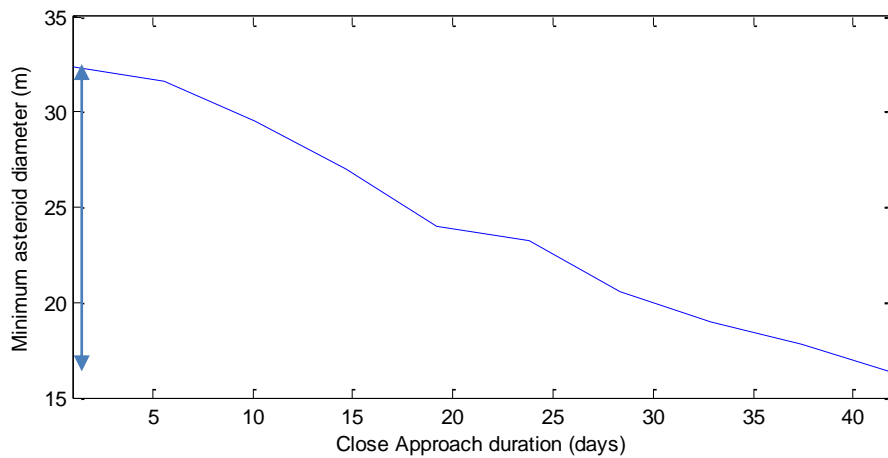


Figure 55 Asteroid diameter vs CAD for OCC = 4 (1 to 42 days)

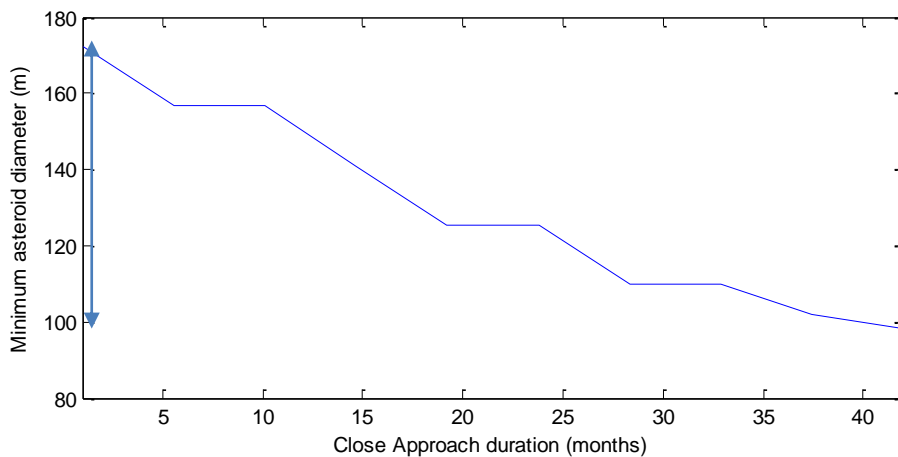


Figure 56 Asteroid diameter vs CAD for OCC = 5 (1 to 42 days)

# 13. ANNEX IV: Study 6 results

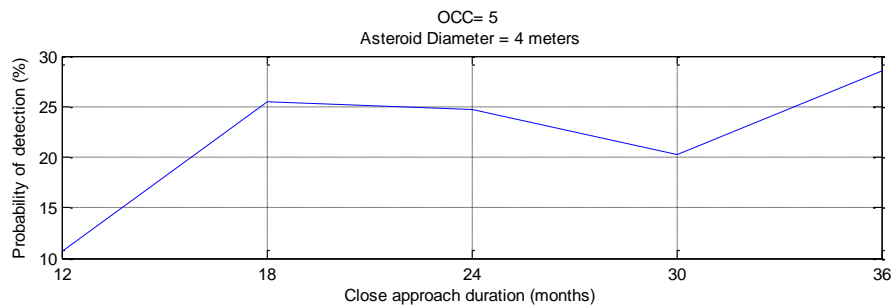


Figure 57 Detection probability for OCC=5, D=4 m and CAD from 12 to 36 months

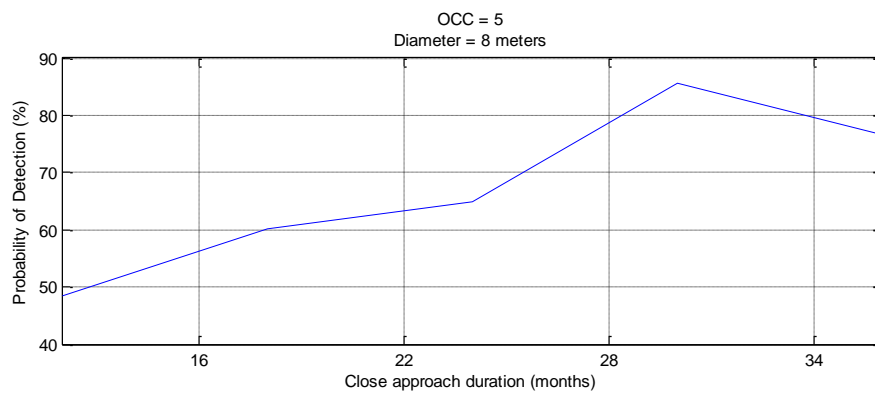


Figure 58 Detection probability for OCC=5, D=8 m and CAD from 12 to 36 months

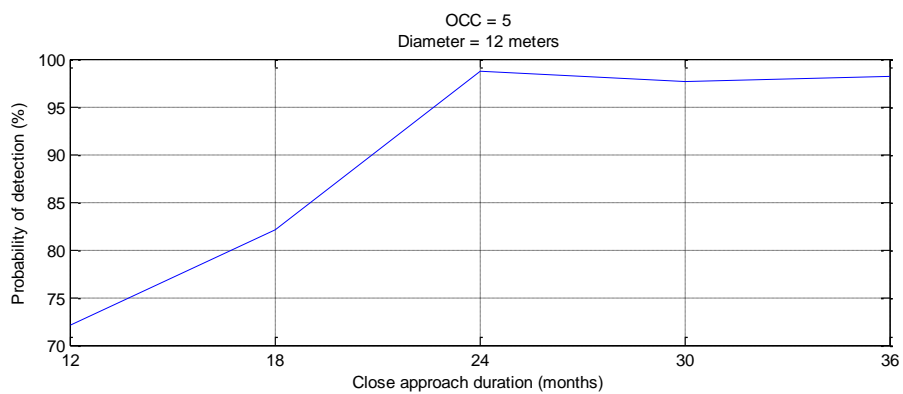


Figure 59 Detection probability for OCC=5, D=12 m and CAD from 12 to 36 months

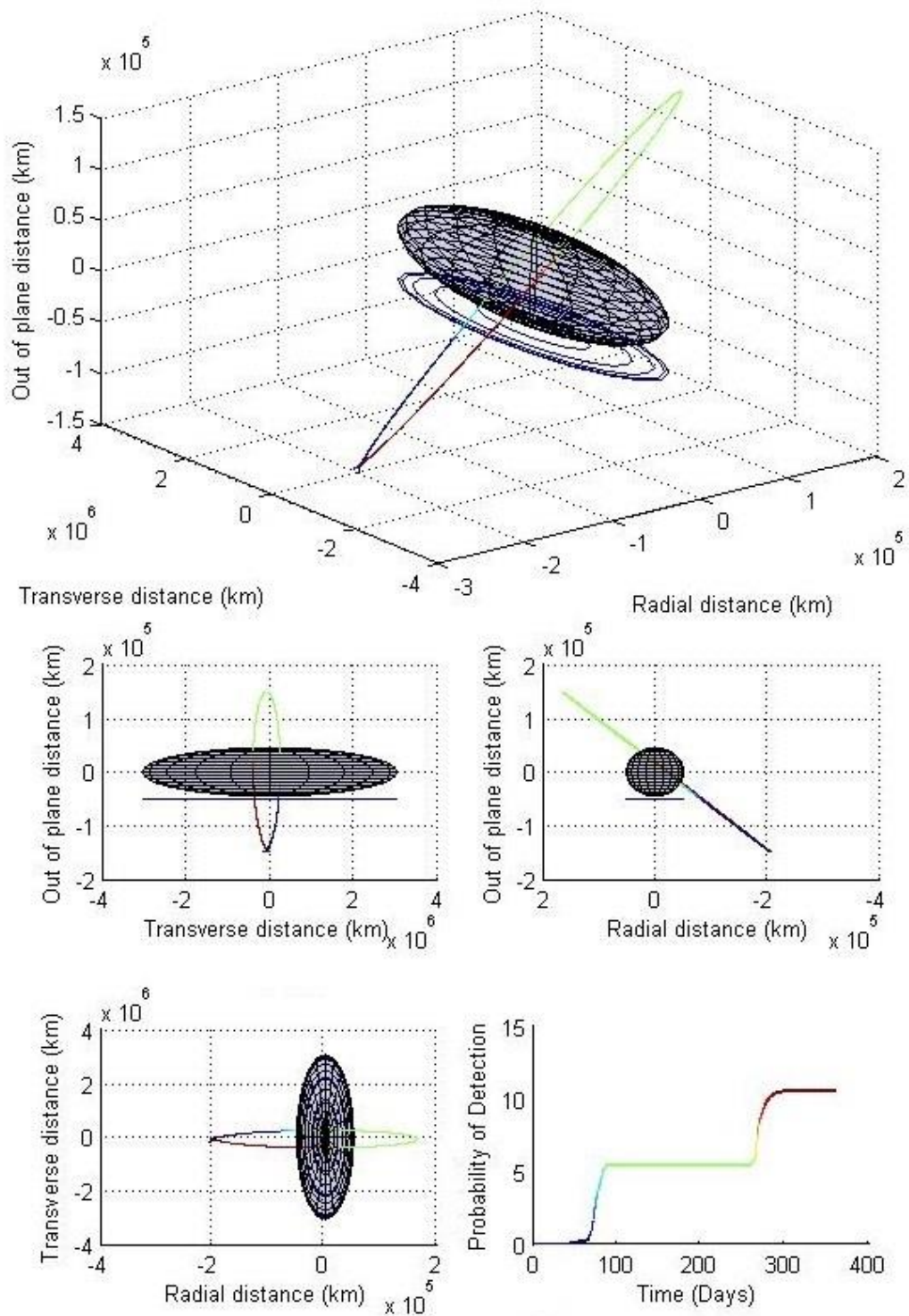


Figure 60 Trajectory for OCC=5, D=4 m and CAD=12 months

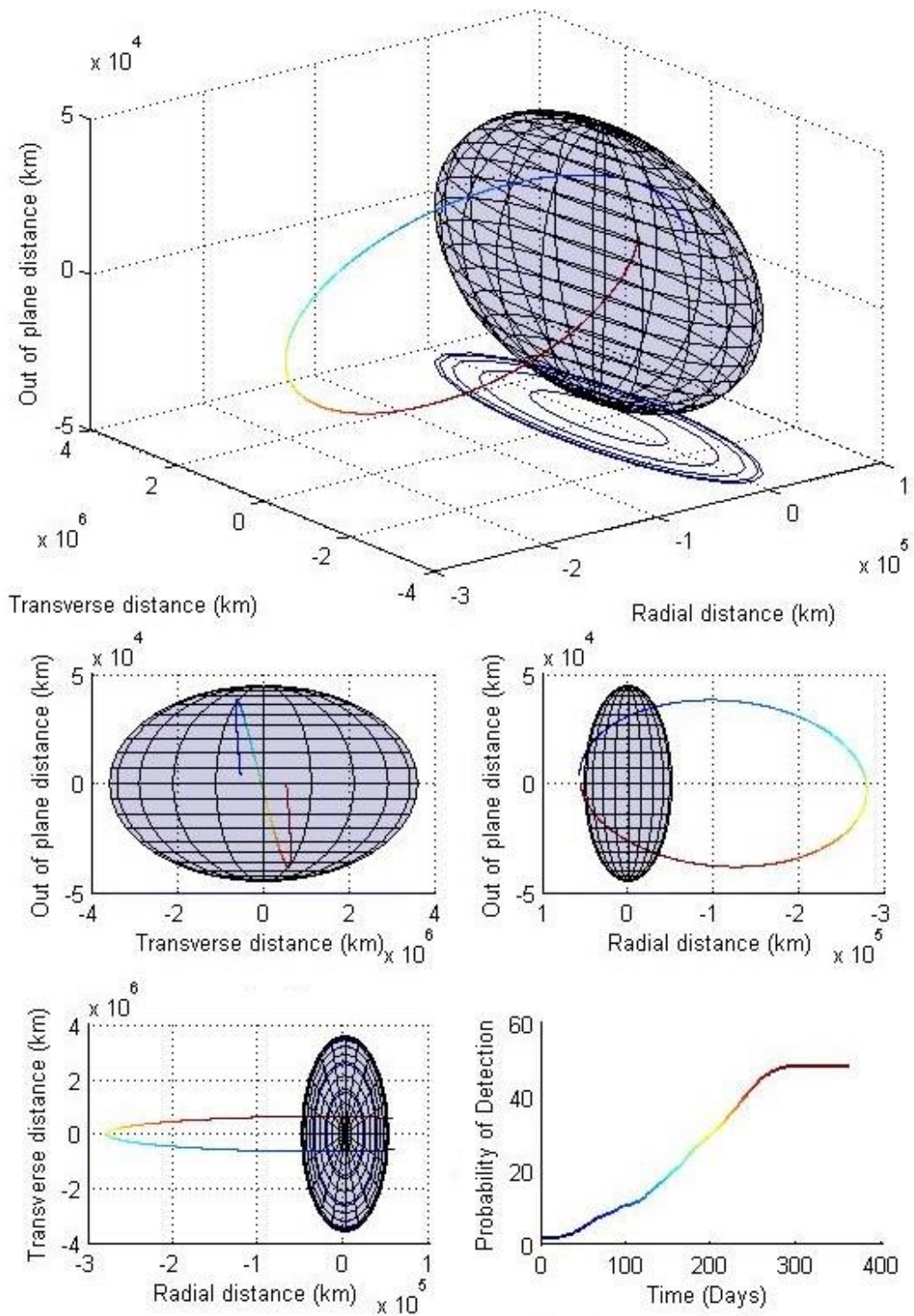


Figure 61 Trajectory for OCC=5, D=8 m and CAD=12 months

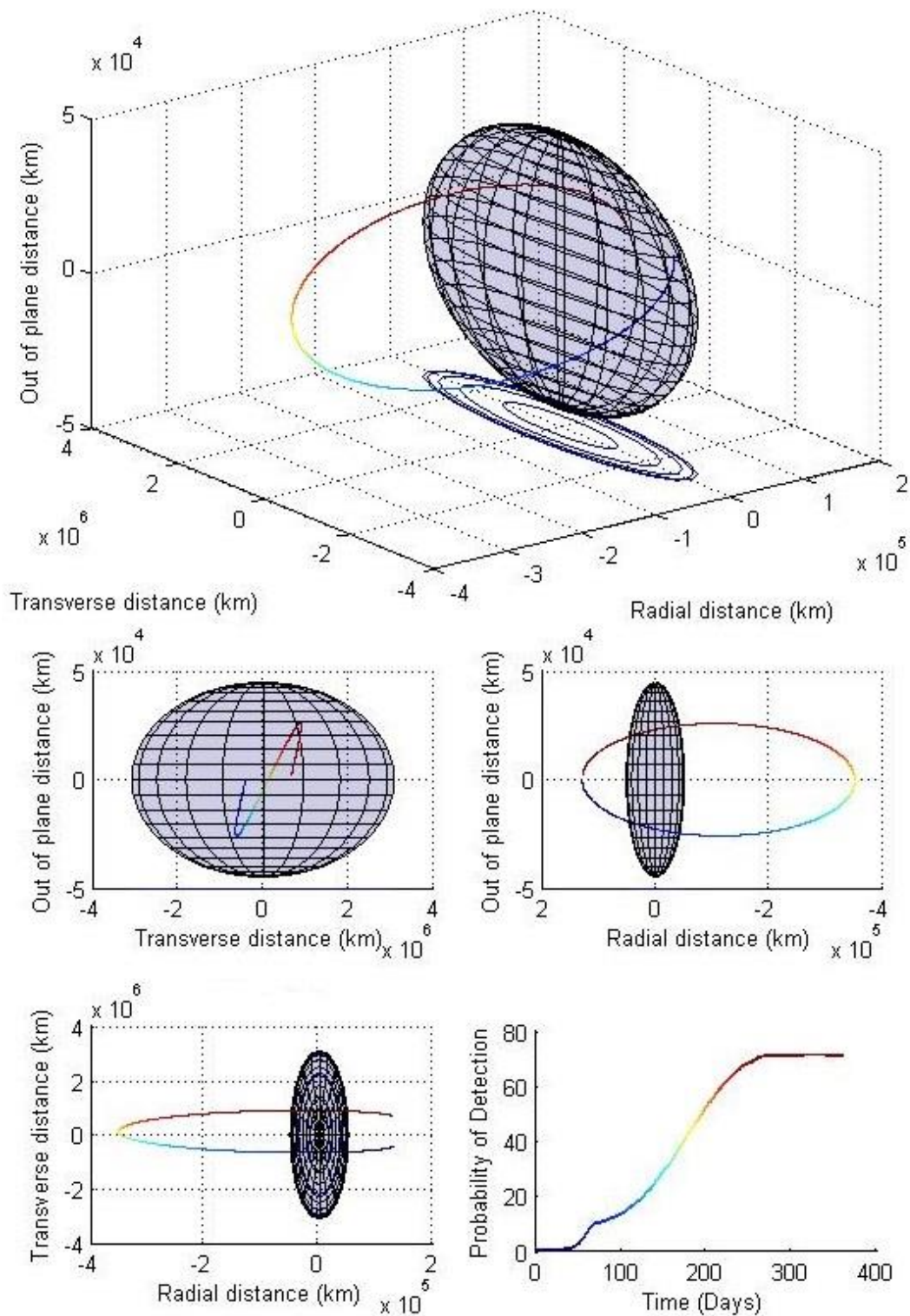


Figure 62 Trajectory for OCC=5, D=12 m and CAD=12 months

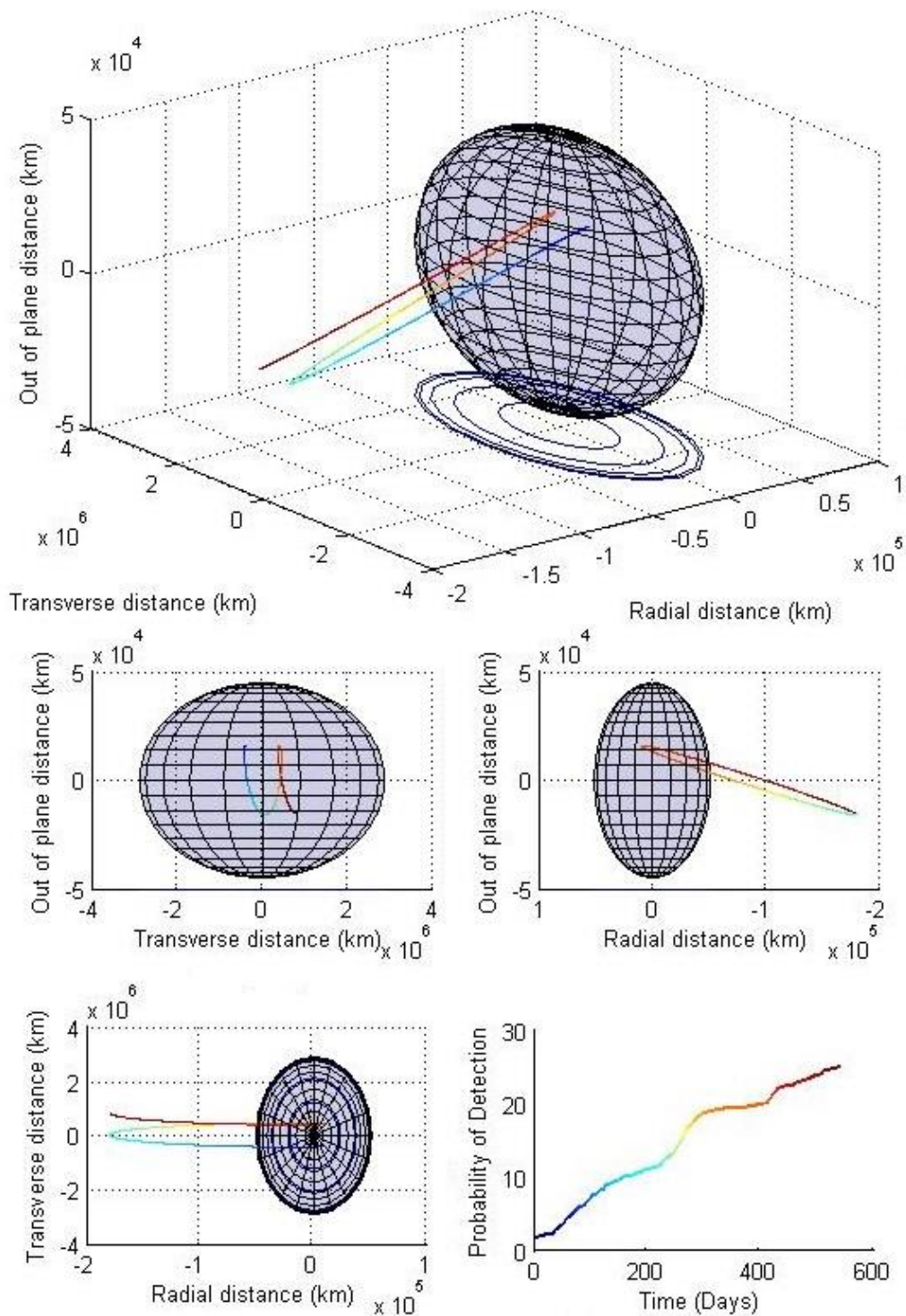


Figure 63 Trajectory for OCC=5, D=4 m and CAD=18 months

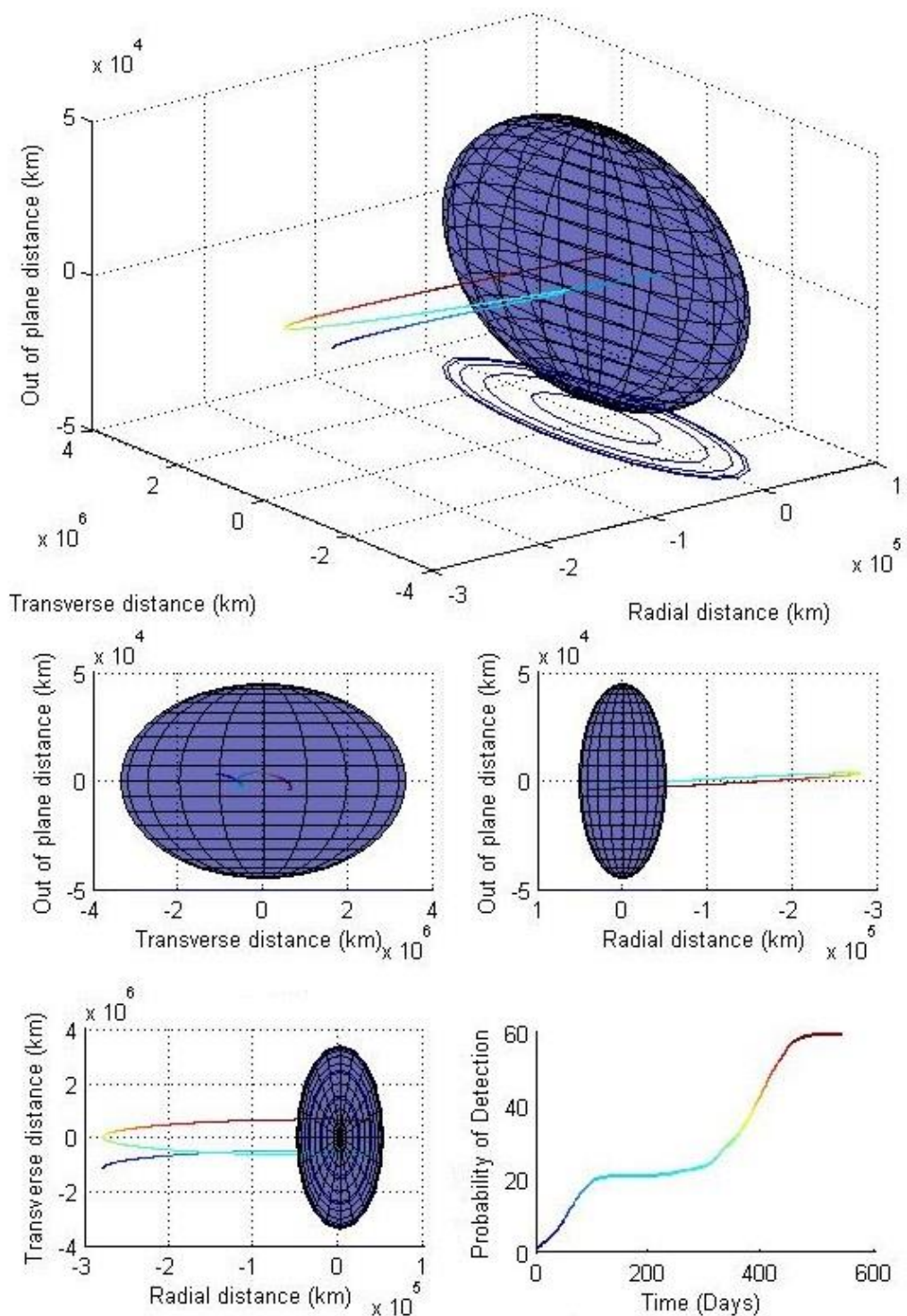


Figure 64 Trajectory for OCC=5, D=8 m and CAD=18 months

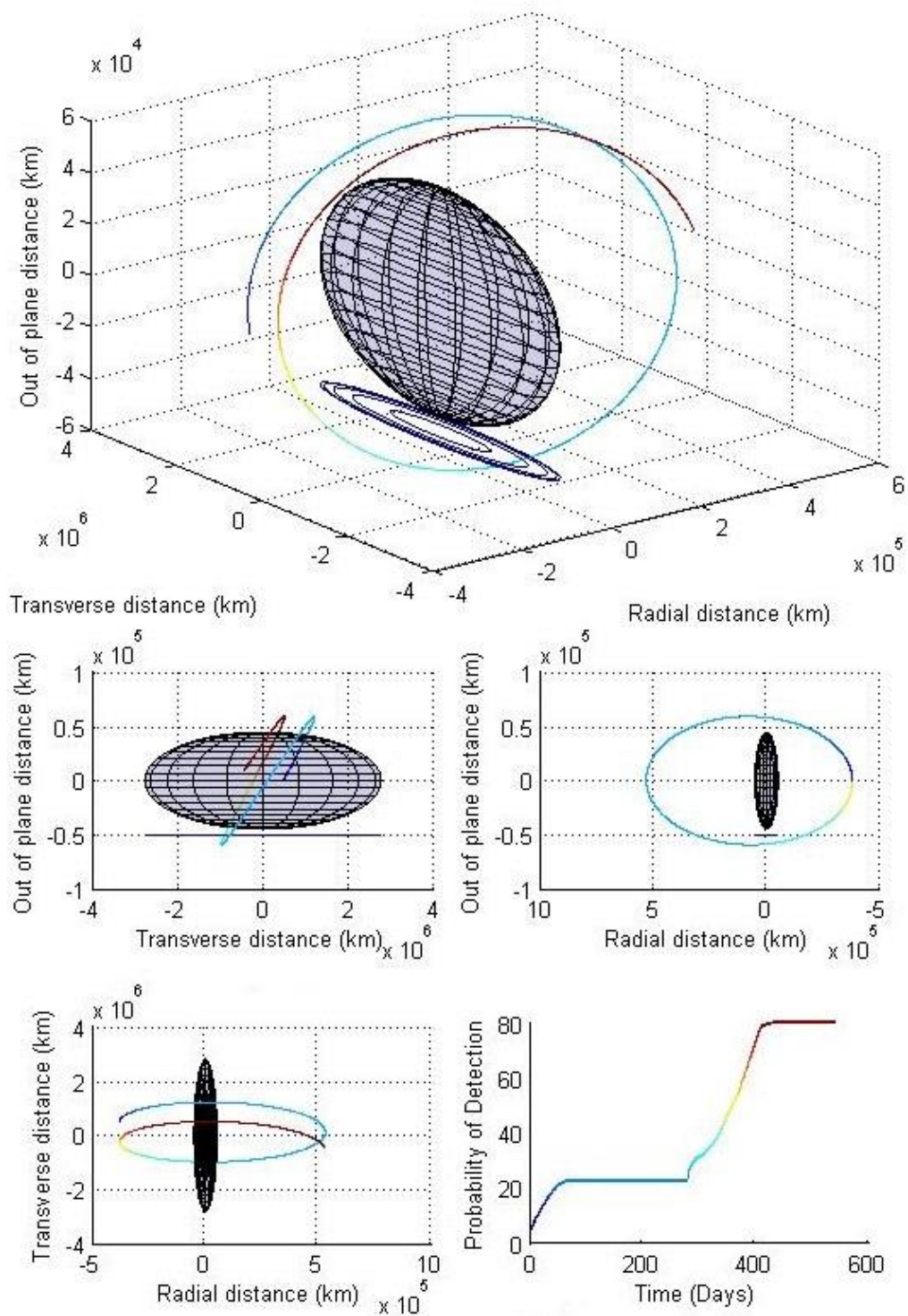


Figure 65 Trajectory for OCC=5, D=12 m and CAD=18 months

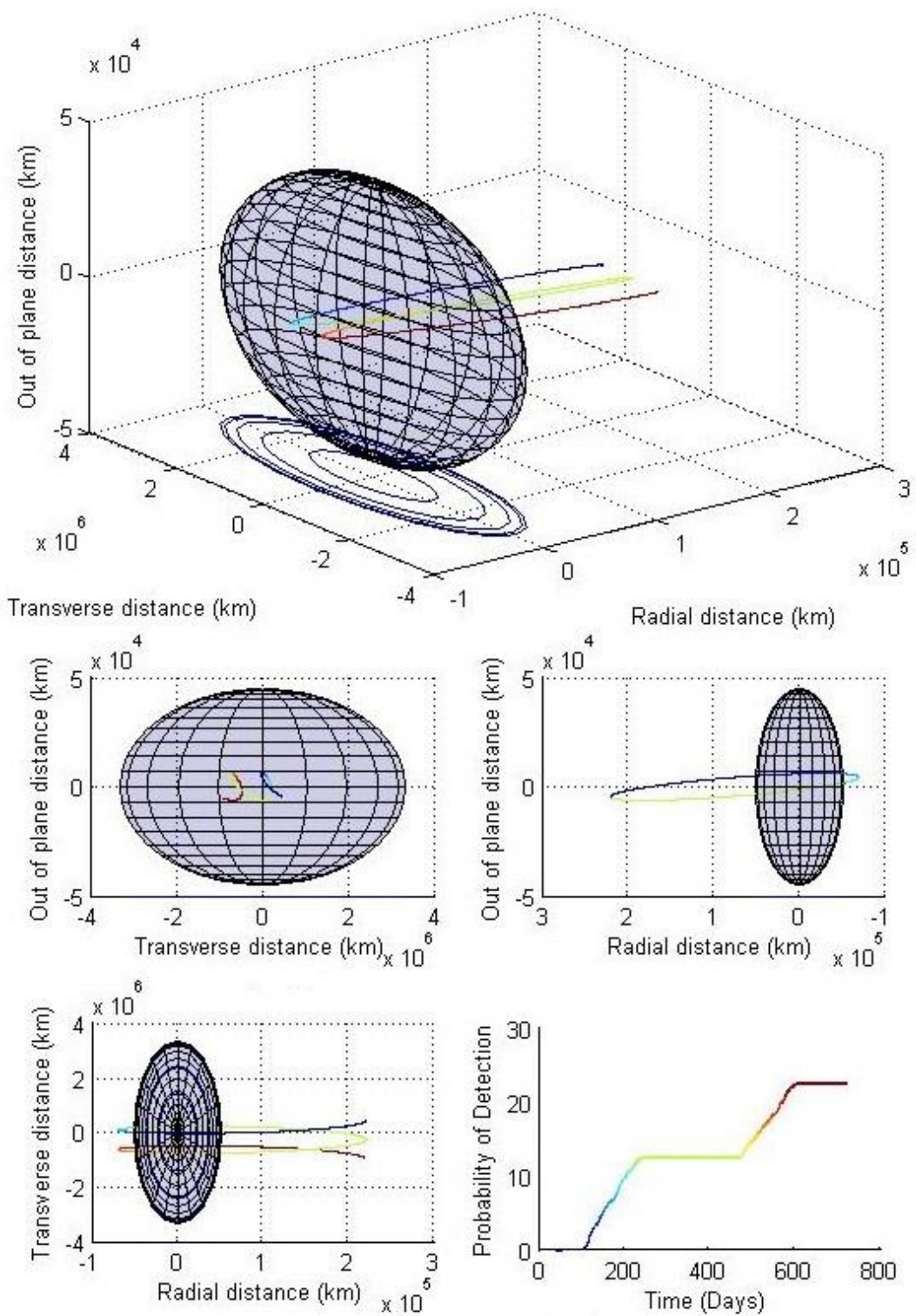


Figure 66 Trajectory for OCC=5, D=4 m and CAD=24 months

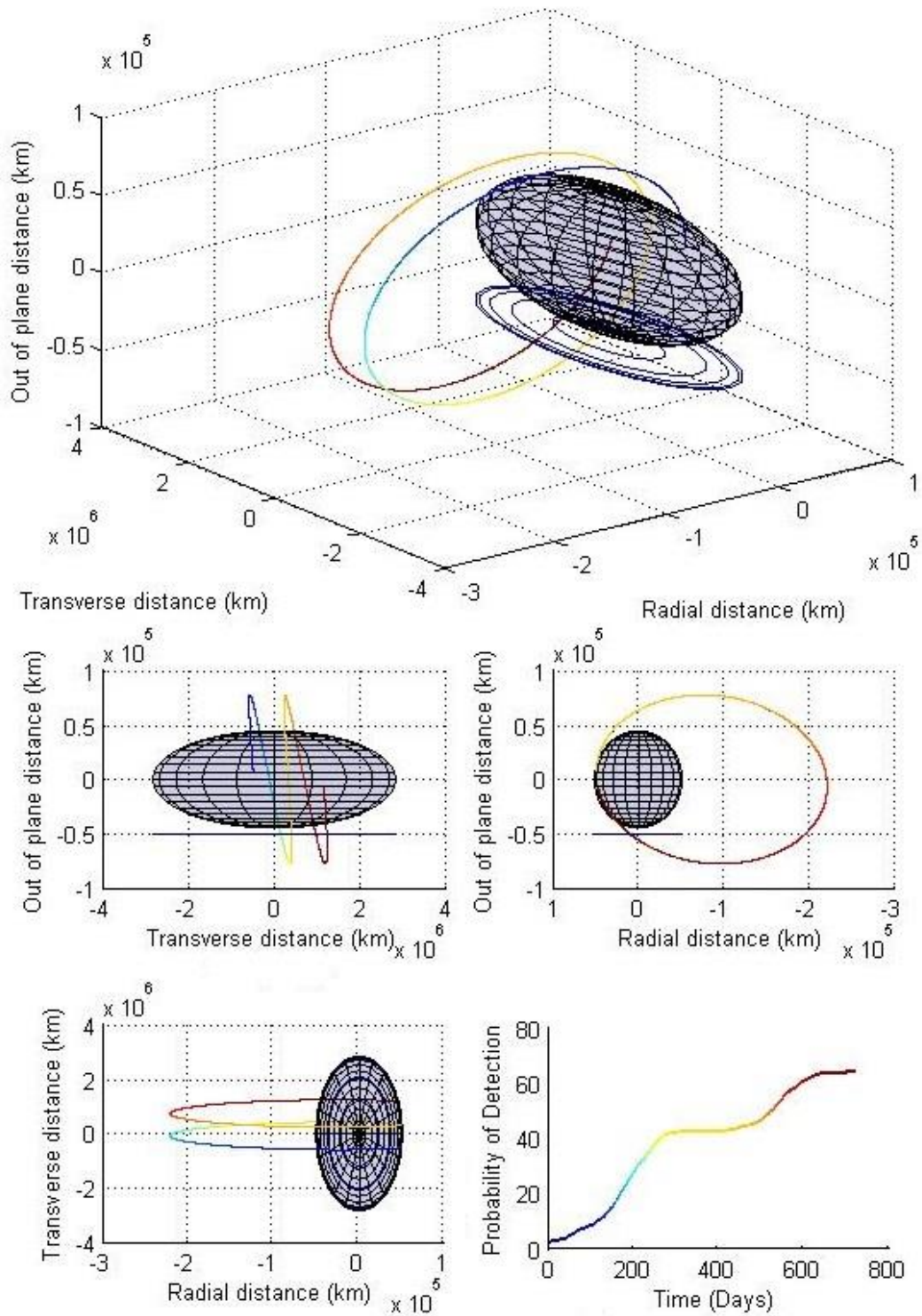


Figure 67 Trajectory for OCC=5, D=8 m and CAD=24 months

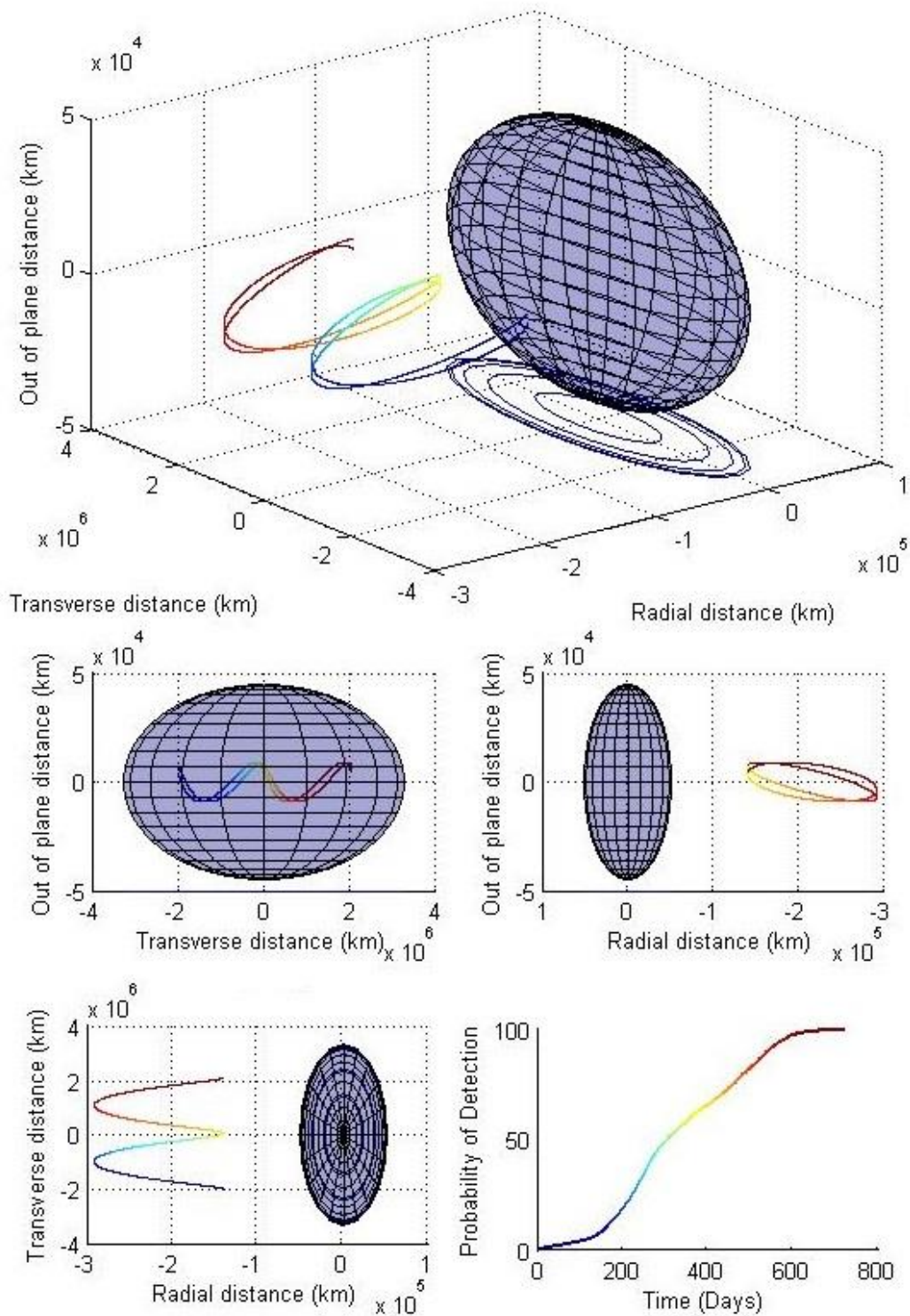


Figure 68 Trajectory for OCC=5, D=12 m and CAD=24 months

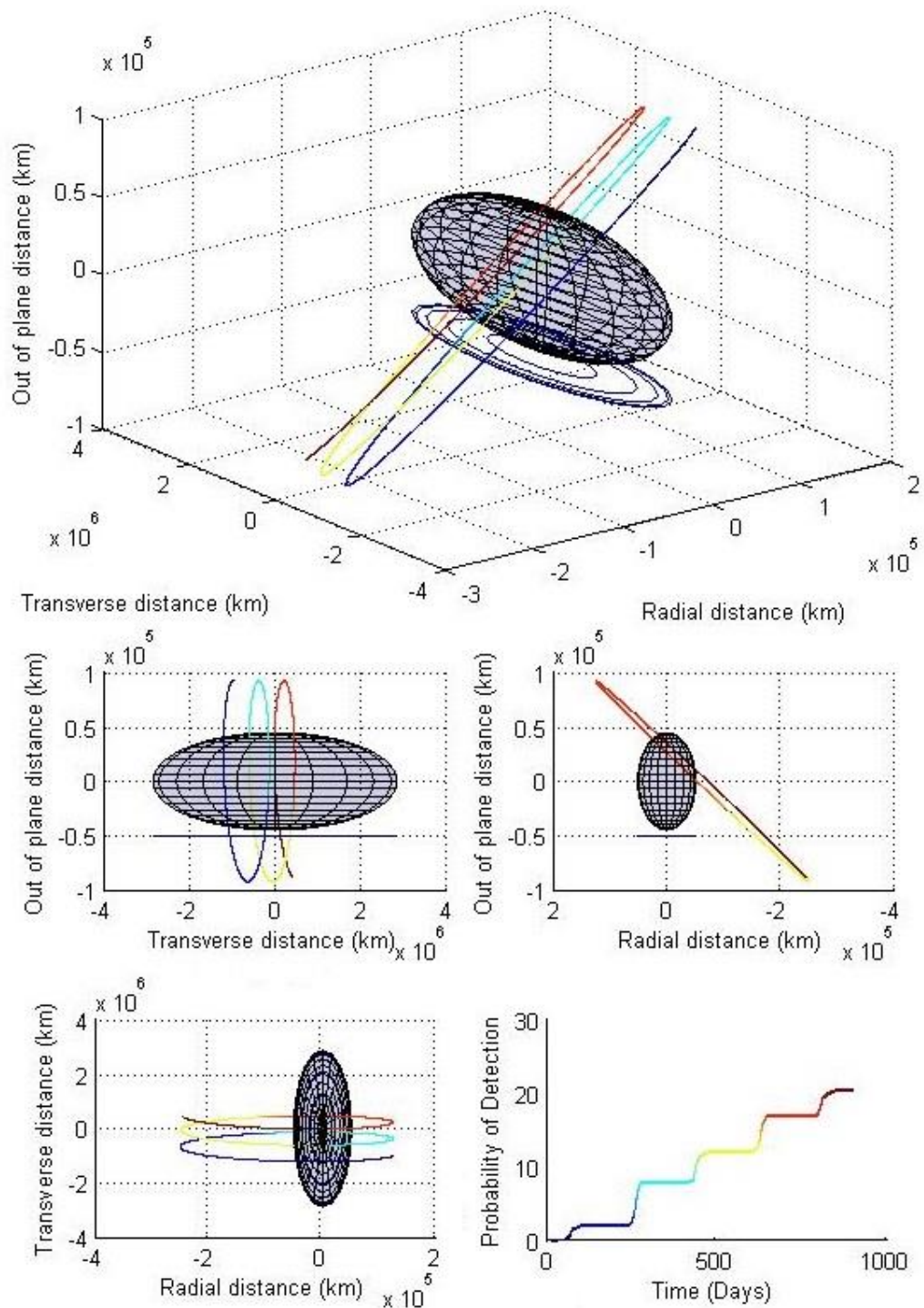


Figure 69 Trajectory for OCC=5, D=4 m and CAD=30 months

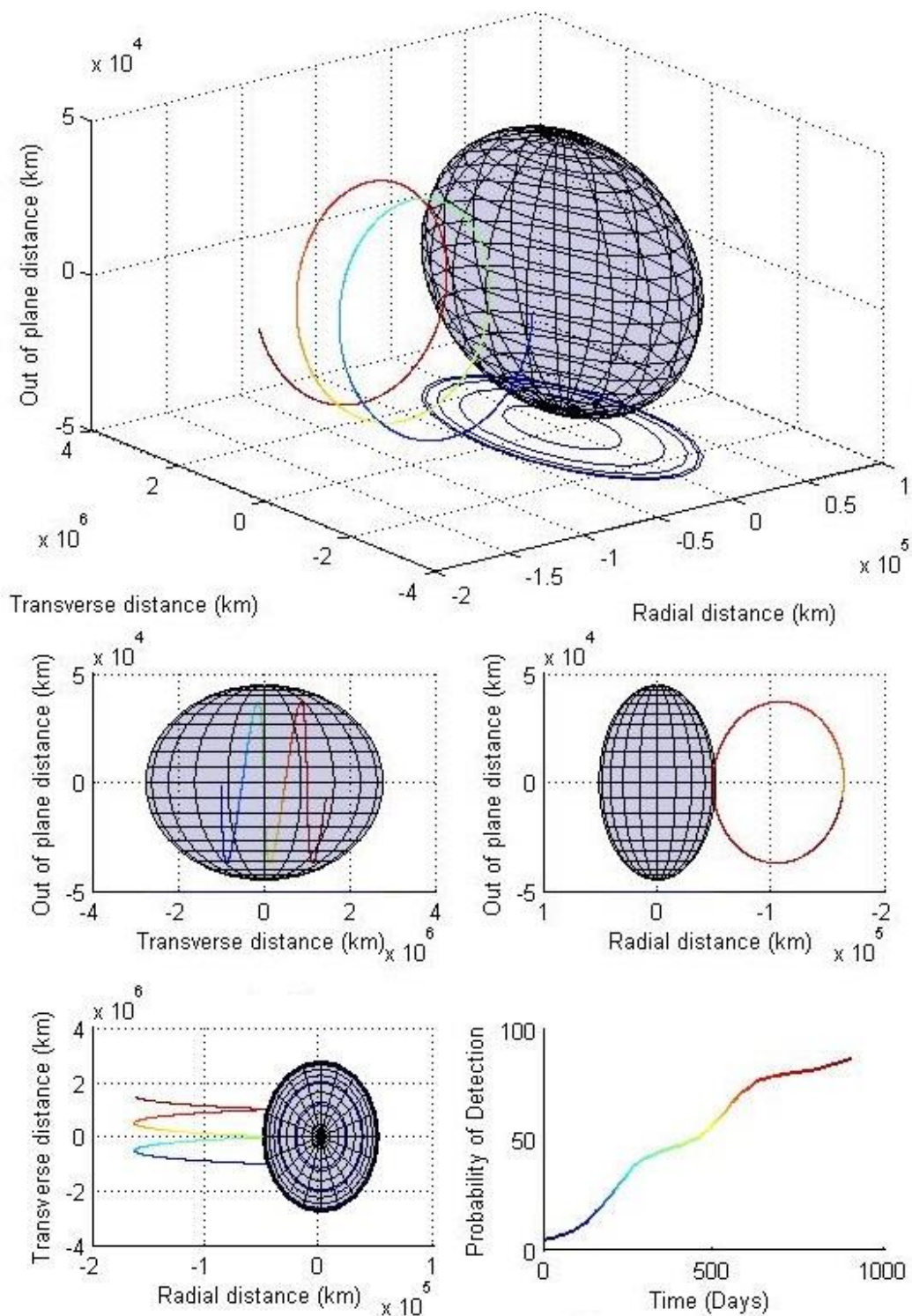


Figure 70 Trajectory for OCC=5, D=8 m and CAD=30 months

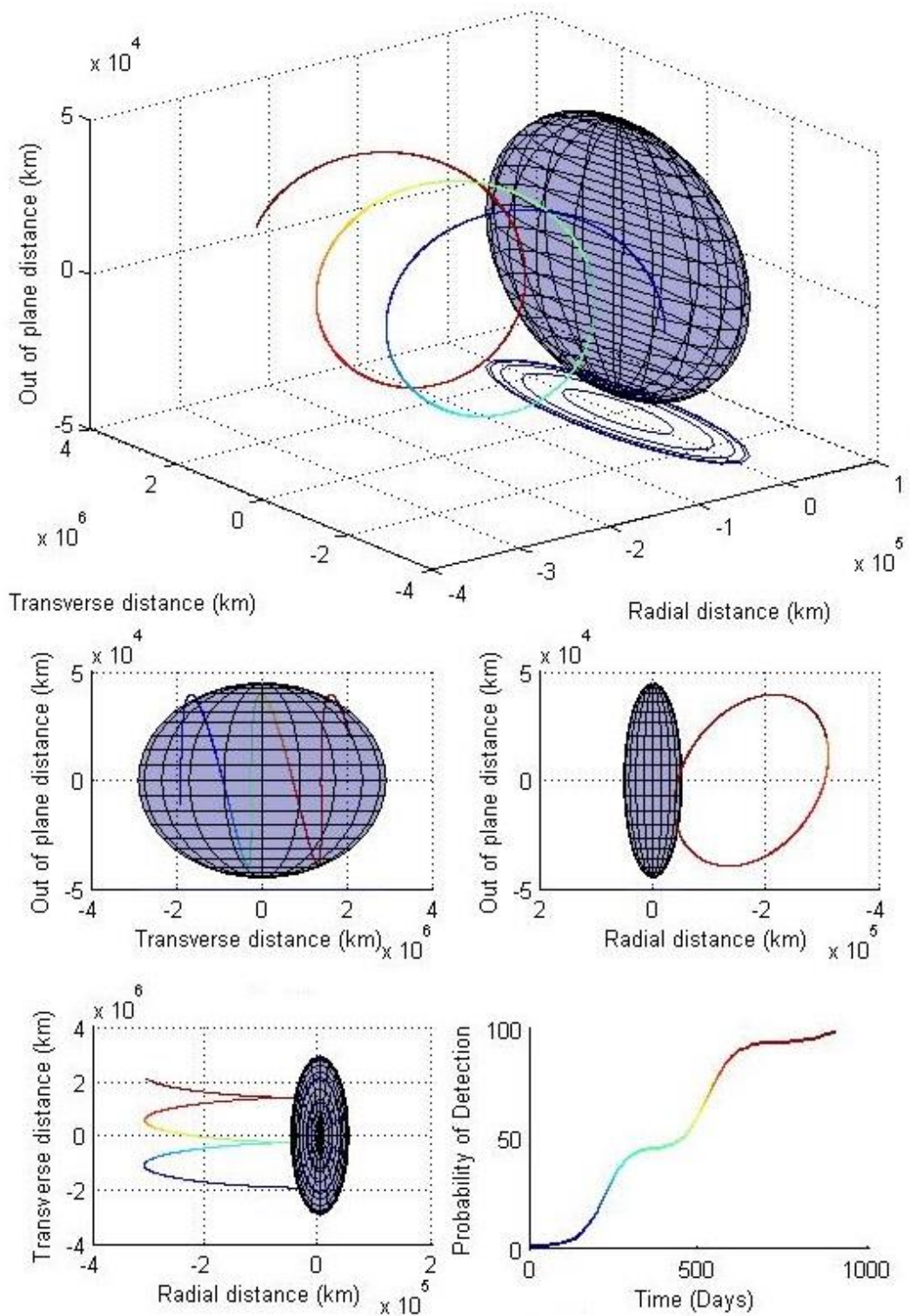


Figure 71 Trajectory for OCC=5, D=12 m and CAD=30 months

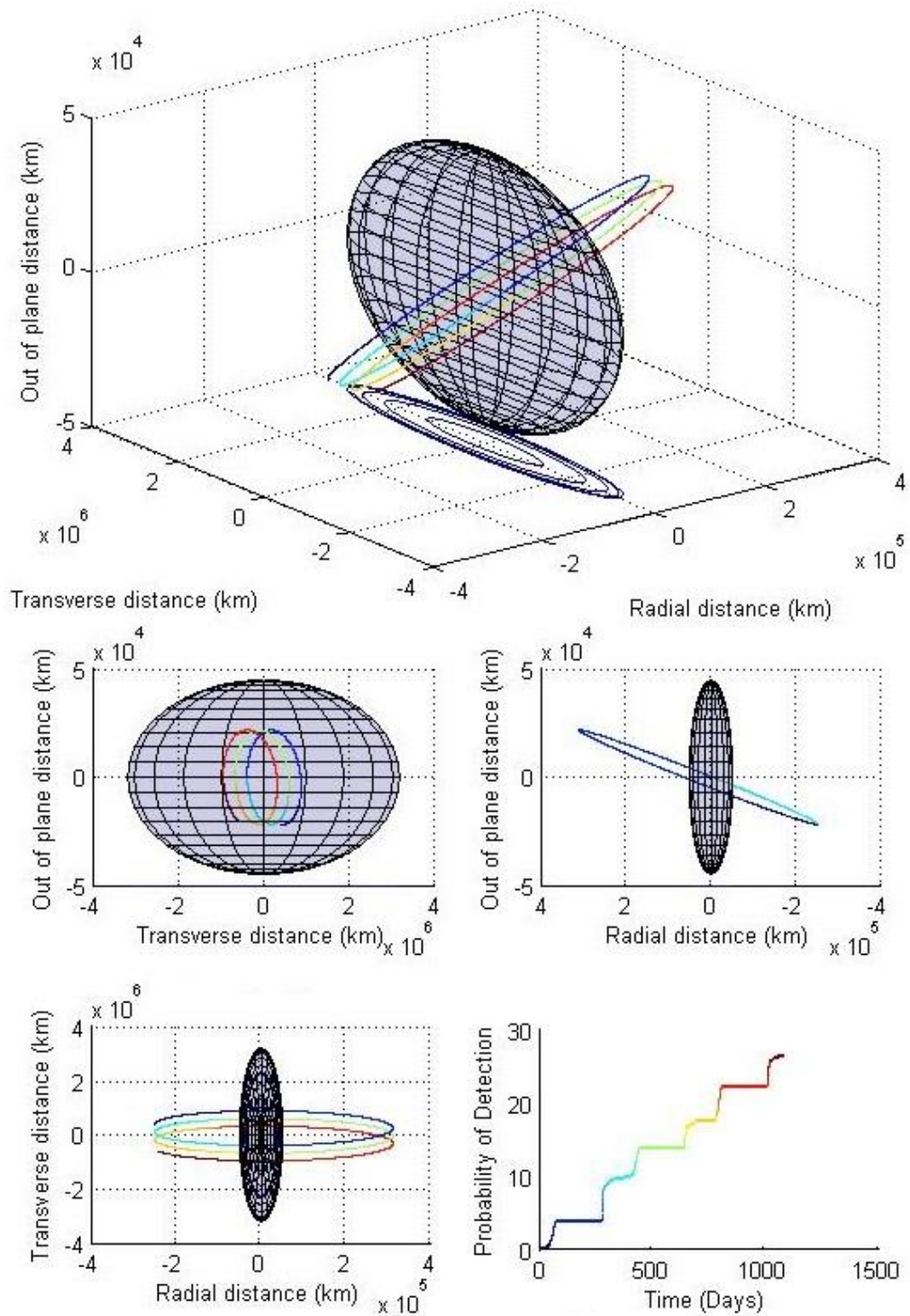


Figure 72 Trajectory for OCC=5, D=4 m and CAD=36 months

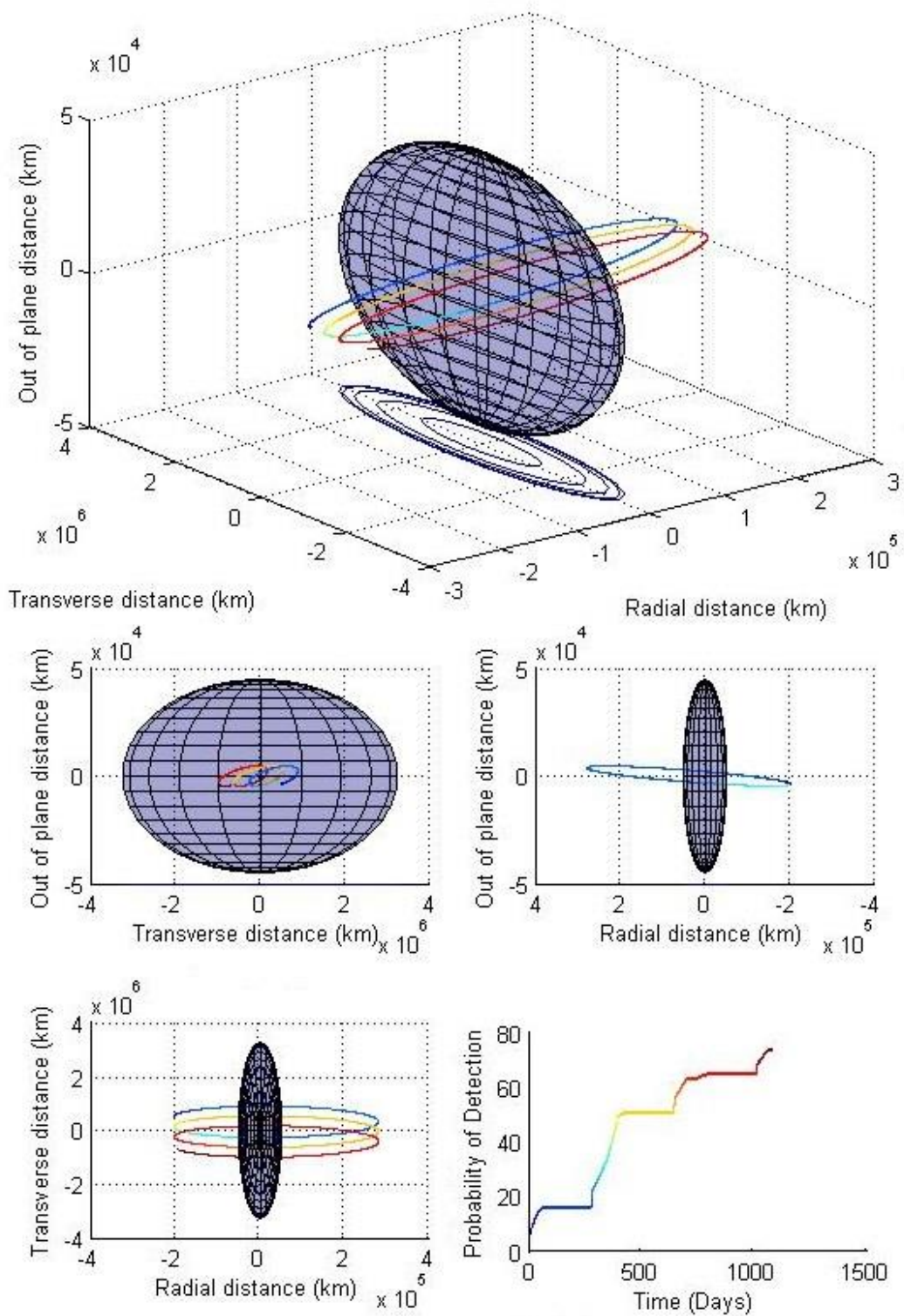


Figure 73 Trajectory for OCC=5, D=8 m and CAD=36 months

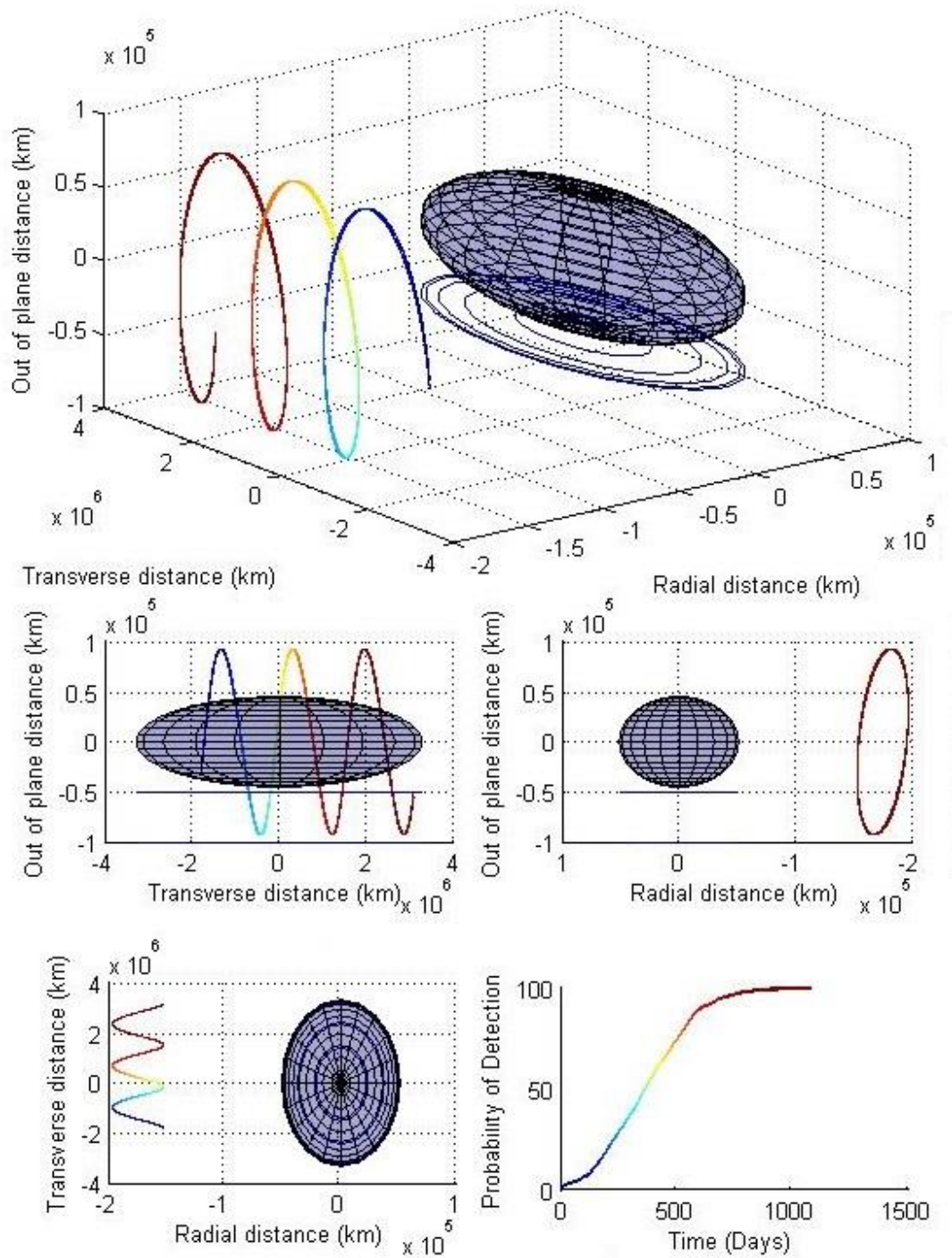


Figure 74 Trajectory for OCC=5, D=12 m and CAD=36 months